WAVE FORCES ON MODELS OF SUBMERGED OFFSHORE STRUCTURES

Prepared

by

Paul E. Versowsky and John B. Herbich
Coastal, Hydraulic and Ocean Engineering Group
Department of Civil Engineering
Texas Engineering Experiment Station
Texas A&M University

Partially supported through Institutional
Grant 04-3-158-18 to Texas A&M University by the
National Oceanic and Atmospheric Administration's
Office of Sea Grants, Department of Commerce

Sea Grant Publications No. TAMU-SG-75-215
C.O.E. Report No. 175

August 1975

$3.00

Order from:

Department of Marine Resources Information
Center for Marine Resources
Texas A&M University
College Station, Texas 77843

ABSTRACT

The results of a model study of the forces caused by oscillatory waves on large rectangular tank-like submerged objects are presented. Three phases of the problem were examined: 1) description of the forces in terms of dimensionless parameters, 2) description of the effect of large wave heights which are of importance to the designer, and 3) the presentation of a format to be used in model studies on submerged structures.

Theoretical studies of the problem have assumed wave heights to be small and the forces to be entirely inertial. However, of interest to the engineer are the forces caused by the larger waves generated by severe storms. In the model study the forces caused by the larger waves were determined and the effect of the water particle velocity in producing a drag force was examined.

The relationships between the fluid particle displacement and the coefficients of mass and drag were evaluated. Previous studies indicate that particle displacement is related to the values of empirical coefficients assumed by previous investigation.

The experimental results are given in a dimensionless form. Provided the laws of modeling are followed, and there are no scale effects, these results may be used to determine the forces on prototype structures in the ocean.

PREFACE

Research described in this report was conducted as part of the research program in coastal and ocean engineering at Texas A&M University. Experimental work was conducted in the Hydromechanics Laboratories and was partially supported by the NOAA Sea Grant Program at Texas A&M University.

TABLE OF CONTENTS

LIST OF FIGURES

LIST OF FIGURES (cont.)

LIST OF FIGURES (cont.)

LIST OF FIGURES (cont.)

CHAPTER I

INTRODUCTION

The huge amount of energy required by modern man to supply electricity to his home, run his car, and operate his industry has prompted the petroleum industry to explore remote offshore areas and deep water regions in search of oil and natural gas. The problems encountered in extracting the oil and gas found in these areas have produced new innovations in the petroleum recovery industry.

The problem of crude oil storage at offshore fields distant from adequate shore and port facilities was solved by the Dubai Petroleum Company and Chicago Bridge and Iron Company with the construction and placement of three large submerged tanks at their field in the Arabian Gulf. With processing equipment located on platforms atop two of the tanks, the facility represents the world's largest self-contained offshore production complex with capabilities for storage and tanker loading (16).

The need to extend the oil recovery capabilities of the petroleum industry to deeper water has led to the development of plans for an entire oil field underwater. Phase One of such a project was completed in August of 1972 when Lockheed Petroleum Services Ltd. and Shell Oil Company completed the installation of the world's first dry

---

The citations on the following pages follow the style of the Journal of the Waterways, Harbors, and Coastal Engineering Division, Proceedings of the American Society of Civil Engineers.

underwater oil well in 375 ft. of water in the Gulf of Mexico (1). The actual well-head structure is thirty ft. high and ten ft. in diameter. Future plans call for additional underwater well-heads with a submerged manifold center to commingle production, and a submerged production station where oil and gas are separated and then pumped to the appropriate holding facilities.

The submerged structures described above represent a considerable outlay of time and money. These and other future concepts of underwater structures require sound design criteria to assure a balance between economy and maximum structural integrity. Of primary concern to the designer working in an ocean environment where water depths range from intermediate to shallow are the forces due to gravity waves. Analytical theories presently put forth for determining wave forces on large submerged objects are adequate only for waves of small amplitude and for objects of idealized shape.

Until such time as theoretical force predictions are available, the designer must rely on either past experience or the results of model experiments. Also, the peculiarities of each design situation may require model testing to complement any theoretical results obtained. The importance of such model tests can only be emphasized by the investment made by Chicago Bridge and Iron Company in building and instrumenting its wave-test facility. Present research by Chicago Bridge and Iron involves a submerged 1-million bbl. storage facility and some multipurpose structures (17).

It is with these thoughts in mind that the objectives of this thesis are stated.

Thesis Objectives. - The primary objective of this thesis was to study the forces caused by oscillatory waves on large submerged objects and to present the information regarding such forces in a suitable dimensionless form. An investigation was made of several dimensionless parameters for plotting against the dimensionless force to determine the best possible representation to be used in model studies. Data previously obtained by Herbich and Shank (35) was used in the investigation along with data from experiments performed by the author on larger models.

CHAPTER II

LITERATURE SURVEY

Studies on Wave Forces. - About 1950, Morison, et al. (23,24,26) presented an equation for calculating the total force on an object under the influence of gravity waves. The equation, known as the "Morison equation", was developed for piles and later extended to submerged objects (27). The equation represents the total force as the sum of two components, drag and inertia. The Morison equation can be written as

$$F_T = C_D \rho \frac{A}{2} |u| u + C_M \rho \forall \frac{\partial u}{\partial t} \quad \ldots\ldots\ldots \quad (2.1)$$

where F_T = total force on the object

C_D, C_M = drag and inertia coefficients, respectively

A = cross-sectional area of object (projected)

$\forall$ = volume of object

ρ = density of fluid

u = velocity of water particle

$\frac{\partial u}{\partial t}$ = acceleration of water particle

The Morison equation uses empirically determined coefficients (C_D, C_M) and the particle velocity and acceleration equations of some appropriate wave theory to relate total force to wave parameters.

An equation for the horizontal wave force on a large rectangular submerged structure was given by Reid and Bretschneider (31). The volume of the object is considered large enough that the force on

the object is entirely inertial; and the force is computed from the horizontal pressure distribution beneath the wave. The Reid and Bretschneider equation for horizontal force is

$$F_H = \gamma C_M \frac{H}{2} \ell_2 \ell_3 \frac{\cosh k(z+d)}{\cosh kd} [\cos\theta_1 - \cos(\theta_1 + \frac{2\pi\ell_1}{L})] \quad (2.2)$$

where F_H = horizontal force component

C_M = mass coefficient to account for disturbance of flow due to presence of object

ℓ_1 = object dimension parallel to direction of wave travel

ℓ_2 = object dimension perpendicular to direction of wave travel

ℓ_3 = object height

γ = unit weight of fluid

H = wave height

θ_1 = phase position of leading edge of object

d = water depth

x,z = horizontal and vertical coordinates, respectively

L = wave length

Chakrabarti (5) showed that this equation reduces to the inertial term of the Morison equation for small objects (i.e., $\ell_1 << L$).

In 1958, Brater, McNown, and Stair (2) studied the magnitude and characteristics of wave forces on submerged structures. Several models which included rectangular barge-like objects were supported from rods instrumented to detect horizontal and vertical loadings. The wave profile and the time history of the resulting horizontal

and vertical forces were obtained for various wave heights, wave periods, and barge locations with respect to the water surface. For the barge-like structure, the force was determined to be almost entirely inertial, with the maximum force usually occurring under the nodes of the wave.

Using the pressure variation beneath a wave (which considered the change in water surface elevation), Brater, McNown, and Stair computed values for the horizontal inertia coefficient. The inertia coefficient was shown to decrease with increasing wave height. For low wave heights, the theoretical force and measured force agreed well for constant values of the inertia coefficient. Fair agreement existed for larger waves except for the region near the bottom where the measured and theoretical values diverged (measured being greater). Maximum wave heights were usually less than .29 feet.

In the previously cited articles, it was assumed that the Morison type equation was valid and results indicate that for objects small relative to the wave length this is true. Garrison and Rao (29) noted, however, that the Morison equation is used under the following assumptions:

a) The object does not appreciably disturb the incident wave.

b) The fluid flow field existing at the center of the object extends to infinity.

c) The total force is the sum of the inertial and drag components of force.

As the size of the object increases relative to the wave length and water depth, three effects occur:

a) The incident wave can be scattered due to the presence of the object.

b) If the object is not deeply submerged, there is an effect due to the proximity of the free surface.

c) If the object is large, the inertial forces predominate.

The first two effects are called "diffraction effects". The simplifying assumptions of the Morison equation are no longer valid, and another approach should be used.

A theory which accounts for the relative size of the object and the free surface effect is commonly called "diffraction theory". In this approach, separation and viscous effects are neglected and the problem is set up in terms of a velocity potential. The velocity potential which satisfies the necessary boundary conditions is sought. Once it is found, the dynamic pressure distribution is determined from the linearized Bernoulli equation. The forces are obtained by integrating the pressure distribution over the surface of the object.

In 1954, MacCamy and Fuchs (22) used diffraction theory to determine the wave force on large circular cylinders extending vertically from the bottom through the free surface. For small cylinders, the equations reduced to the inertial force term of the Morison equation, provided one considers the inertia coefficient in the Morison equation to equal its potential flow value of 2.0.

In recent studies at Texas A&M University, Garrison, et al. (11,12,29) investigated the forces due to waves on large submerged objects using both theory and experiment.

Garrison and Snider (11) determined the horizontal and vertical wave forces on a submerged hemisphere. The theoretical approach was compared with experimental results using the equations,

$$f_x = \frac{F_{x_{max}}}{\gamma a^2 \frac{H}{2}} = \frac{\pi}{\cosh \frac{h}{a}\frac{2\pi a}{L}} \quad \frac{2\pi a}{L} \quad \ldots\ldots\ldots\ldots \quad (2.3)$$

and

$$f_y = \frac{F_{y_{max}}}{\gamma a^2 \frac{H}{2}} = 2\pi \left[\frac{\frac{2\pi a}{L} - \sinh \frac{2\pi a}{L} - \cosh \frac{2\pi a}{L} + 1}{(\frac{2\pi a}{L})^2 \cosh \frac{h}{a} \frac{2\pi a}{L}} \right] \quad (2.4)$$

where f_x, f_y = horizontal and vertical force coefficients, respectively

$F_{x_{max}}, F_{y_{max}}$ = maximum horizontal and vertical force, respectively

γ = unit weight of fluid

a = radius of hemisphere

H = wave height

h = water depth

L = wave length

The theoretical approach was based on two assumptions: 1) the wave length is large compared to the object size, and 2) viscous effects are negligible. Equations 2.3 and 2.4 are derived from the pressure distribution as given by Airy wave theory. Comparison of theory and experiment showed good agreement for conditions covered by the assumptions.

Garrison and Rao (29) developed in detail the diffraction theory for wave forces on a rigid semiellipsoid submerged in an inviscid, incompressible fluid. The formulation of the problem using diffraction theory is difficult even for the simple shape involved. More complex shapes produce formidable calculations requiring computer numerical analysis.

Herbich and Shank (14,35) represented the results of model studies on half-cylindrical and rectangular-shaped objects. They found that the force on the models was almost entirely inertial, and using the equation given by Reid and Bretschneider (Eq. 2.2) determined an inertial coefficient for the models. The results of the model studies were given in the form of dimensionless graphs of a dimensionless force versus relative depth (L/d) for constant values of wave steepness (H/L) for both the forizontal and vertical directions. The dimensionless force was given by

$$(F_{DIM}) = \frac{F_{max}}{\gamma \frac{A^3}{d} \frac{H}{2}} \quad \ldots\ldots\ldots\ldots\ldots (2.5)$$

where F_{DIM} = dimensionless force

F_{max} = maximum measured force

A = significant linear dimension equal to the height of the model squared divided by the length of the model in the direction of wave propagation for all models except the flat plate

$A = H_m$ = height of model for flat plate

d = water depth

H = wave height

γ = specific weight of fluid

Garrison and Chow (10) outlined a diffraction theory valid for submerged objects of arbitrary shape. The theory was applied to a rounded rectangular-shaped structure and compared with the results of model tests. Comparison was made in terms of theoretical and measured dimensionless force graphs and the agreement was good. The model used was by far the largest of any tests cited, being 73" long, 13" high, and 25.5" wide.

Much of the work done in determining wave forces on submerged structures assumed that viscous forces are negligible. Sarpkaya and Garrison (33) determined that for small fluid particle displacement to diameter ratios, drag forces on cylinders could be neglected. This assumption is extended to larger objects and different shapes by Garrison, et al. However, as the fluid particle displacement to object size ratio increases, a point will be reached where viscous effects become important and need to be considered.

Studies Using Dimensionless Parameters. - Keulegan and Carpenter (19) developed a Fourier series analysis for the force on flat plates and cylinders due to a sinusoidally varying fluid motion. By comparing the Morison equation to the Fourier series, they were able to relate the coefficient of inertia to the coefficient of the first sine term of the Fourier expansion, and the coefficient of drag to the modified first term of the cosine part of the expansion. A

remainder function, ΔR, was used to represent the truncated part of the Fourier series not considered in the Morison equation. The remainder function was considered by Keulegan and Carpenter to give a truer representation of force when considering the coefficients C_M and C_D as being constant throughout a given wave cycle.

Keulegan and Carpenter established the significance of the "period parameter" in this work. Using experimental studies, they related the period parameter to both the coefficients of drag and inertia and to the coefficients of the Fourier series. The period parameter is given by $U_M T/D$ where U_M = maximum velocity, T = period of oscillation, and D = diameter of cylinder or width of plate. It was noted that vortex formation and shedding could also be predicted using the period parameter.

Paape and Breusers (28) suggest that forces for prototype structures be derived from model tests applying the ratio of particle displacement to characteristic dimension (e.g., H/ℓ, $2\pi a/\ell$: where H = wave height, ℓ = characteristic dimension, and a = amplitude of fluid motion) as an independent variable. They found that in wave motion the time dependency of the flow pattern leads to an influence of pile dimensions relative to the dimensions of orbital motion.

The Iversen modulus, described by Crooke, is another dimensionless term used to describe fluid forces on piles. Wiegel (38), however, showed that the Iversen modulus was related to the Keulegan-Carpenter period parameter. The Iversen modulus is given by

$$I_V = \frac{(\partial u/\partial t)\, D}{u^2} \quad \ldots\ldots\ldots\ldots\ldots\ldots \quad (2.6)$$

where $\partial u/\partial t$ = fluid particle acceleration

u = fluid particle velocity

D = for piles, cylinder diameter

Substituting for particle acceleration and velocity as defined by Airy wave theory, Equation 2.6 may be rewritten as

$$I_V = \frac{2\pi D}{uT} \frac{\sin(kx-\sigma t)}{\cos(\ell x-\sigma t)} \quad (2.7)$$

For maximum acceleration and velocity, Equation 2.7 becomes

$$I_V = 2\pi \frac{D}{U_{max} T} = 2\pi \left[\frac{1}{\text{period parameter}} \right] \quad (2.8)$$

It should also be noted that for total particle displacement and maximum velocity, the following parameters are proportional to each other for a given water depth, wave length, and object submergence:

a) $\frac{\text{total particle displacement}}{\text{characteristic length}}$

b) period parameter

c) $\frac{\text{wave height}}{\text{characteristic length}}$

CHAPTER III

THEORETICAL CONSIDERATIONS

Wave Theory. - The research presented in this paper is essentially a model study in which physical quantities were directly measured. There are, however, certain quantities necessary to this study which do not avail themselves to easy measurement. Fortunately, these difficult to determine quantities have been mathematically described in any of several wave theories.

In the laboratory, wave characteristics such as wave period, wave height, and water depth are easily measured. These values are then used to calculate the wave length, particle kinematics, and pressure distribution under the wave. Fig. 1 pictorially represents the relationship between the measured and theoretical quantities as used in this study. The measured and calculated wave characteristics along with the measured force are used to determine dimensionless force. The pressure distribution given by theory is used to determine a theoretical dimensionless force.

A wave theory which is easy to work with, accurate, and gives an easily understood interpretation of the physical situation is Airy wave theory. Sometimes referred to as Stokes' first order wave theory, it is a first approximation to a mathematical description of water wave phenomenon. The theory assumes the existence of a velocity potential based on irrotational fluid motion. The fluid is

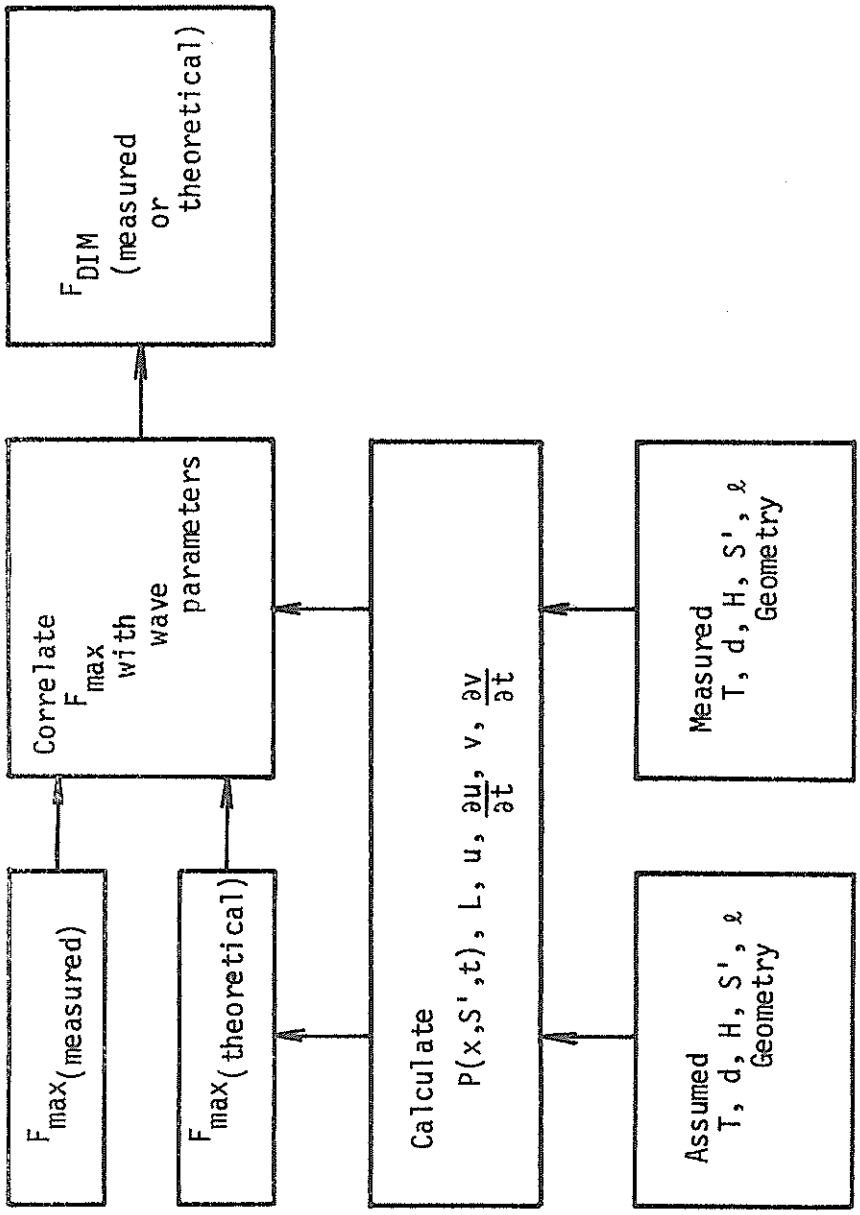

Fig. 1 - Relationship between Theoretical and Measured Quantities used in determining Dimensionless Force.

assumed to be inviscid and incompressible, and the velocity potential must satisfy Laplace's Equation subject to certain boundary conditions.

Laplace's Equation in two dimensions is given by

$$\frac{\partial^2 \Phi}{\partial x^2} + \frac{\partial^2 \Phi}{\partial z^2} = 0 \quad \ldots\ldots\ldots \quad (3.1)$$

where Φ = the velocity potential

x,z = horizontal and vertical coordinates, respectively

The boundary conditions which must be satisfied by the velocity potential are given by

$$\frac{\partial \Phi}{\partial z} = 0 \Bigg|_{z=-d} \quad \ldots\ldots\ldots \quad (3.2)$$

$$\eta = \frac{1}{g} \frac{\partial \Phi}{\partial t} \Bigg|_{z=0} \quad \ldots\ldots\ldots \quad (3.3)$$

where d = water depth

η = free surface elevation

g = acceleration of gravity

t = time

These boundary conditions are based on the following assumptions:

1. Gravity is the only major body force present.
2. Atmospheric pressure is constant over the free surface and is referenced to zero.

3. Water depth is constant and the bottom surface is impermeable.

4. The wave height is small compared with the wave length and water depth.

5. All nonlinear terms are small and can be neglected.

Solving Equations 3.1, 3.2, and 3.3 for the velocity potential yields

$$\Phi = -\frac{ag}{\sigma}\,\frac{\cosh k(z+d)}{\cosh kd}\,\sin(kx-\sigma t) \quad \ldots\ldots\ldots \quad (3.4)$$

where a = wave amplitude

g = acceleration of gravity

$\sigma = 2\pi/T$ = wave angular frequency

T = wave period

$k = 2\pi/L$ = wave number

L = wave length

Fig. 2 is the definition sketch for the terms used in Airy wave theory and presented here.

Substituting for Φ in Equation 3.3 yields the equation for the wave surface profile.

$$\eta = a\cos(kx-\sigma t) \quad \ldots\ldots\ldots\ldots\ldots \quad (3.5)$$

By definition of the velocity potential , the horizontal and vertical components of water particle velocity are given by,

$$u = -\frac{\partial \Phi}{\partial x} \quad \ldots\ldots\ldots\ldots\ldots \quad (3.6)$$

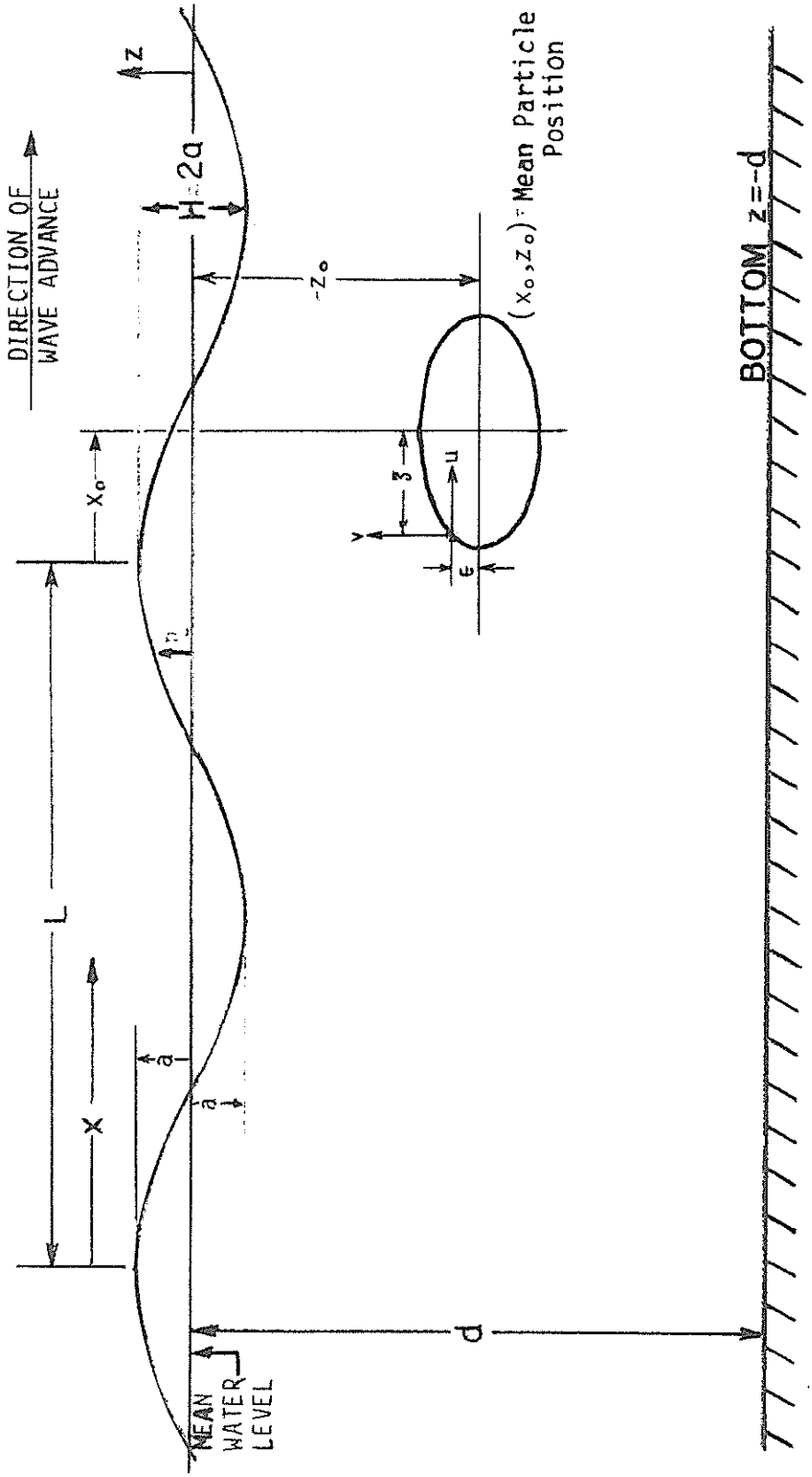

Fig. 2 - Definition Sketch for Terms used in Airy Wave Theory.

$$w = -\frac{\partial \Phi}{\partial z} \quad \ldots\ldots\ldots\ldots\ldots \quad (3.7)$$

and on substituting Equation 3.4 into 3.6 and 3.7, we have

$$u = \frac{agk}{\sigma} \frac{\cosh k(z+d)}{\cosh kd} \cos(kx-\sigma t) \quad \ldots\ldots \quad (3.8)$$

$$w = \frac{agk}{\sigma} \frac{\sinh k(z+d)}{\cosh kd} \sin(kx-\sigma t) \quad \ldots\ldots \quad (3.9)$$

Local water particle acceleration components are the time derivatives of the velocity components.

$$\frac{\partial u}{\partial t} = agk \frac{\cosh k(z+d)}{\cosh kd} \sin(kx-\sigma t) \quad \ldots\ldots \quad (3.10)$$

$$\frac{\partial w}{\partial t} = -agk \frac{\sinh k(z+d)}{\cosh kd} \cos(kx-\sigma t) \quad \ldots\ldots \quad (3.11)$$

Particle displacement from its mean position can be found by integrating the velocity components with respect to time. Letting ξ be the horizontal displacement and ε be the vertical displacement, it can be shown that

$$\xi = -\frac{H}{2} \frac{\cosh k(z+d)}{\sinh kd} \sin(kx-\sigma t) \quad \ldots\ldots \quad (3.12)$$

$$\varepsilon = \frac{H}{2} \frac{\sinh k(z+d)}{\sinh kd} \cos(kx-\sigma t) \quad \ldots\ldots \quad (3.13)$$

The equation for the wave length (L) in Airy wave theory is the same as the equation for wave length in Stokes' second order wave theory. Notice that the equation is transcendental, as L appears on both sides of the equation.

$$L = \frac{gT^2}{2\pi} \tanh \frac{2\pi d}{L} \quad \ldots\ldots\ldots \quad (3.14)$$

The speed of wave propagation or the wave celerity (C) is given by

$$C = L/T \quad \ldots\ldots\ldots\ldots\ldots \quad (3.15)$$

Finally, the pressure beneath a wave is found by substituting for Φ in the linearized integrated equation of motion:

$$-\frac{\partial \Phi}{\partial t} + \frac{P}{\rho} + gz = 0 \quad \ldots\ldots\ldots \quad (3.16)$$

and

$$P = \gamma a \cdot \frac{\cosh k(z+d)}{\cosh kd} \cdot \cos(kx-\sigma t) - \gamma z \quad \ldots \quad (3.17)$$

Details of the complete formulation of small amplitude (Airy) wave theory are given by Wiegel (38), and Dean and Eagleson (18).

As mentioned previously, Airy wave theory is easy to work with. It also has the advantage of allowing the user to visualize mathematically the phenomenon associated with wave motion. However, it is a first approximation and a word should be said about the extent of its applicability.

In 1953, Morison and Crooke (25) performed a set of experiments in which they measured the wave surface profile, horizontal and vertical particle velocity, and the size and shape of particle orbits. The results of the laboratory experiments were compared with Stokes' first order (Airy) and Stokes' second order wave theories. They

determined that good agreement between theory and experiment existed where the relative water depth (d/L) was greater than about 0.2, even for waves of appreciable wave steepness (H/L). Fair agreement existed in the range of $0.2 > d/L > 0.1$.

Dimensional Analysis. - In model studies, one of the most powerful tools the investigator has to work with is dimensional analysis. By grouping significant variables into dimensionless parameters, it is possible to reduce the number of variables in the problem. Dimensional analysis yields an equation describing the phenomenon which can be written as

$$\pi_1 = f(\pi_2, \pi_3, \ldots, \pi_n) \quad \ldots\ldots\ldots \quad (3.18)$$

where the π_n's represent the resulting dimensionless parameters. Equation 3.18 is the most general equation describing the problem. Careful selection of the important variables in question will result in the most useful form of Equation 3.18. It is therefore necessary that there be some idea as to which variables are important in the analysis of the phenomenon.

The primary objective of this thesis is to study the forces caused by oscillatory waves on large submerged objects and present the information regarding such forces in a suitable dimensionless form. Dimensional analysis yields the dimensionless parameters which are used in the dimensionless plots presented. Dimensionless graphs, properly done, are important for several reasons: 1) The dimensionless graph provides more information than a graph in which the

coordinates have dimensions. 2) Being dimensionless, any system of measurement can be used (i.e., CGS system, MKS force system, American Engineering System, etc.). 3) Prototype phenonemon can be predicted from model studies using the dimensionless plots if the proper model-prototype similitude is observed.

Similitude of model and prototype requires that geometric, kinematic, and dynamic ratios in each system be equal. The length ratio for the model dimensions must be the same as the corresponding length ratio in the prototype for geometric similarity. Kinematic and dynamic similarity requires, for example, that the velocity ratio and mass ratio respectively, be equal in model and prototype. Satisfying these conditions, the dimensionless plots are valid for both model and prototype.

The first step in the dimensional analysis is the selection of the variables pertinent to the problem of wave forces on a submerged structure. This requires knowledge of the process, and a study of fluid force in oscillatory flow will aid in determining these quantities. The variables fall into three basic categories: 1) geometric variables, 2) kinematic and dynamic variables, and 3) fluid properties. Thus, it has been determined that the force on a body due to oscillatory waves can be written as the functional relationship:

$$F = f_1(\forall, \ell, H, d, L, \rho, \mu, U, T, g) \quad . \quad . \quad . \quad . \quad . \quad . \quad (3.19)$$

The first five terms on the right-hand side of the above relationship are geometric properties of the system. The volume ($\forall$) is important because the force in accelerated flow is proportional to the volume. The quantity ℓ can be any characteristic length of the system. The wave height (H), water depth (d), and wave length (L), characterize the wave motion. The next two terms are the fluid properties, density (ρ), and dynamic viscosity (μ). Finally, the kinematic and dynamic terms chosen are velocity (U), wave period (T), and gravitational acceleration (g). The force (F) is also a dynamic variable.

Using the method described by Street (37) and choosing the repeating variables to be density (ρ), gravitational acceleration (g), and volume ($\forall$), the following eight dimensionless terms were computed.

$$\left.\begin{aligned} \pi_1 &= \frac{F}{\rho g \forall} & \pi_2 &= \frac{\mu}{\rho\sqrt{g\forall}} & \pi_3 &= \frac{H^3}{\forall} \\ \pi_4 &= \frac{g^3T^6}{\forall} & \pi_5 &= \frac{d^3}{\forall} & \pi_6 &= \frac{L^3}{\forall} \\ \pi_7 &= \frac{\ell^3}{\forall} & \pi_8 &= \frac{U^6}{g^3\forall} \end{aligned}\right\} \quad . \; . \; . \quad (3.20)$$

This forms a complete set of the variables in question. If we choose, we may multiply or divide dimensionless terms or raise them to any power to obtain new dimensionless terms which more appropriately describe the process. For example, multiplying π_5 by the inverse of π_6 and taking the cube root of the result, we obtain the relative depth parameter (d/L).

$$\pi_{14} = \left(\frac{\pi 5}{\pi_6}\right)^{1/3} = \left(\frac{d^3}{\forall} \cdot \frac{\forall}{L^3}\right)^{1/3} = \frac{d}{L} \quad . \; . \; . \quad (3.21)$$

This type of manipulation results in the following new dimensionless quantities.

$$\left.\begin{aligned} \pi_9 &= \frac{F}{\rho g \forall \cdot \frac{H}{d} \cdot \frac{\ell}{L}} \qquad \pi_{10} = \frac{\mu}{\rho\sqrt{g\ell^3}} \qquad \pi_{11} = \frac{H}{\ell} \\ \pi_{12} &= \frac{d}{\ell} \qquad \pi_{13} = \frac{\ell}{L} \qquad \pi_{14} = \frac{d}{L} \\ \pi_{15} &= \frac{UT}{\ell} \qquad \pi_{16} = \frac{U}{\sqrt{g\ell}} \end{aligned}\right\} \; . \; . \quad (3.22)$$

These π-values can then be substituted into the functional relationship having the form of Equation 3.18.

$$\frac{F}{\rho g \forall \cdot \frac{H}{d} \cdot \frac{\ell}{L}} = f_2\left(\frac{\mu}{\rho\sqrt{g\ell^3}}, \frac{H}{\ell}, \frac{d}{\ell}, \frac{\ell}{L}, \frac{d}{L}, \frac{UT}{\ell}, \frac{U}{\sqrt{g\ell}}\right) \quad . \; . \; . \; . \quad (3.23)$$

The left hand side of Equation 3.23 is the general representation for the dimensionless force. The reason for the form of this term will become apparent in the discussion in the next section. The first term on the right hand side of Equation 3.23 can be shown to be the ratio of Froude number to Reynolds number. Garrison and Chow (10) suggest that this term may be neglected provided it is small, which is generally the case for large objects submerged in water.

The next three π-parameters in Equation 3.23 (H/ℓ, d/ℓ, ℓ/L) indicate the condition of flow around the object. Garrison and Rao (29) identify these terms as: 1) the relative displacement parameter (H/ℓ), 2) the surface effect parameter (d/ℓ), and 3) the relative size parameter (ℓ/L). Their importance to the problem of wave forces on submerged objects can best be understood by considering their effect on the validity of the Morison equation and diffraction theory. Fig. 3 (after Garrison, Rao, and Snider (12)) gives a graphic representation of the relationship between these parameters.

Fig. 3 is drawn for a constant value of the surface effect parameter. The coefficient of mass in the Morison equation will depend on this value. As the ratio of d/ℓ decreases, the effect of the object on the free surface will increase and diffraction effects will predominate.

The relative displacement parameter (H/ℓ) is related to viscous effects. Sarpkaya and Garrison (33) have shown from unsteady flow experiments on cylinders that for small values of the ratio of fluid particle displacement to cylinder diameter (the initiation of motion) the values of the inertial and drag coefficients are equal to their potential flow values of 2.0 and 0.0, respectively. However, as the ratio of fluid particle displacement to cylinder diameter increased, separation occurred and the drag coefficient increased from zero. Using linear wave theory, it can be shown that for a given wave length and water depth the ratio of total fluid particle displacement to object characteristic length is proportional to H/ℓ. Diffraction

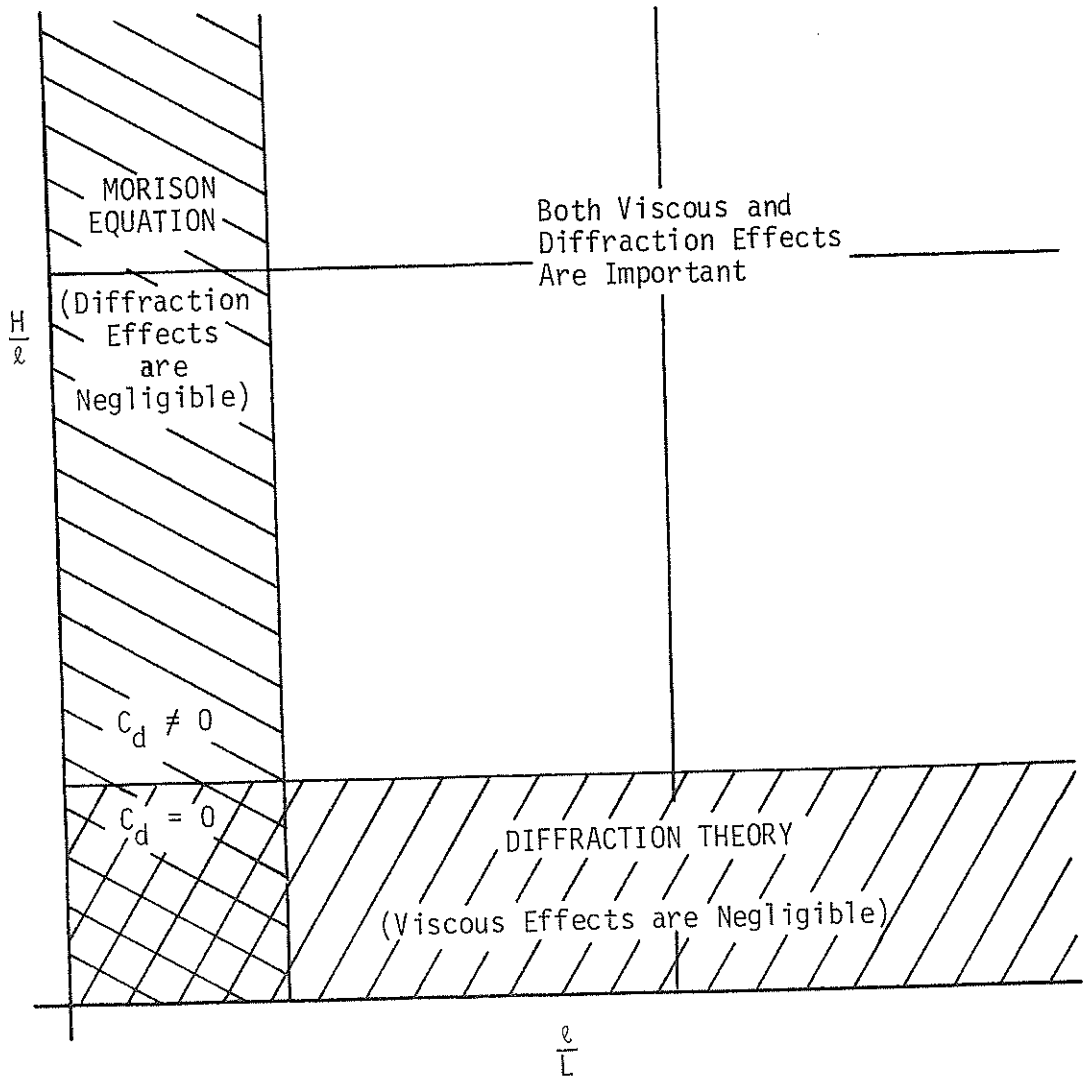

Fig. 3 - Region of Applicability of Morison Equation and Diffraction Theory with respect to the Relative Size Parameter (ℓ/L) and Relative Displacement Parameter (H/ℓ) for a Constant Surface Effect Parameter (d/ℓ). [after Garrison, Rao, and Snider]

theory neglects viscous effects and therefore is valid for small values of the relative displacement parameter.

The relative size parameter is important in determining the validity of the Morison equation. For small structures, such as piles, the relative size parameter is small and the Morison equation is valid. For large structures, the flow becomes disturbed and diffraction effects predominate. If viscous effects are small, diffraction theory can be used to find the forces on large objects. The relative size parameter is also important in describing the variation in force over the dimensions of the object.

The next dimensionless term is the relative depth (d/L). The relative depth and wave steepness (H/L) characterize the incident wave.

The dimensionless term UT/ℓ is called the period parameter. Keulegan and Carpenter (19) correlated this term with the coefficients of mass and drag for unsteady flow around a cylinder. This parameter is similar to the relative displacement parameter in that for linear wave theory, they are both proportional to the total particle displacement to characteristic length ratio as shown in Equations 3.24 and 3.25 below. For a given water depth and wave length, we may write

$$\frac{\xi_{total}}{\ell} = \frac{H}{\ell} \cdot \frac{\cosh k(z+d)}{\sinh kd} = K_1 \frac{H}{\ell} \quad . \quad . \quad . \quad (3.24)$$

and

$$\frac{U_{max} T}{\ell} = \frac{H}{\ell} \cdot \pi \cdot \frac{\cosh k(z+d)}{\sinh kd} = \pi K_1 \frac{H}{\ell} \qquad (3.25)$$

The last dimensionless term in Equation 3.23 is the Froude number ($U/\sqrt{g\ell}$). Although important in the problem of waves generated by moving ships, the Froude number does not appear significant in the problem of wave forces on submerged structures.

Theoretical Wave Forces. - The pressure distribution under a wave is given by Equation 3.17. Neglecting the hydrostatic term, we may write the wave induced pressure as,

$$P(x,S,t) = \gamma \frac{H}{2} \frac{\cosh kS}{\cosh Kd} \cos(kx-\sigma t) \quad \ldots\ldots\ldots \quad (3.26)$$

where $P(x,S,t)$ = wave induced pressure

γ = unit weight of fluid

H = wave height

$S = (z+d)$ = elevation above bottom

$k = 2\pi/L$

L = wave length

$\sigma = 2\pi/T$

T = wave period

t = time.

Consider a rectangular structure submerged so that the center of the structure is located a distance S' above the bottom as shown in Figure 4. Let ℓ_1 be the structure dimension in the direction of wave propagation, ℓ_2 is the structure dimension perpendicular to the direction of wave propagation, and ℓ_3 is the vertical dimension of the structure. The structure is considered deeply submerged so that surface effects are negligible. Neglecting viscous effects,

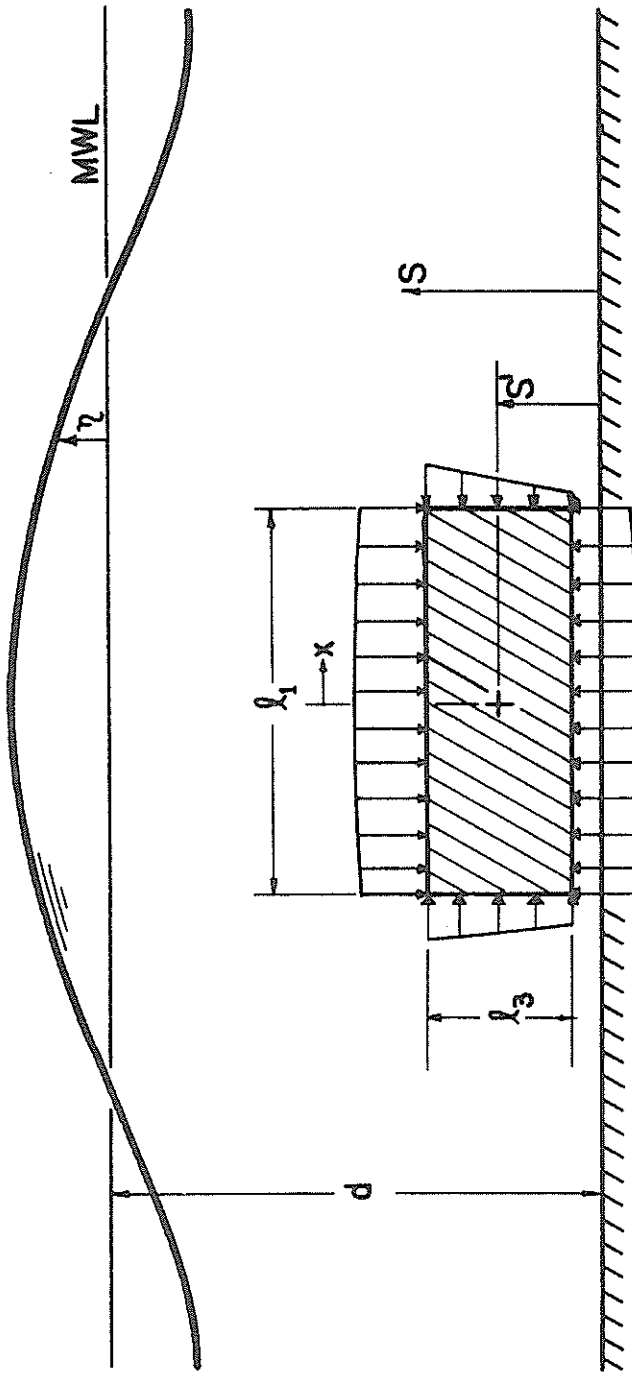

Fig. 4 - Definition Sketch of Pressure Distribution on Model.

we may write the force due to a wave on the structure as a result of the wave induced pressure distribution. For the force in the horizontal direction, we have

$$F_H = C_{M_H} \cdot \ell_2 \left[\int_{-\frac{\ell_3}{2}}^{\frac{\ell_3}{2}} P(x-\tfrac{\ell_1}{2}, S' + S, t)\,dS - \int_{-\frac{\ell_3}{2}}^{\frac{\ell_3}{2}} P(x+\tfrac{\ell_1}{2}, S' + S, t)\,dS \right] \quad \ldots\ldots (3.27)$$

The coefficient C_{M_H} accounts for the disturbance of the flow due to the presence of the object. It is the coefficient of mass in the Morison equation and has a value greater than unity.

Substituting Equation 3.26 into Equation 3.27 yields

$$F_H = C_{M_H} \cdot \ell_2 \left[\int_{-\frac{\ell_3}{2}}^{\frac{\ell_3}{2}} \gamma \tfrac{H}{2} \frac{\cosh k(S'+S)}{\cosh kd} \cos k(x-\ell_1/2) - \sigma t \; dS - \int_{-\frac{\ell_3}{2}}^{\frac{\ell_3}{2}} \gamma \tfrac{H}{2} \frac{\cosh k(S'+S)}{\cosh kd} \cos k(x+\ell_1/2) - \sigma t \; dS \right] \quad \ldots (3.28)$$

This equation can be rewritten as

$$F_H = C_{M_H} \cdot \ell_2 \gamma \frac{H}{2} \cdot \frac{1}{\cosh kd} \cdot \left\{ \cos \left(k(x-\ell_1/2)-\sigma t \right) - \cos \left(k(x+\ell_1/2)-\sigma t \right) \right\} \cdot \int_{-\frac{\ell_3}{2}}^{\frac{\ell_3}{2}} \cosh k(S'+S)dS \quad \ldots (3.29)$$

Evaluating the integral in Equation 3.29 yields

$$\int_{-\frac{\ell_3}{2}}^{\frac{\ell_3}{2}} \cosh k(S'+S)dS = \frac{1}{k} \left[\sinh k(S'+\ell_3/2) - \sinh k(S'-\ell_3/2) \right] \quad \ldots (3.30)$$

Using the relation

$$\sinh(u+v) - \sinh(u-v) = 2 \cosh u \sinh v$$

Equation 3.30 reduces to the expression

$$\frac{2}{k} \cosh kS' \sinh(k\ell_3/2) \quad \ldots\ldots\ldots (3.31)$$

Using the relation

$$\cos u - \cos v = -2 \sin 1/2(u+v) \sin 1/2(u-v),$$

the bracketed {} part of Equation 3.29 becomes

$$2 \sin(kx-\sigma t) \sin(k\ell_1/2) \quad \ldots\ldots\ldots \quad (3.32)$$

We may now substitute expressions 3.31 and 3.32 into Equation 3.29. This yields

$$F_H = C_{M_H} \gamma \frac{H}{2} \cdot \ell_2 = \frac{2}{k} \frac{\cosh kS'}{\cosh kd} \sinh \frac{k\ell_3}{2} \cdot 2\sin \frac{k\ell_1}{2} \sin(kx-\sigma t) \quad (3.33)$$

By multiplying and dividing Equation 3.33 by ℓ_1, ℓ_3, and k, we produce an equation of the form

$$F_H = \gamma \frac{H}{2} \cdot \ell_1 \ell_2 \ell_3 \, k \frac{\cosh kS'}{\cosh kd} \cdot \left(\frac{\sinh k\ell_3/2}{k\ell_3/2}\right)\left(\frac{\sin k\ell_1/2}{k\ell_1/2}\right) \cdot$$

$$\sin(kx-\sigma t) \quad \ldots\ldots\ldots\ldots\ldots\ldots\ldots \quad (3.34)$$

It is noted here that $\ell_1 \cdot \ell_2 \cdot \ell_3$ is the volume of the rectangular structure and the Equation 3.10 is present in 3.34.

$$F_H = C_{M_H} \rho \forall \frac{\partial u}{\partial t} \cdot \left(\frac{\sinh k\ell_3/2}{k\ell_3/2}\right)\left(\frac{\sin k\ell_1/2}{k\ell_1/2}\right) \quad \ldots\ldots \quad (3.35)$$

Dean and Dalrymple (9) in a similar derivation give the equation for the vertical force. The derivation is identical to the one

done here for the horizontal force and need not be repeated. The vertical force is given as

$$F_V = C_{M_V} \rho \forall \frac{\partial w}{\partial t} \cdot \left(\frac{\sinh k\ell_3/2}{k\ell_3/2}\right)\left(\frac{\sin k\ell_1/2}{k\ell_1/2}\right) \quad \ldots . \quad (3.36)$$

Equations 3.35 and 3.36 represent the theoretical wave force on a large rectangular structure, for the horizontal and vertical directions, respectively. It should be noted that the x- and z- components of acceleration are evaluated at the center of the structure.

The hyperbolic sine term

$$SHL3 = \frac{\sinh (k\ell_3/2)}{k\ell_3/2} \quad \ldots \ldots \ldots \quad (3.37)$$

accounts for the variation in pressure over the end vertical faces of the structure. For values of ℓ_3 less than ten percent of the wave length, the maximum error in neglecting this term is about one percent.

The circular sine term

$$SL1 = \frac{\sin (k\ell_1/2)}{k\ell_1/2} \quad \ldots \ldots \ldots \quad (3.38)$$

accounts for the variation in pressure over the length of the structure parallel to the direction of wave propagation. For values of ℓ_1 less than nine percent of the wave length, the maximum error in neglecting this term is about one percent.

For objects which are small (i.e., follow the above criteria), the value of Equations 3.37 and 3.38 is approximately equal to one and Equations 3.34 and 3.35 reduce to the inertia force term of the Morison equation.

$$F_H = C_{M_H} \rho \forall \frac{\partial u}{\partial t} \quad \ldots\ldots\ldots\ldots\ldots\ldots (3.39)$$

$$F_V = C_{M_V} \rho \forall \frac{\partial w}{\partial t} \quad \ldots\ldots\ldots\ldots\ldots\ldots (3.40)$$

The values of the coefficients C_{M_V} and C_{M_H} are obviously different due to variations in flow kinematics in the x- and z- directions, and also due to possible shape variations in the x, y and z, y planes.

Dimensionless Force. - For a large object which is deeply submerged, Equation 3.23 may be written in the following manner

$$\frac{F}{\rho g \forall \cdot \frac{H}{d} \cdot \frac{\ell}{L}} = f_3 \, (S'/L, \, d/L) \quad \ldots\ldots\ldots\ldots (3.41)$$

where F = force

ρ = density of fluid

g = gravitational acceleration

V = volume

H = wave height

d = water depth

L = wave length

S' = characteristic length of system represented as the distance of the center of the tank above the bottom

ℓ = characteristic length of system

Dean and Dalrymple (9) have suggested a dimensionless force term for the vertical and horizontal force components on a large rectangular structure. The dimensionless force is necessarily given for the maximum force for the conditions stated. Slightly modified, the equations given by Dean and Dalrymple (9) are

$$(F_{DIM})_H = \frac{(F_{MAX})_H}{\gamma \frac{H}{d} \cdot \Psi \cdot SHL3 \cdot SL1} \quad \ldots\ldots\ldots (3.42)$$

$$(F_{DIM})_V = \frac{(F_{MAX})_V}{\gamma \frac{H}{d} \cdot \Psi \cdot SHL3 \cdot SL1} \quad \ldots\ldots\ldots (3.43)$$

where SHL3 and SL1 are given by Equations 3.37 and 3.38, respectively.

A theoretical dimensionless force equation is determined by solving Equations 3.35 and 3.36 for the maximum force component and combining the results with Equations 3.42 and 3.43, respectively. The theoretical dimensionless forces are

$$(F_{DIM})_H = C_{M_H} \cdot \pi \cdot \frac{d}{L} \cdot \frac{\cosh kS'}{\cosh kd} \quad \ldots\ldots\ldots (3.44)$$

$$(F_{DIM})_V = C_{M_H} \cdot \pi \cdot \frac{d}{L} \cdot \frac{\sinh kS'}{\cosh kd} \quad \ldots\ldots\ldots (3.45)$$

Another set of dimensionless force equations result from dividing Equation 3.34 by the expression $\gamma \frac{H}{L} \Psi \cdot SHL3 \cdot SL1$ for the maximum force. This gives the theoretical dimensionless force equation

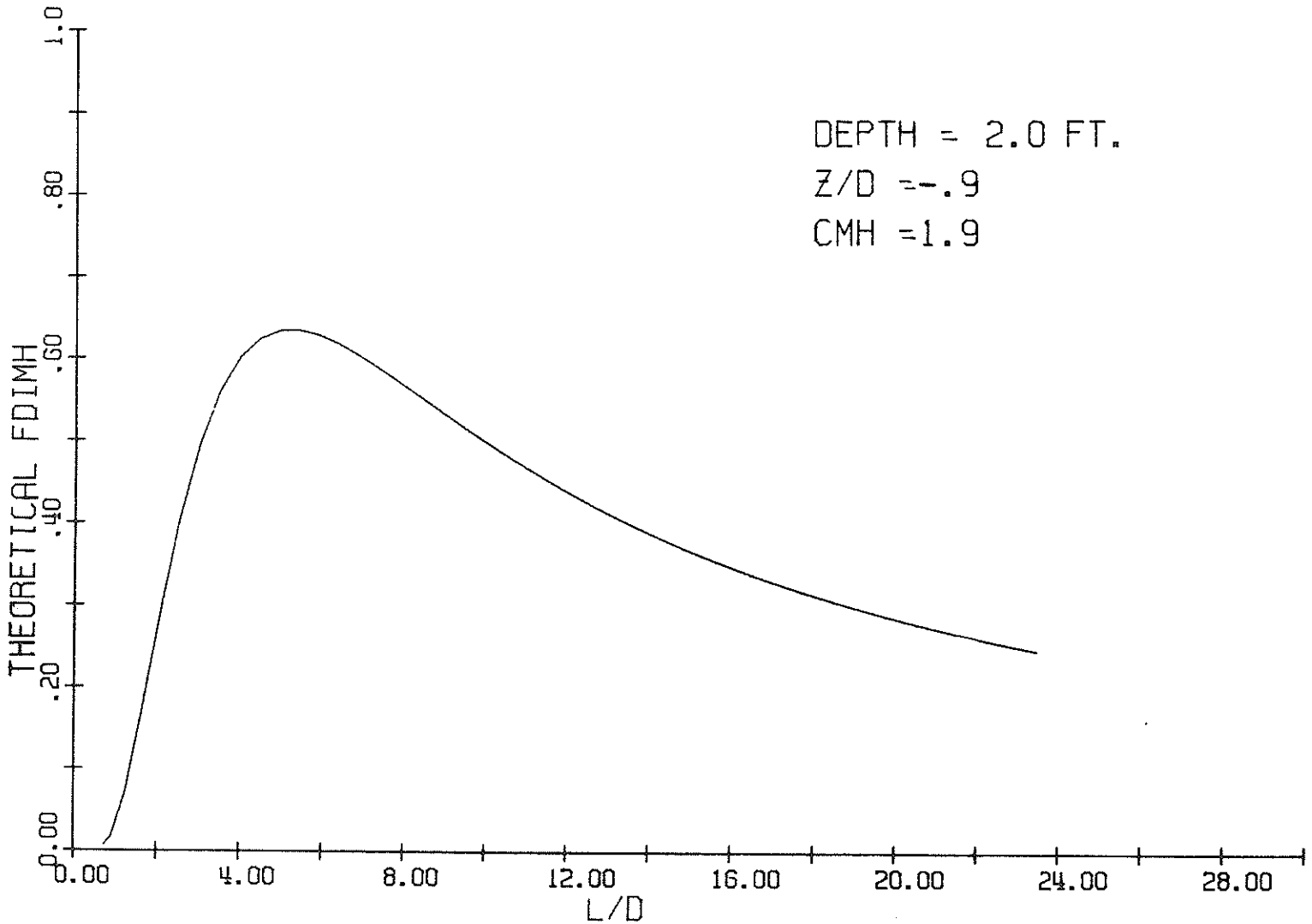

FIG.5 — THEORETICAL D-LESS HORIZONTAL FORCE VS. RELATIVE DEPTH

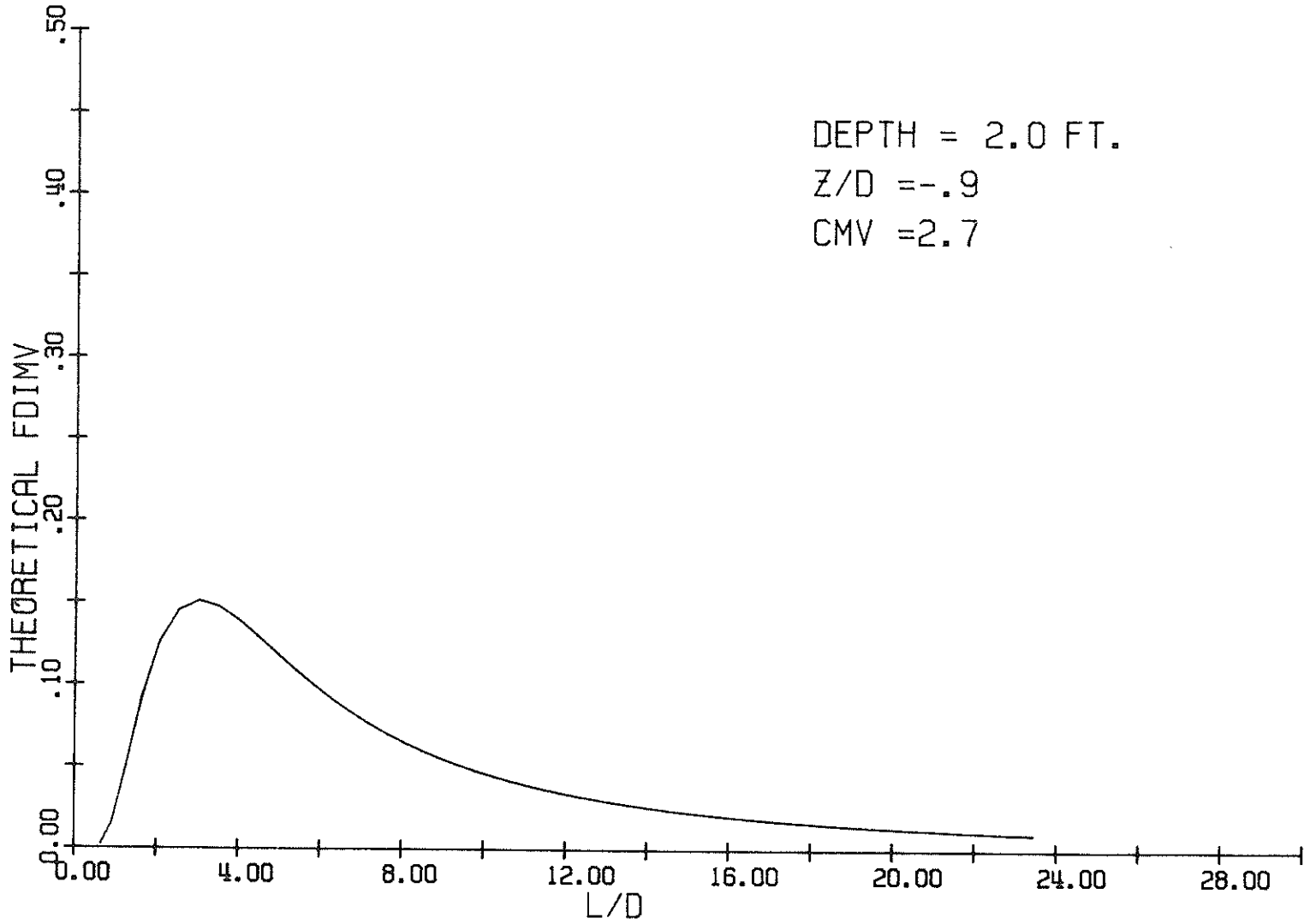

FIG.6 — THEORETICAL D-LESS VERTICAL FORCE VS. RELATIVE DEPTH

$$(F_{DIM})_H = C_{M_H} \cdot \pi \cdot \frac{\cosh kS'}{\cosh kd} \quad \ldots\ldots\ldots \quad (3.46)$$

Similarly for the vertical component of force

$$(F_{DIM})_V = C_{M_V} \cdot \pi \cdot \frac{\sinh kS'}{\cosh kd} \quad \ldots\ldots\ldots \quad (3.47)$$

The use of Equations 3.46 and 3.47 requires the dimensionless force terms for the vertical and horizontal direction to be

$$(F_{DIM})_V = \frac{(F_{MAX})_V}{\gamma \frac{H}{L} \forall \cdot SHL3 \cdot SL1} \quad \ldots\ldots\ldots \quad (3.48)$$

$$(F_{DIM})_H = \frac{(F_{MAX})_H}{\gamma \frac{H}{L} \forall \cdot SHL3 \cdot SL1} \quad \ldots\ldots\ldots \quad (3.49)$$

Equations 3.42 through 3.45 are represented by the functional Equation 3.41. The terms SHL3 and SL1 are dimensionless representations of the dimensionless parameter ℓ/L for the height and length of the structure as shown in Equations 3.37 and 3.38. Equations 3.46 through 3.49 are represented by the functional equation

$$\frac{F}{\gamma \cdot \frac{H}{L} \cdot \forall \cdot \frac{\ell}{L}} = f_4 \, (d/L, S'/L) \quad \ldots\ldots \quad (3.50)$$

which can also be determined by dimensional analysis.

Equations 3.44 to 3.47 give theoretical values for dimensionless force which depend on the value of the coefficient of mass used. Figs. 5 and 6 show the theoretical dimensionless force plotted versus L/d for the indicated values of C_M and S'/d. Model studies

using Equations 3.42 and 3.43 or 3.48 and 3.49 will require that the ratio of S'/d be equal in model and prototype. In addition, geometric similarity requires that the ratios ℓ_1/L, ℓ_2/L, ℓ_3/L, H/L and d/L be the same for model and prototype. Changes in the width of the structure are reflected in the volume ($\forall$).

CHAPTER IV

EXPERIMENTAL EQUIPMENT AND PROCEDURE

Experimental Facility. - The experimentation described in this report was performed in the three dimensional wave facility of the Coastal and Ocean Engineering Division of Texas A&M University (Fig. 8). The wave basin is eighty feet long by thirty two feet wide, and has a maximum water depth of two feet. The test position of the models in the basin was such that no side wall effects could be felt by the models.

Waves were produced by the paddle-type wave generator shown in Fig. 7. Three paddles (each thirty in. high and ten ft. long) span the width of the basin and were adjusted to oscillate in phase. A seven horsepower variable speed motor rotated the main crankshaft which was connected to the paddles by three drive rods. The stroke of the paddles (and thus the wave height) was varied by changing the position of attachment of the drive rods to the crankshaft arms with respect to the center line of the shaft.

Peculiar to this wave generator is the fact that the smallest eccentricity of the drive rod arms from the center of the crankshaft is three inches. This made it impossible to get small wave heights when the wave period was small, as the faster the paddle oscillates the more water it moves (thus higher wave height). Translated into numbers, this means that for the smallest stroke a rotation period of 2.5 sec. produced a 0.1 ft. wave, whereas, a rotation period of

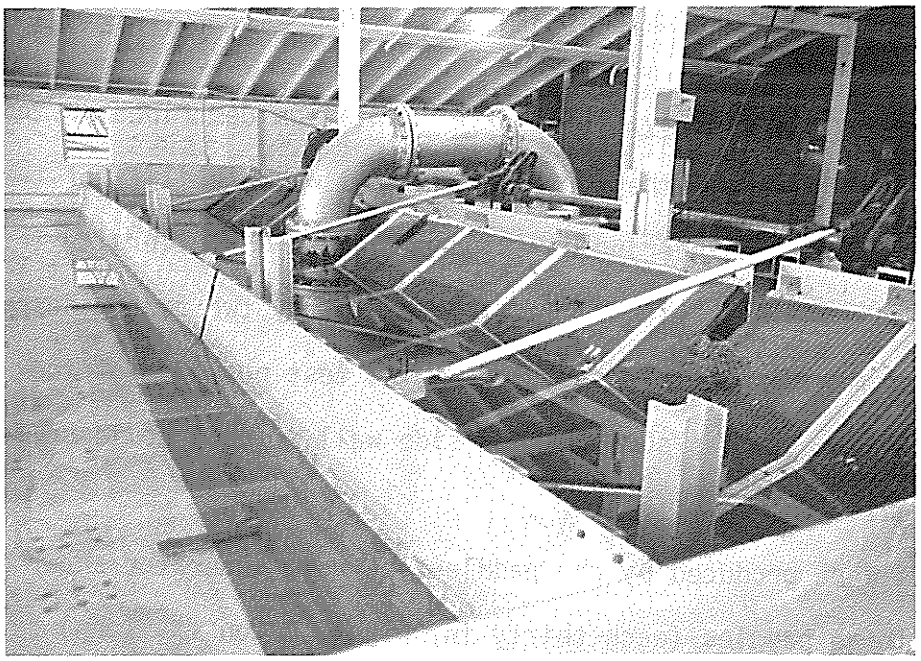

FIG. 7 - WAVE GENERATOR.

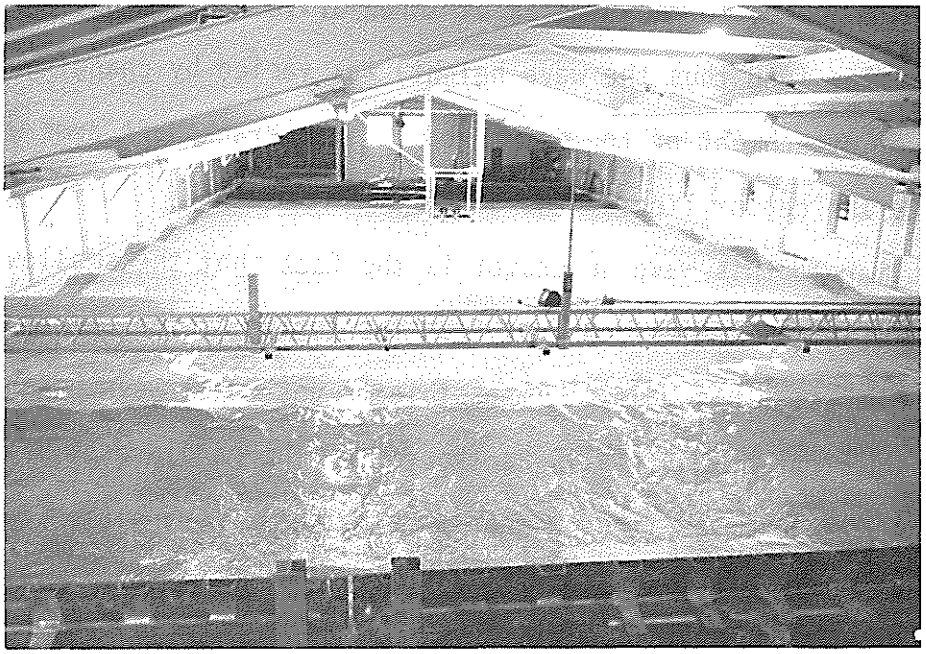

FIG. 8 - WAVE BASIN.

1.3 sec. produced a 0.3 ft. wave. The wave period was changed by varying the speed of the drive motor.

Located opposite the wave generator at the other end of the basin was a wave absorber (Fig. 8a). The wave absorber was an artificial beach consisting of a 30° impermeable slope covered with approximately four inches of a permeable fibrous material. Waves incident on the beach were dissipated by breaking and/or by absorption of runup by the permeable layers. Reflection tests indicated that more than 80% of the incident wave was dissipated by the wave absorber depending on the wave steepness.

Models. - The data used in this study have resulted from tests on four models. Each model was constructed of 3/8" plexiglass and was rectangular in shape with open bottom. The model designation and dimensions are given below.

Model 1 - ℓ_1 = .33 ft.; ℓ_2 = .66 ft.; ℓ_3 = .37 ft.
Model 2 ℓ_1 = .66 ft.; ℓ_2 = .66 ft.; ℓ_3 = .37 ft.
Model 3 ℓ_1 = .96 ft.; ℓ_2 = .66 ft.; ℓ_3 = .37 ft.
Model 4 ℓ_1 =1.29 ft.; ℓ_2 = .66 ft.; ℓ_3 = .37 ft.

The quantities ℓ_1 and ℓ_2 refer to the dimension of the model with respect to the direction of wave travel. The term ℓ_1 is the model dimension parallel to the direction of wave advances; ℓ_2 is the model dimension perpendicular to the direction of wave advance; and, ℓ_3 is always the model height. It can be noted that models 1, 2, 3 and 4, have the same height (ℓ_3) and width (ℓ_2), but the dimension of the

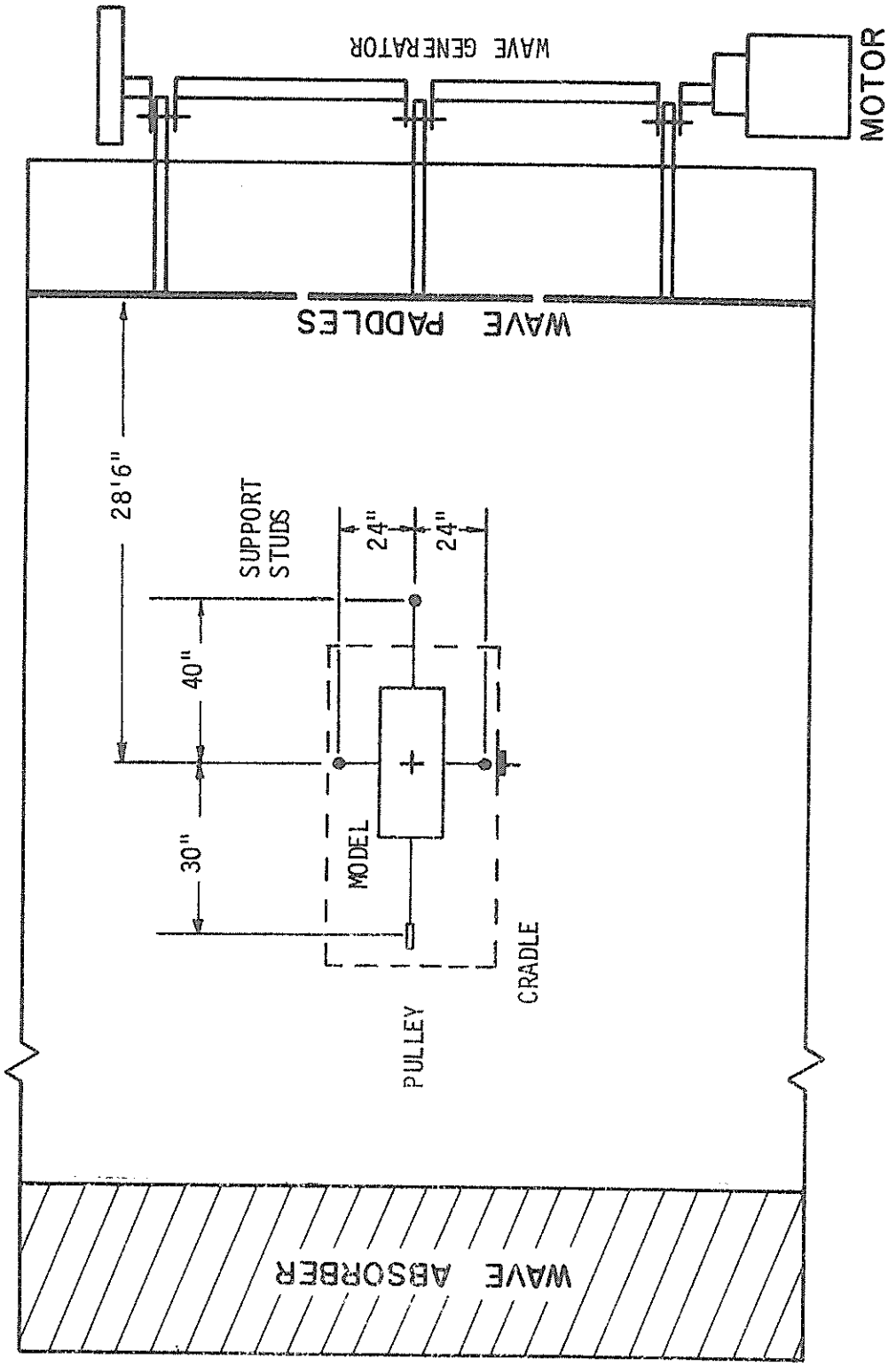

Fig. 8a - Position of Cradle and Model with respect to the Wave Basin.

model in the direction of wave travel (ℓ_1) varies.

By rotating models 3 and 4 ninety degrees and using model 2 we can form another model set.

Model 2 - ℓ_1 = .66 ft.; ℓ_2 = .66 ft.; ℓ_3 = .37 ft.

Model 5 - ℓ_1 = .66 ft.; ℓ_2 = .96 ft.; ℓ_3 = .37 ft.

Model 6 - ℓ_1 = .66 ft.; ℓ_2 =1.29 ft.; ℓ_3 = .37 ft.

Models 2, 5 and 6 have the same height (ℓ_3) and length in the direction of wave advance (ℓ_1), but the widths of the models vary. Fig. 9 shows the models, their dimensions, and their relationship to the advancing wave.

Experimental data for models 1 and 2 was collected by Herbich and Shank (6) and made available to the author by Dr. Herbich. The data for models 3, 4, 5 and 6 was taken by the author in the experimental program described in this thesis.

Experimental Apparatus. - To facilitate the positioning of the model in the wave basin a cradle was suspended from the ceiling of the laboratory as shown in Fig. 11. The cradle supported five force transducers and a wave gauge.

Four holes (1.5 in. dia.) were cut in a 30 in. by 24 in. piece of plywood which was fitted into the base of the cradle. The holes were cut so that when the front edge of the board and the front edge of the cradle were adjacent and parallel the holes were over the four corners of the model test position. The four vertical force transducers were placed over these holes. The fifth transducer used to

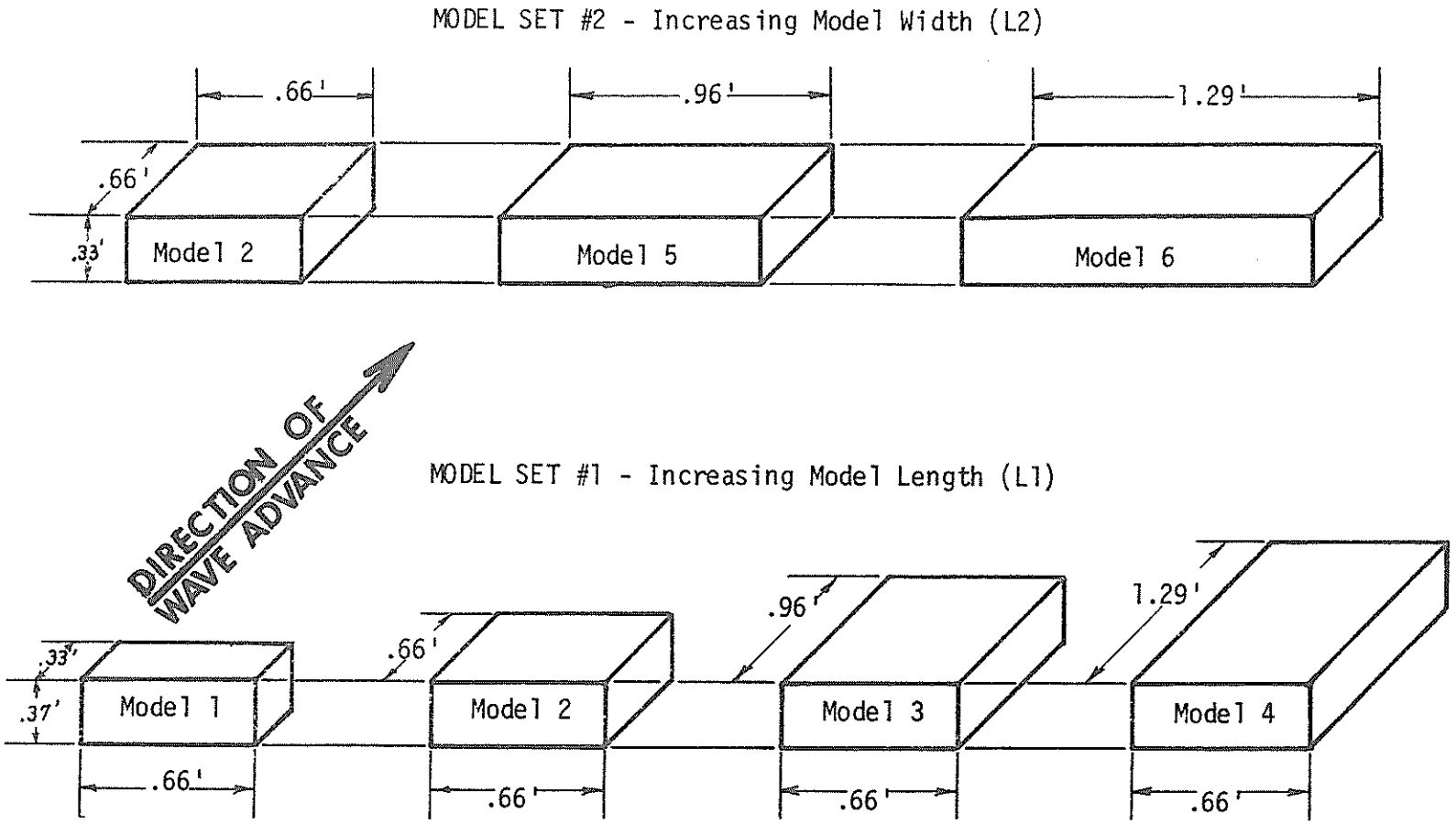

Fig. 9 - Model description and Position with respect to the Advancing Waves.

measure the horizontal force was located on a second board at the rear of the cradle as shown in Fig. 10.

The force transducers consisted of two strain gauges cemented to an aluminum cantilever beam as shown in Fig. 12. A load applied to the end of the cantilever produced a change in the resistance of the strain gauges by compressing or lengthening the gauge wires. This resistance change produced a small varying voltage which, for small deflections, was proportional to the load. The strain gauge voltage was recorded on either of two electronic recorders used. Four force transducers were used to measure the vertical loading on the model and a four-channel Sanborn carrier-preamplifier recorder (model 150) was used to record the loading. Only one force transducer was necessary to measure horizontal force and this was recorded on a Hewlett-Packard dual-channel carrier pre-amplifier recorder (model 321). Recorder outputs are shown in Figs. 13 and 14. Basic sensitivity of the force transducers was 5.0 grams per millimeter of pen deflection.

Because of space requirements the electronic recording units had to be placed at some distance from the test position. The leads from the force transducers were connected to a terminal strip on the transducer board shown in Fig. 10. Five lengths of two conductor shielded wire were run from the terminal strip to the Sanborn and Hewlett-Packard recorders shown in Fig. 15.

The models were supported at each corner by fine stainless steel connected to the four vertical force transducers as shown in Fig. 16 and 17. Clearance between the bottom of the model and the basin

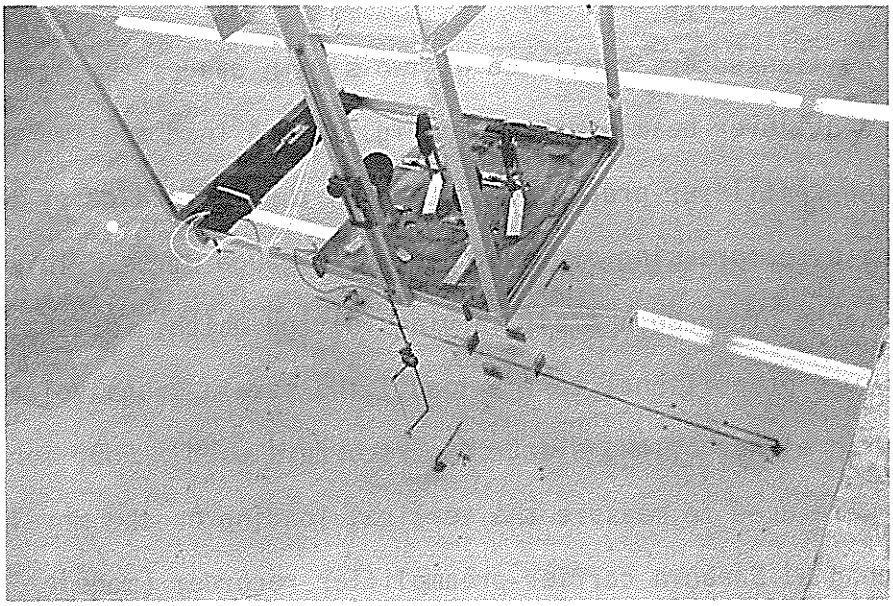

Fig. 10 - Cradle, wave gauge, and force transducer relationship.

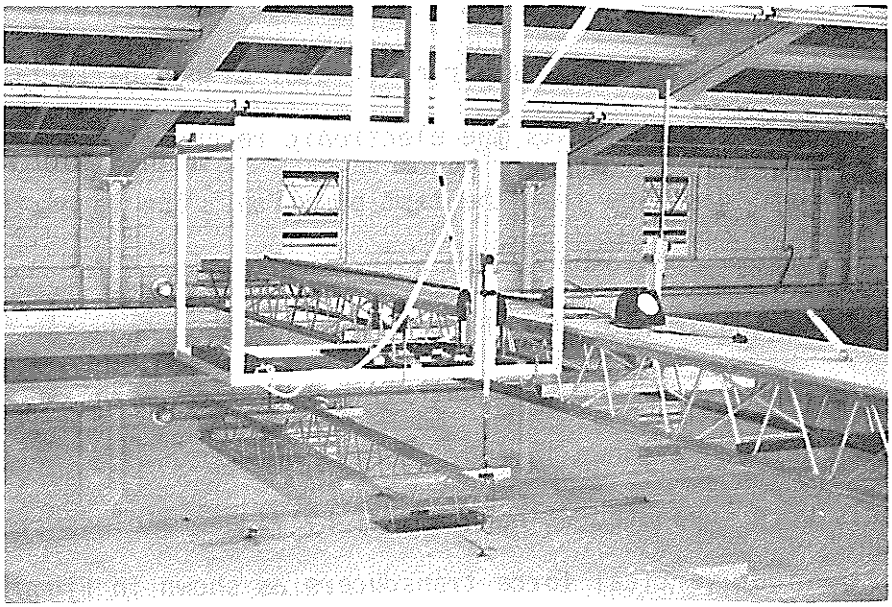

Fig. 11 - Overall view of model test position.

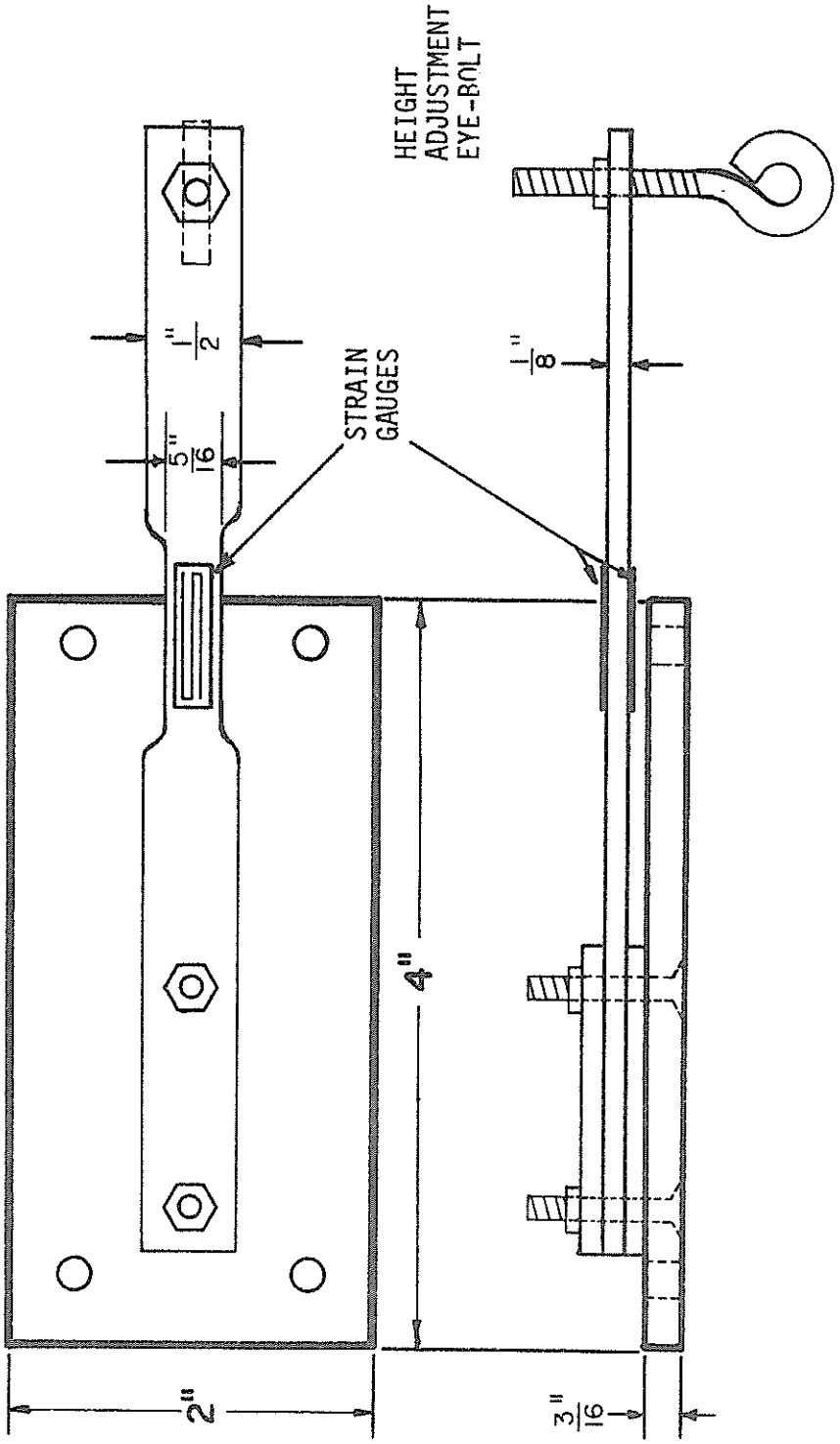

Fig. 12 - Force Transducer.

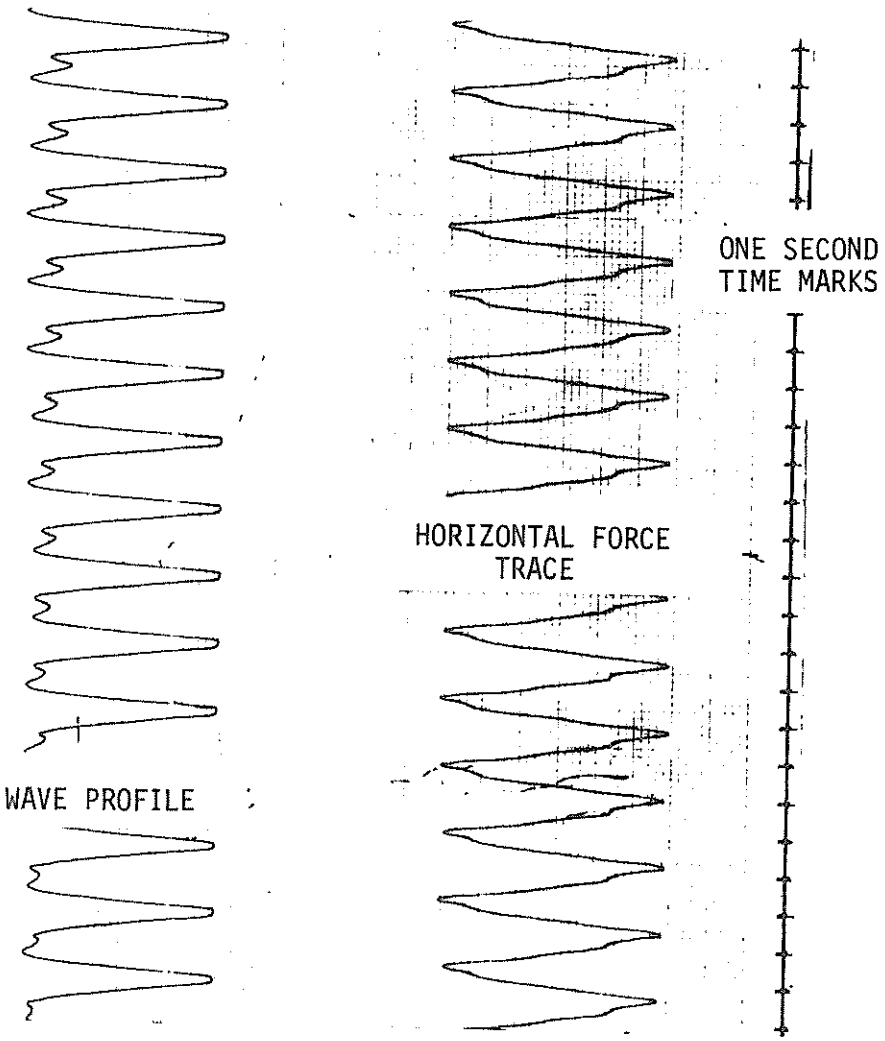

FIG. 13 - SAMPLE WAVE PROFILE - HORIZONTAL FORCE RECORD

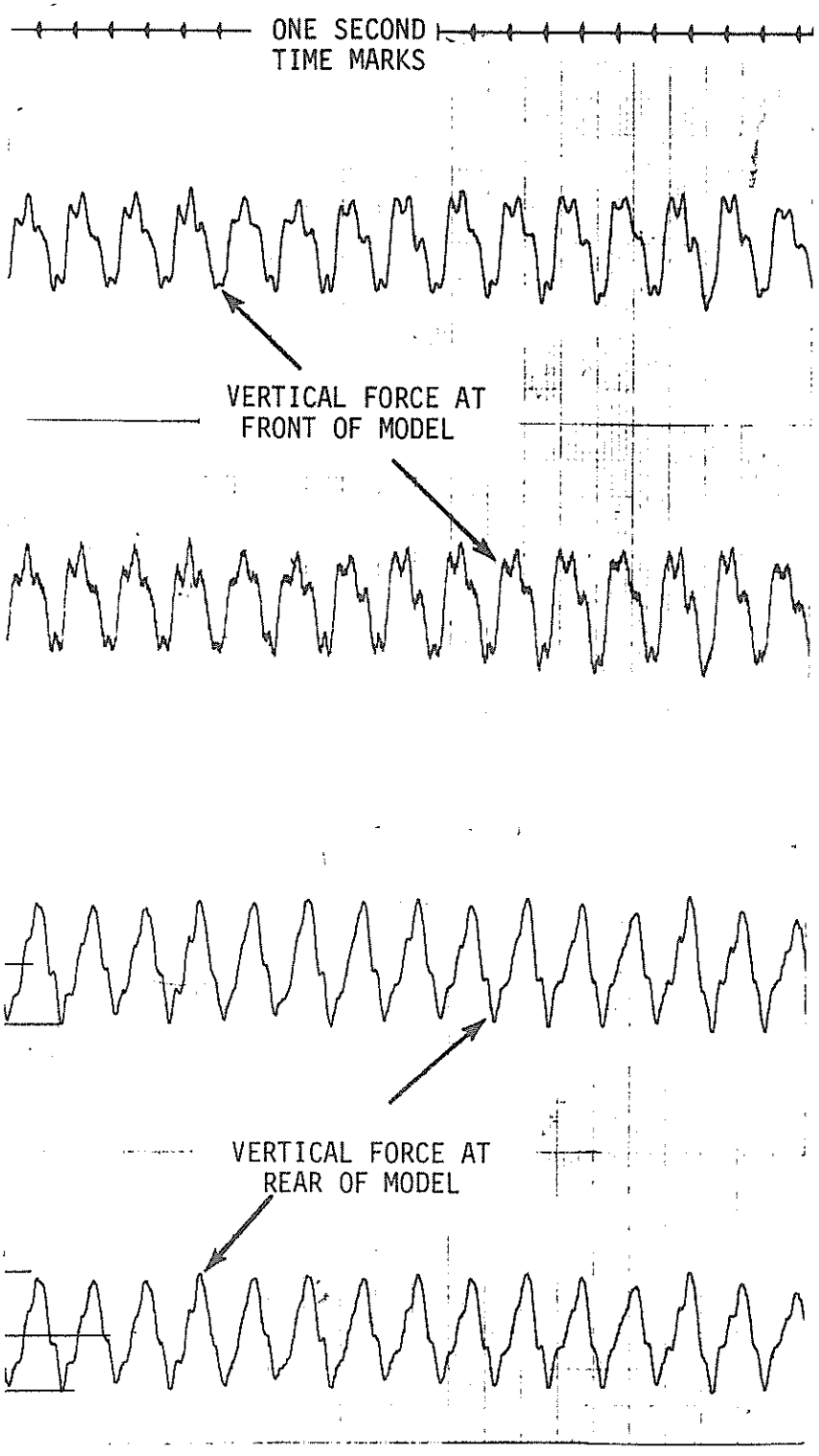

FIG. 14 - SAMPLE VERTICAL WAVE FORCE RECORD

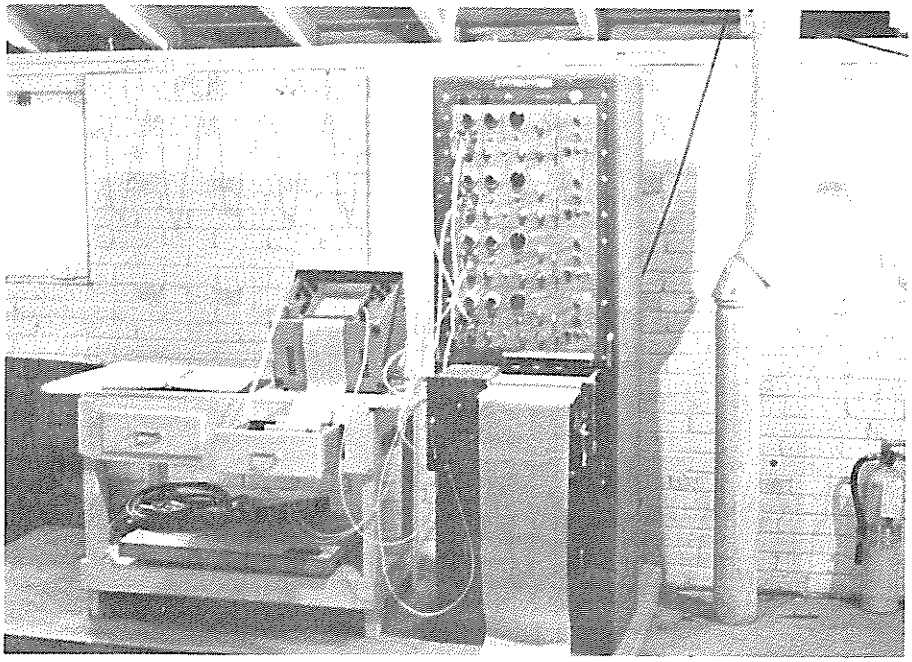

Fig. 15 - Electronic recording equipment.

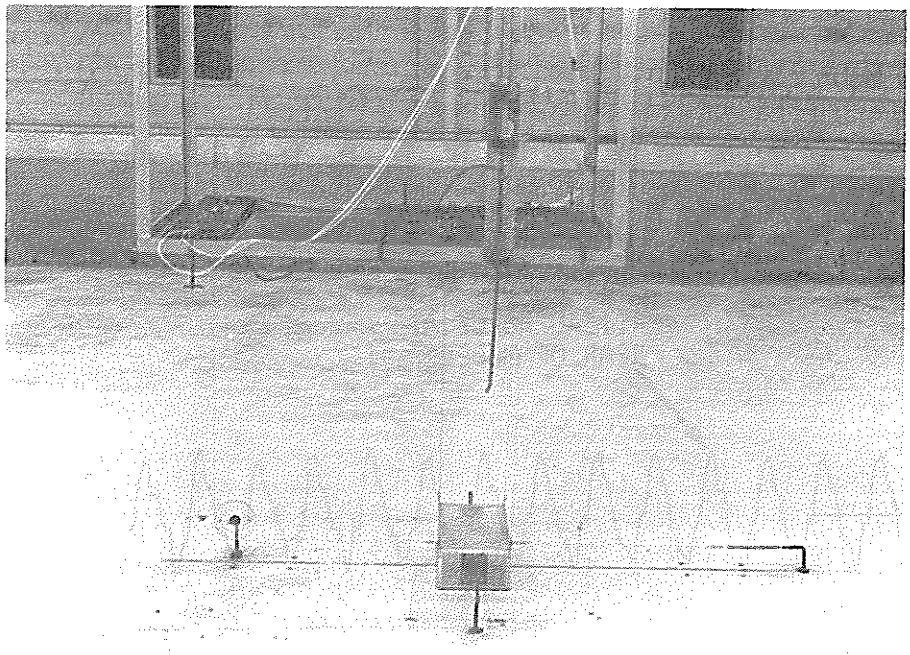

Fig. 16 - Test set-up with wave basin empty.

floor was kept at 0.25" by adjusting the threaded eye-bolts on the force transducer. Since the force on the models in the vertical direction oscillates up and down it was necessary to weight the models to keep the load-carrying wires from going slack when the force was directed upward.

The model was constrained from horizontal motion in the direction perpendicular to the wave crest line by fine stainless steel wires which also transmitted the force to the horizontal force transducer as shown in Fig. 17. The wire leads ran down from the force transducer to a five inch diameter minimum friction pulley where it was diverted 90° and then fastened to the center of the rear face of the model. From the center of the front face another lead ran to a tensioning spring fastened to a stud fixed to the basin floor. The spring kept sufficient tension in the leads at all times. Not shown in Fig. 17 but present in the experimental set up (Fig. 16) were lateral constraints consisting of leader, spring, and stud on each side of the model. These reduced the change of lateral oscillations of the model. The pulley and the three support studs were placed sufficiently far from the model to keep the flow conditions at the model as undisturbed as possible (Fig. 8a).

In the experimental setup described above, the model was in a fixed, rigid position. This was necessary to keep the disturbance of the flow due to model movement to a minimum. Tests showed that a 500 gram load produced a model deflection of less than .1 inch. This flexibility of the system was required, however, for the force

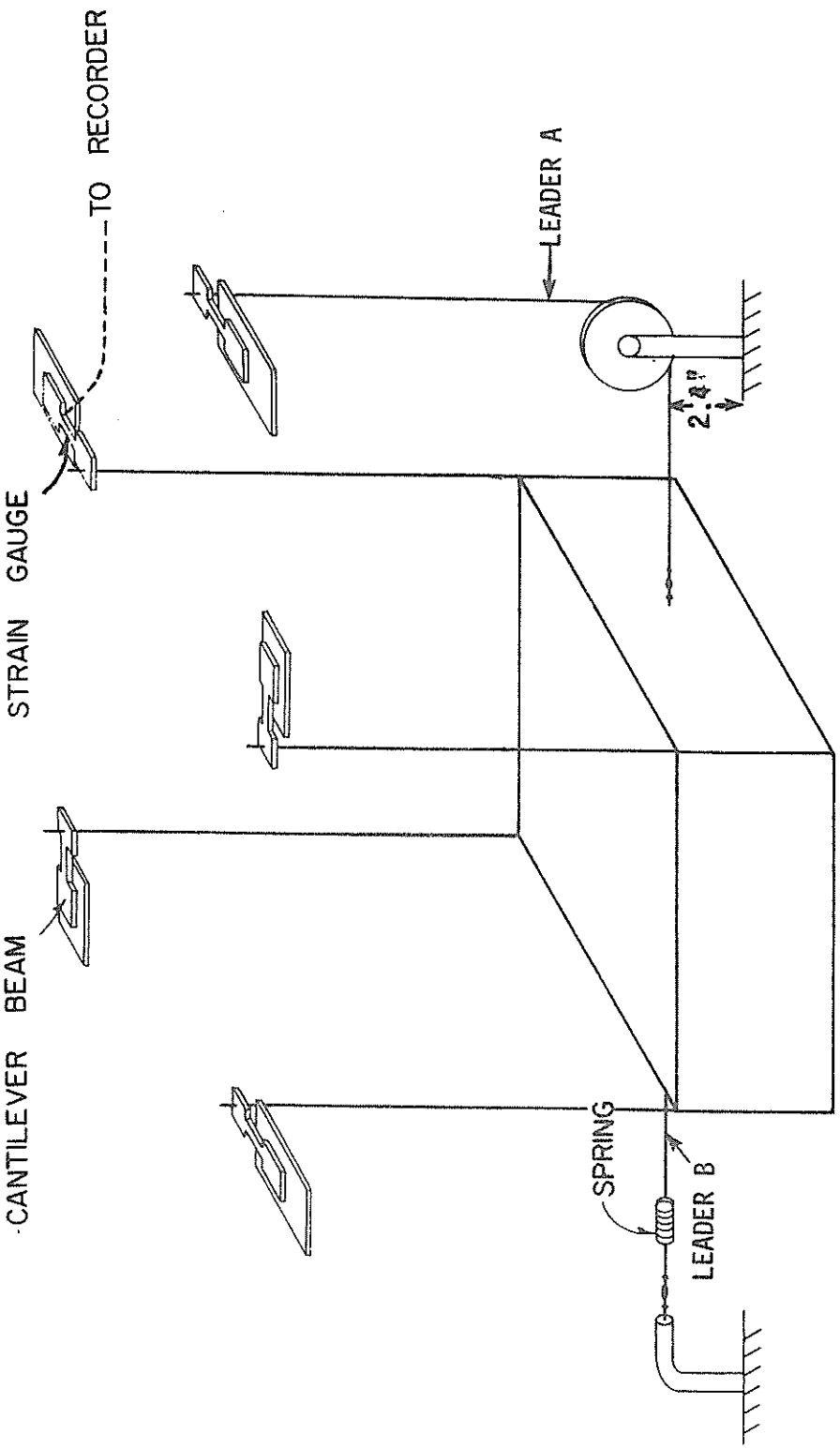

FIG. 17 SCHEMATIC DIAGRAM OF MODEL AND LOAD CELL

transducers to detect the wave forces on the model and is assumed to have a negligable effect on the flow about the model.

Calibration is the procedure used to translate recorder pen deflection into values of the physical quantity of interest (i.e. force). The procedure used to calibrate the force transducers is given in Appendix IV.

The independence of the horizontal and vertical force transducers was tested by loading the system in either of the two directions and noting pen deflection (indicating force) in the other direction. These tests showed that the horizontal and vertical force transducers were independent. Since the vertical force on the model was the sum of four force transducer readings, tests were performed to determine the effect each vertical transducer had on the other. These tests showed that loading one transducer separately produced a reaction in the other three transducers. However, if the loading was symmetrical about the center of the model the four transducers acted as though they were independent. Under a wave loading the forces are symmetrical about the model axis parallel to the direction of wave advance. Thus, if the model were properly positioned, and each transducer carried one quarter of the static weight of the model, the four transducers could be considered independent.

Each model was positioned at approximately the center of the wave basin. Appendix III gives the detailed description of the procedure used to insure that each model was constrained in the same position with respect to the advancing waves. With the model properly

aligned, the vertical and horizontal forces were transmitted to the proper force transducer.

Continuous time-histories of the water surface elevation at the center of the model were taken using a capacitance-type wave gauge. The output of the gauge was recorded on the Hewlett-Packard dual channel carrier preamplifier recorder (Fig. 15). The amplitude of the recorder trace was proportional to the amplitude of the wave and was easily determined after calibration.

Calibration of the wave gauge is described in Appendix III. The basic sensitivity of the wave gauge was 0.1 ft. per centimeter of pen deflection. Wave gauge calibration was performed at the beginning and end of each set of runs. The wave heights given by the electronic wave gauge compared favorably with visual observation on a wave staff located near the gauge.

The wave period was determined by dividing by ten the time it took for ten complete rotations of the crankshaft of the wave generator. A trip switch on the wave generator flashed a light bulb which signaled a complete rotation. This average wave period for ten waves compared favorably with the wave period determined from the recorder trace by measuring the distance between two corresponding points in a wave cycle and dividing by the rate of recorder paper feed which is an accurately known constant (the Sanborn and Hewlett-Packard had common paper speeds of 1, 5, and 100 mm/sec. Five millimeters per second was chosen as most feasible). A mobile instrument carriage shown in Fig. 11, provided access to the model in the center of the

tank.

Experimental Procedure. - After positioning the model according to the procedure detailed in Appendix IV the wave basin was filled to the test water depth of 18.0 or 24.0 inches. The horizontal force transducer and the four vertical force transducers were then calibrated, and then a test run was performed. The lab data for a run included the run number, water depth, the force and water elevation time-histories, the wave height visually observed on the wave staff, the average of ten oscillations of the wave generator, the wave generator stroke, and motor speed setting.

Due to frequent malfunctions of the Sanborn recording equipment (oscillations of the pen zero, changes in basic sensitivity, and complete failure were observed) it was deemed necessary to check the calibration of the four vertical force transducers after each run. Recalibration was performed if necessary and the next test was then run.

At the end of a set of test runs (a test set usually consisted of 12 to 20 wave runs for a given model position and water depth) the wave gauge and horizontal force transducer calibration was checked. The Hewlett-Packard recorder functioned quite well with only minor variations noted.

As previously mentioned, two recorders were used to record the time-history of the forces and water surface elevation. To correlate the two outputs, a synchronized timing mark was placed on the record during each test run.

CHAPTER V

DATA ANALYSIS

Data from the laboratory tests on the models was in the form of recorder output as shown in Figs. 13 and 14. The center of each recorder trace corresponds to the pen position for zero force or zero water surface elevation (SWL). The magnitude of the forces and the wave height were determined using the calibration curves obtained for each transducer.

The values for the forces and wave height were the average values determined from a continuous group of 6-8 waves. Since the wave generator speed had to be increased from zero to the test speed for each run, the first waves were usually of variable height and period. After a short period of time, transverse water surface oscillations were set up in the basin causing irregular wave records. The waves from which the experimental data were obtained were from the section of the wave record after the wave generator had settled down and before the transverse oscillations set in.

For the oscillatory horizontal force, the maximum force in the direction of wave advance (FHW) was evaluated separately from the maximum force in the direction opposed to wave advance (FHO). The total vertical force is the sum of the maximum force readings of the four force transducers supporting the model. The vertical force upward (FVU) was measured separately from the downward vertical force (FVD).

The wave height was measured as the total distance between two extreme water surface elevations on the recorder trace. The wave height and wave period determined from the water surface profile compared well with the measured wave height and the timed period of the wave generator observed during the experiments.

The phase angles between the wave crest and the forces on the model were determined for some of the data. The phase angles between the wave crest and the two horizontal forces were easily determined as both records were on the same recorder output. However, the phase angles of the maximum vertical forces were more difficult to determine in that the wave trace was separate from the vertical force traces. To correlate the two records in time, a timing mark was simultaneously placed on each record. Determining the phase angle was also complicated by the fact that the only feasible recorder paper feed common to both recorders was 5 mm/sec. This tended to jam the profiles together for the shorter period wave making phase angle interpretation very difficult. Only a random sampling of phase angles was taken to aid in evaluation of the data.

To reduce the raw data once it had been converted to numerical values, the author made use of the IBM 360/65 computer in Texas A&M University's Data Processing Center. The fortran computer program given in Appendix V calculated the wave length for each set of data, the dimensionless force and other dimensionless terms used in evaluating the experiments; and plotted the dimensionless graphs used in this thesis. Figs. 30 and 31 show the computer results for the

measured data. The plotting was done in conjunction with the Data Processing Center's Calcomp 565 Plotter and Industrial Engineering's Gerber Plotter.

CHAPTER VI

PRESENTATION AND DISCUSSION OF RESULTS

The primary objective of this thesis was to study the forces caused by oscillatory waves on large submerged objects and to present the information regarding such forces in a suitable dimensionless form. To accomplish this, a series of model tests were performed in which the wave parameters and the wave forces were measured. The resulting experimental data was then reduced to dimensionless form.

The dimensionless force term used in this study is given by either Equation 3.42 or 3.43 and is presented here without the subscripts indicating direction.

$$F_{DIM} = \frac{F_{MAX}}{\gamma \cdot \frac{H}{d} \cdot \forall \cdot SHL3 \cdot SL1} \qquad \ldots\ldots\ldots (6.1)$$

where

F_{DIM} = dimensionless force term

F_{MAX} = measured maximum force

γ = unit weight of water

H = wave height

d = water depth

$\forall$ = object volume

and SHL3, SL1 are defined by equations 3.37 and 3.38 respectively.

In determining the theoretical dimensionless force, the equations for the maximum horizontal and vertical forces were derived assuming that the force was entirely inertial. In Airy wave theory, if the force is entirely inertial, it is proportional to wave height. The theoretical dimensionless force terms derived by combining Equations 3.35 and 3.42, and Equations 3.36 and 3.43 are therefore independent of the wave height as indicated by Equations 3.44 and 3.45. Equations 3.44 and 3.45 are theoretical equations for the above dimensionless force for the horizontal and vertical directions respectively, and are plotted versus L/d in Figs. 5 and 6. Note that these curves depend on the value of the coefficient of mass.

The formation of model sets 1 and 2 in Chapter IV was done in order to examine the effect of changes in model size on the dimensionless force. The comparison of the dimensionless force between all the models in a set could not be accomplished due to the difference in wave periods used by the author (for models 3, 4, 5, and 6) and those used by Herbich and Shank (for models 1 and 2). The range of wave periods for the Herbich and Shank data was 0.71 sec. to 1.50 sec. The three dimensional wave facility used by the author had a minimum period of 1.35 sec. Since the water depths were the same in all experiments, the relative depth ratios differed. It was therefore only possible to compare the results for models 1 and 2 and for models 3 and 4 in model set 1, and for models 5 and 6 in model set 2.

The horizontal force on the model was measured in the direction of wave advance (FHW) and in the direction opposed to wave advance (FHO). The results indicate that these forces were approximately equal with FHW only slightly larger. In the vertical, the upward force (FVU) and the downward force (FVD) were measured and were approximately equal for values of relative depth less than 10.0. For values of the relative depth greater than 10.0, the upward force was usually somewhat less than the downward directed force. To simplify the discussion of the results, only the data for the horizontal force in the direction of wave advance and the downward directed vertical force will be presented. The data presented will be in dimensionless form. FDIMHW is the dimensionless representation of FHW, and FDIMVD is the dimensionless representation for FVD. FDIMHW and FDIMVD are determined by equation 6.1 with the corresponding maximum measured FHW and FVD substituted for F_{MAX}.

The results of the model tests are presented in graphs of dimensionless force (FDIM) versus relative depth (L/d). This form of graph is suggested by Equations 3.44 and 3.45. The dimensionless force was also plotted versus the relative size parameter (Ll/L). This type of graph was similar to the graphs of dimensionless force versus relative depth. However, they did not account for changes in water depth as the flow conditions at the model depend partially on the relative depth (L/d).

The results for models 1 and 2 are presented in Figs. 18 and 20 for the horizontal force and in Figs. 19 and 21 for the vertical force.

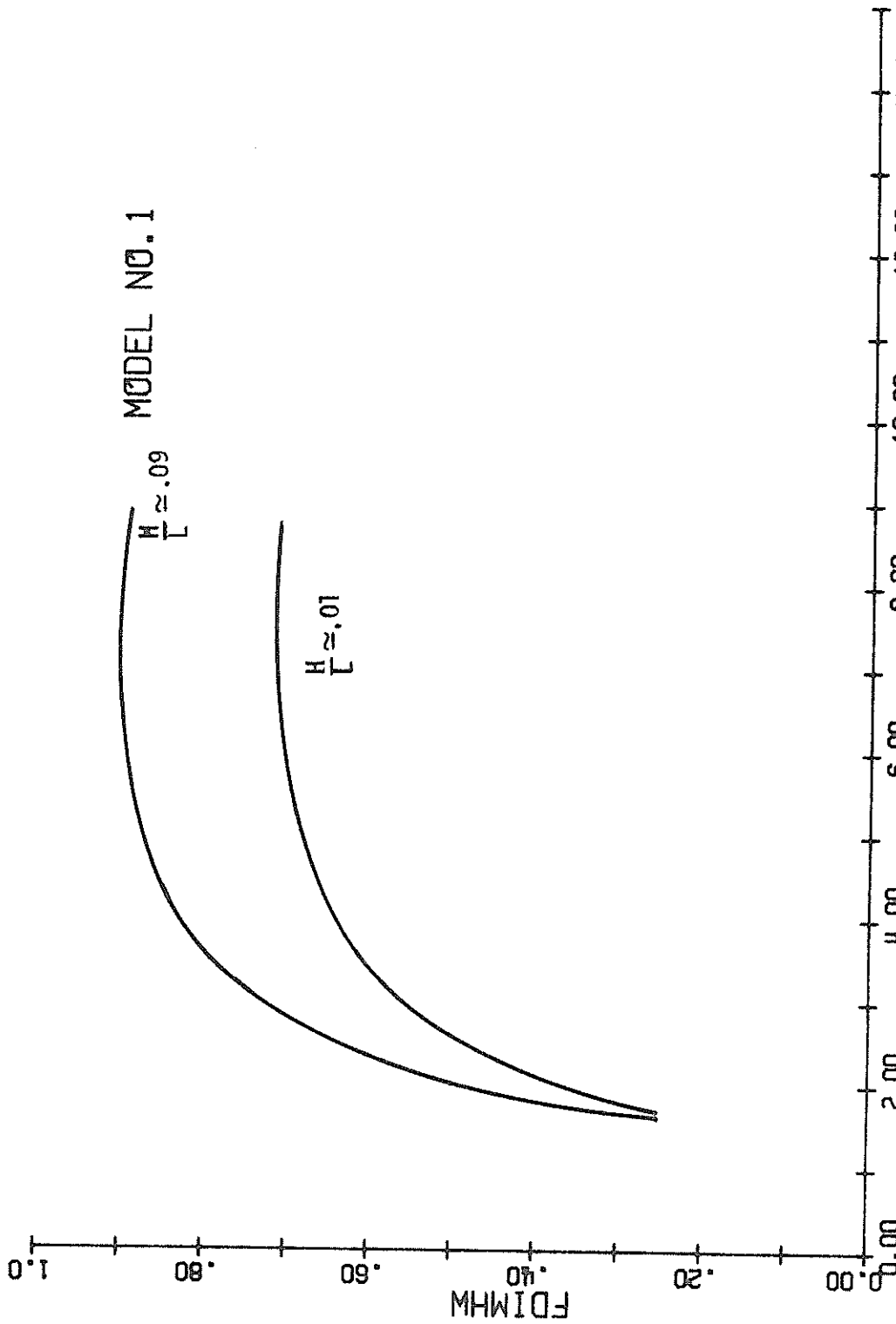

FIG. 18 HORIZONTAL DIMENSIONLESS FORCE VS. RELATIVE DEPTH

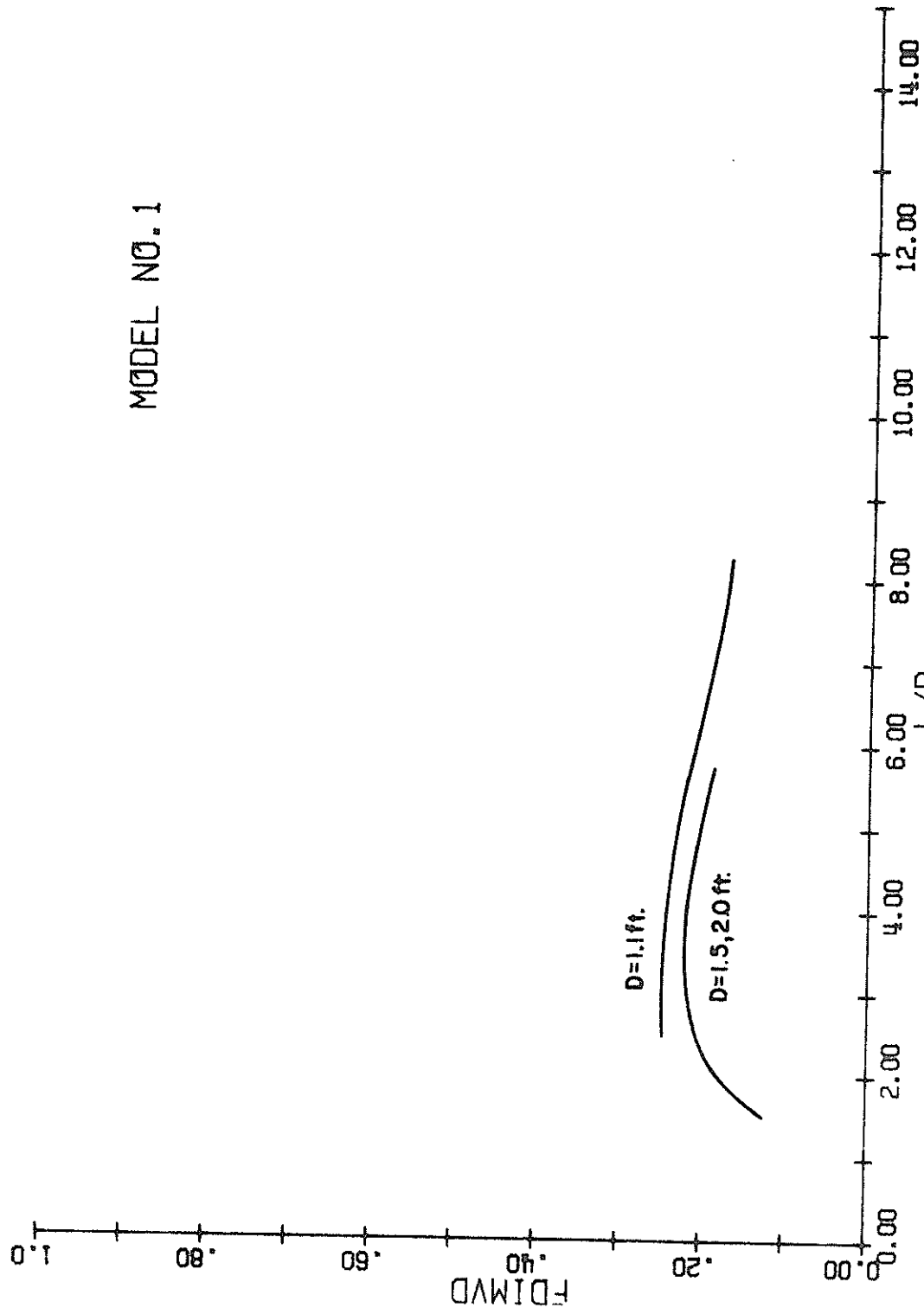

FIG. 19 VERTICAL DIMENSIONLESS FORCE VS. RELATIVE DEPTH

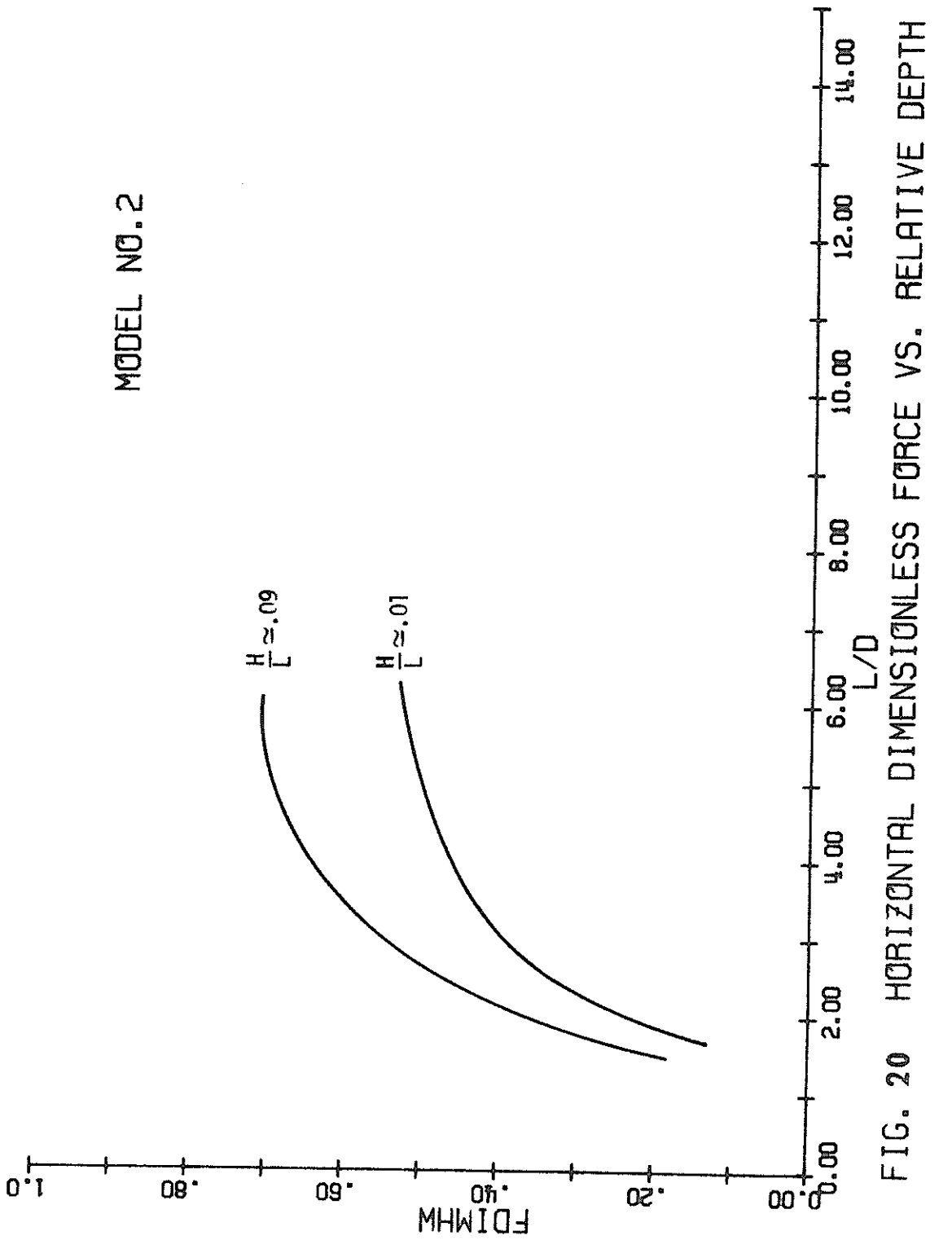

FIG. 20 HORIZONTAL DIMENSIONLESS FORCE VS. RELATIVE DEPTH

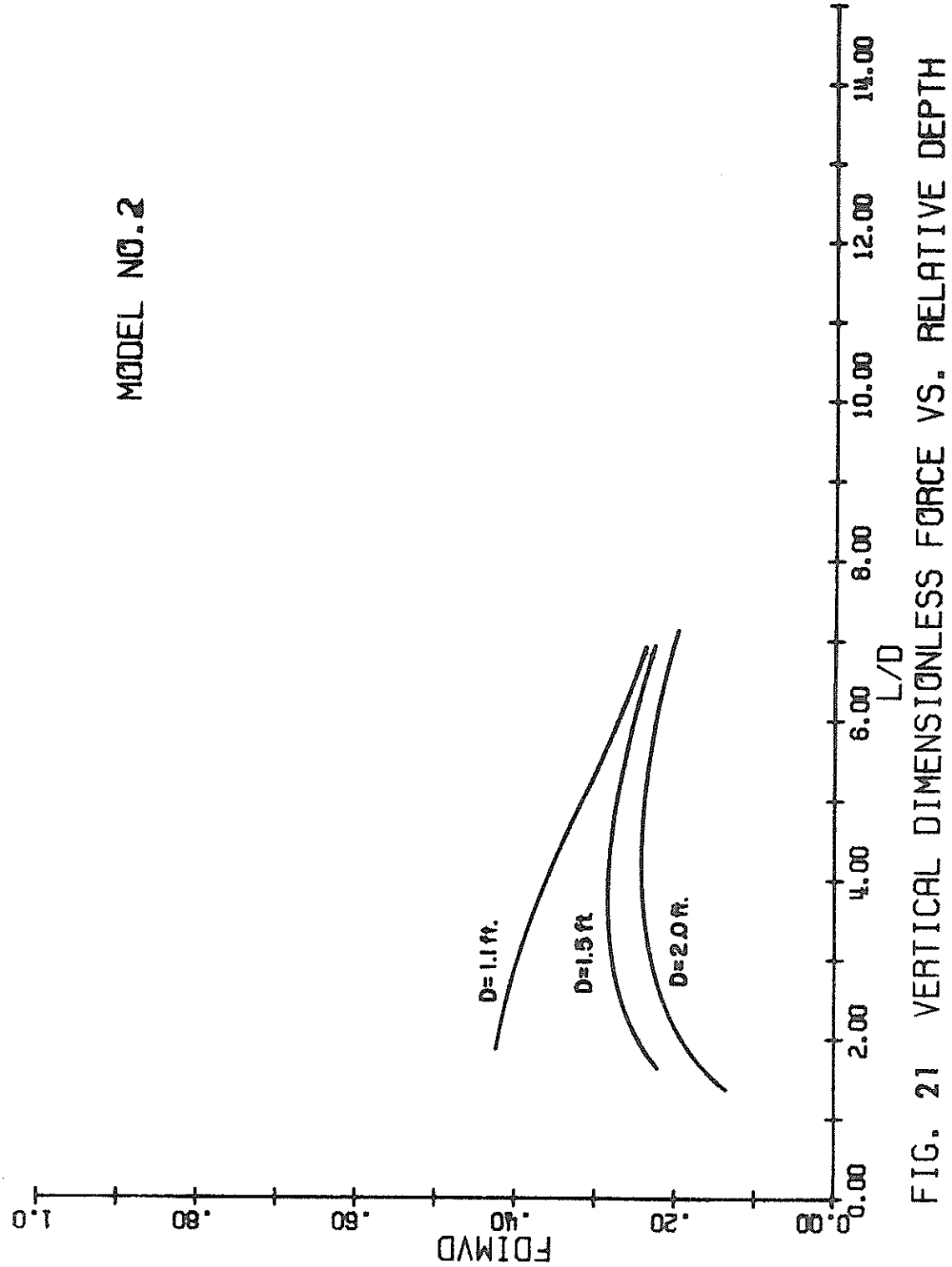

FIG. 21 VERTICAL DIMENSIONLESS FORCE VS. RELATIVE DEPTH

These graphs are for all three depths of water in which the two models were tested (d = 1.1 ft., 1.5 ft., 2.0 ft.). The data indicates that the horizontal dimensionless force depends on the wave steepness. However, the data was such that it was difficult to draw, with any confidence, lines of constant wave steepness. The upper and lower lines in Figs. 18 and 20 are drawn for the largest and smallest dimensionless force measured at a given value of relative depth. The large values of wave steepness ($H/L \simeq .08, .09$) fell on or just below the upper line on each graph. Low wave steepness values ($H/L \simeq .009, .01, .02$) fell above the lower line. The range of wave steepness values for each L/d value for models 1 and 2 was .009 to .09.

Figs. 18 and 20 indicate that the effect of wave steepness on the horizontal dimensionless force increases with increasing relative depth (L/d) for the range of relative depth shown. Equations 3.44 and 3.45 which were derived assuming that the force was entirely inertial indicates that the dimensionless force is not dependent on wave steepness. To account for this discrepancy, we can examine the velocity induced (drag) force. Figs. 22 and 23 show the horizontal component of acceleration and velocity (Eqs. 3.11 and 3.10) plotted versus relative depth for the indicated depths of submergence ($\frac{z}{d}$) and a wave height of 0.5 ft. The horizontal component of acceleration (Fig. 22), which gives rise to the inertial force on the model, increases from zero to a maximum value at $L/d \simeq 5.0$ for large negative depths of submergence. The horizontal velocity component (Fig. 23)

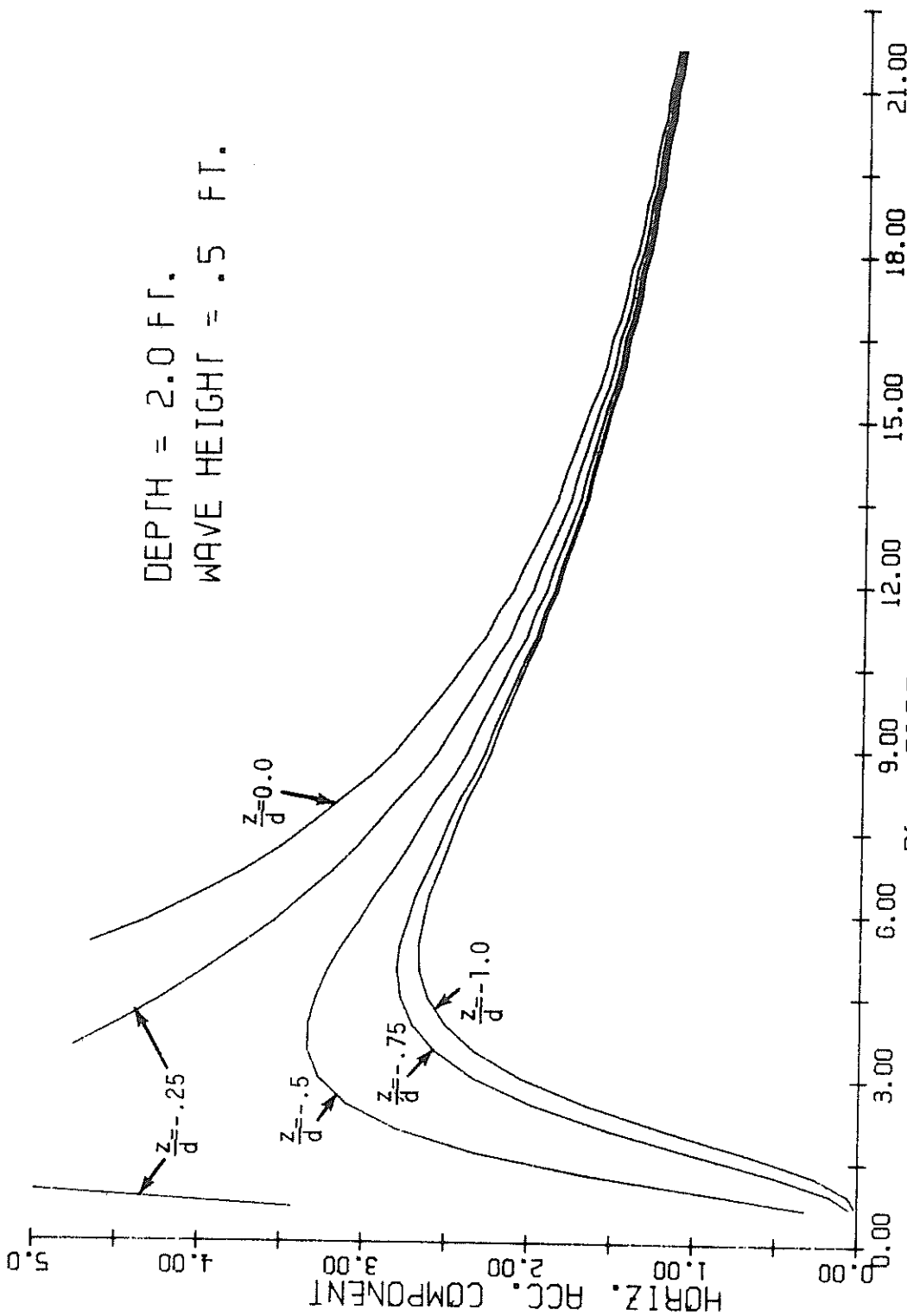

FIG. 22 HORIZONTAL PARTICLE ACCELERATION VS. RELATIVE DEPTH

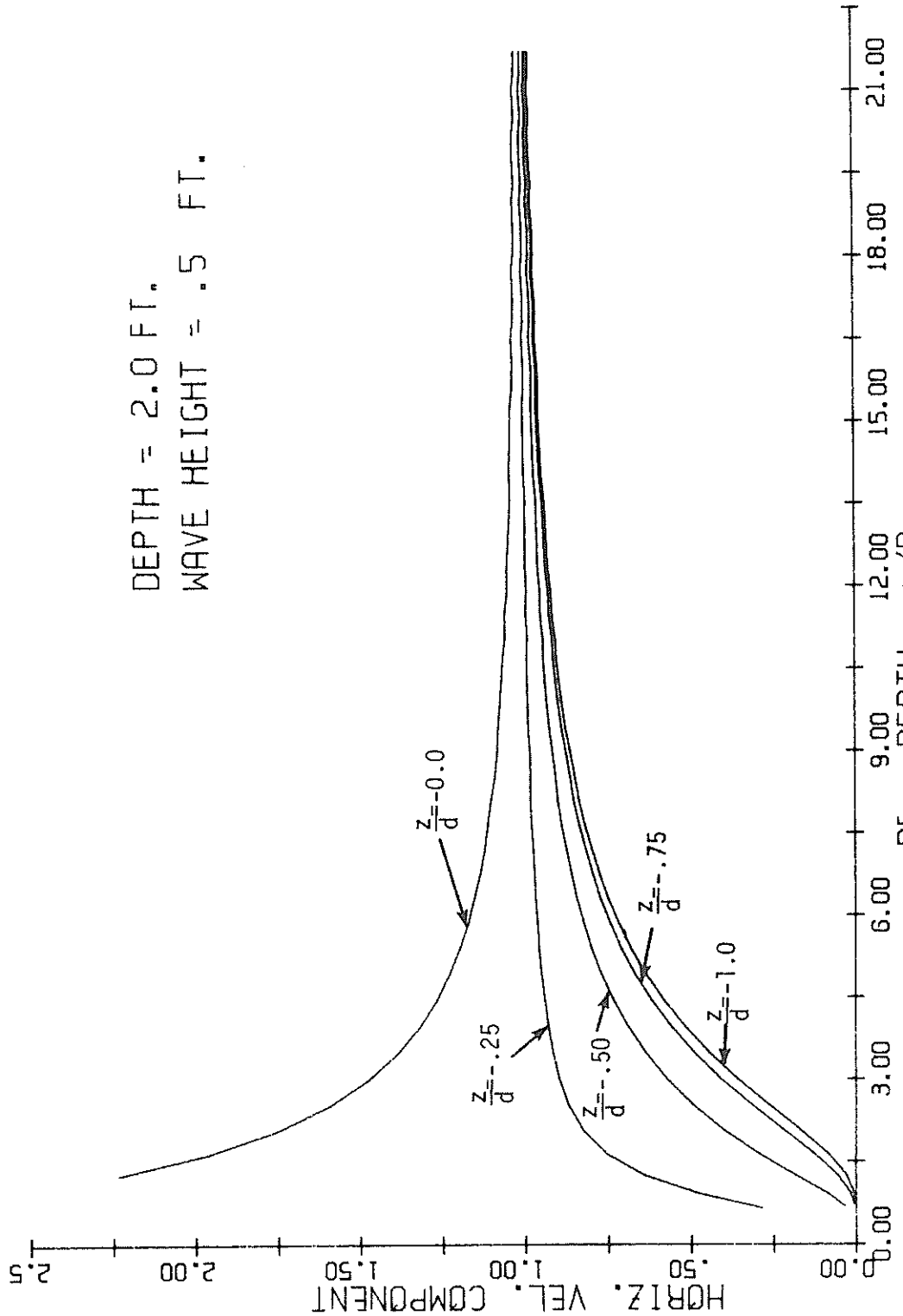

FIG. 23 HORIZONTAL PARTICLE VELOCITY VS. RELATIVE DEPTH

increases at a slower rate but soon contributes to the total force on the model as the "drag" force. Since the drag force is proportional to the velocity squared and the velocity is proportional to the wave height, then as the wave height increases the contribution of the drag force to the total force can become significant.

Examination of the phase angles at which the maximum force occurs should indicate the existence of the velocity induced force on the model. The maximum horizontal velocity and acceleration components are 90° out of phase, the maximum horizontal acceleration occuring under the crest and trough of the wave. However, for these two models, the determination of the phase angles could not be accomplished for the reasons stated in Chapter V.

To observe the effect of increasing wave height on the horizontal dimensionless force, the relative displacement parameter (H/L1) was plotted versus the horizontal dimensionless force (Fig. 24). For a given model and depth of water the dimensionless force can be written as

$$F_{DIM} = \frac{F_{MAX}}{H \cdot SHL3 \cdot SL1 \cdot constant}$$

where

$$constant = \gamma \frac{\forall}{d}$$

For a given relative depth, if equation 3.35 gives the maximum force on the model, then lines of constant relative depth on the

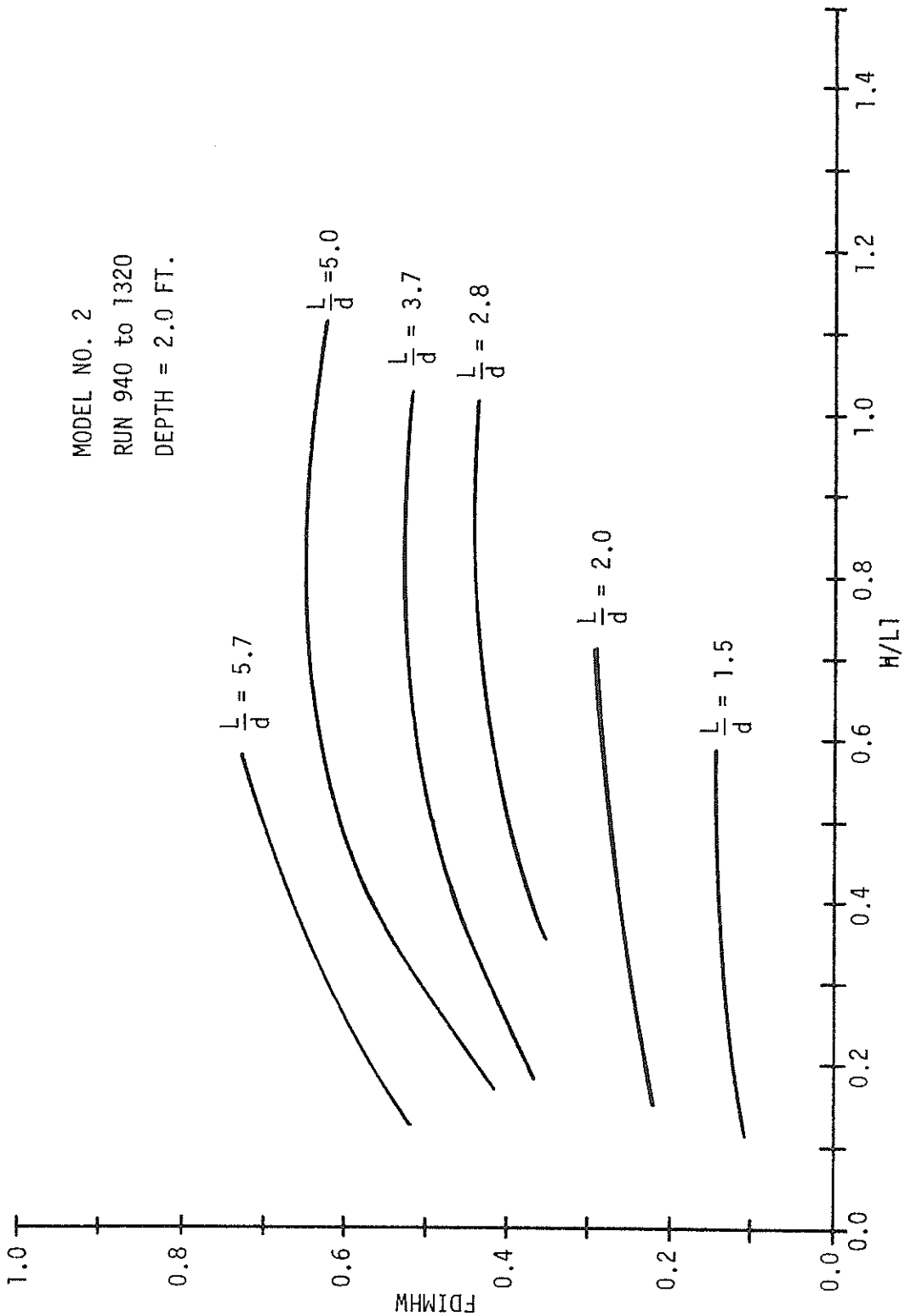

FIG. 24 - HORIZONTAL DIMENSIONLESS FORCE VS. RELATIVE DISPLACEMENT PARAMETER.

graph of FDIMHW versus H/L1 should be horizontal lines. Fig. 24 is drawn for model 2 in 1.5 ft. of water. The lines of constant relative depth are not horizontal, but slope slightly upward indicating that the horizontal dimensionless force increases with increasing wave height. For the larger values of relative depth the dimensionless force begins to decrease with increasing wave height.

We may discuss Fig. 24 in terms of increasing wave height, because the data presented there is for only one model and L1 is constant. However, the shape of the curves in Fig. 24 can be looked at from the standpoint of the relative displacement of the fluid particles. Sarpkaya and Garrison (33) showed that for small values of relative displacement (H/L1), the coefficients of mass and drag are related. As the relative displacement increased from zero, the coefficient of mass decreased from its potential flow value. For a given relative depth (L/d), the amplitude of the fluid particle displacement increases with increasing wave height, and the decrease in dimensionless force with increasing relative displacement (H/L1) can be attributed to a decrease in the coefficient of mass.

Sarpkaya and Garrison (33) also showed that as the coefficient of mass decreased, the coefficient of drag increased at small values of relative displacement. Thus the contribution of the drag force to the total force increased with increasing wave height. To determine the importance of the drag force, the phase angle should be examined. Experiments should be performed which accurately

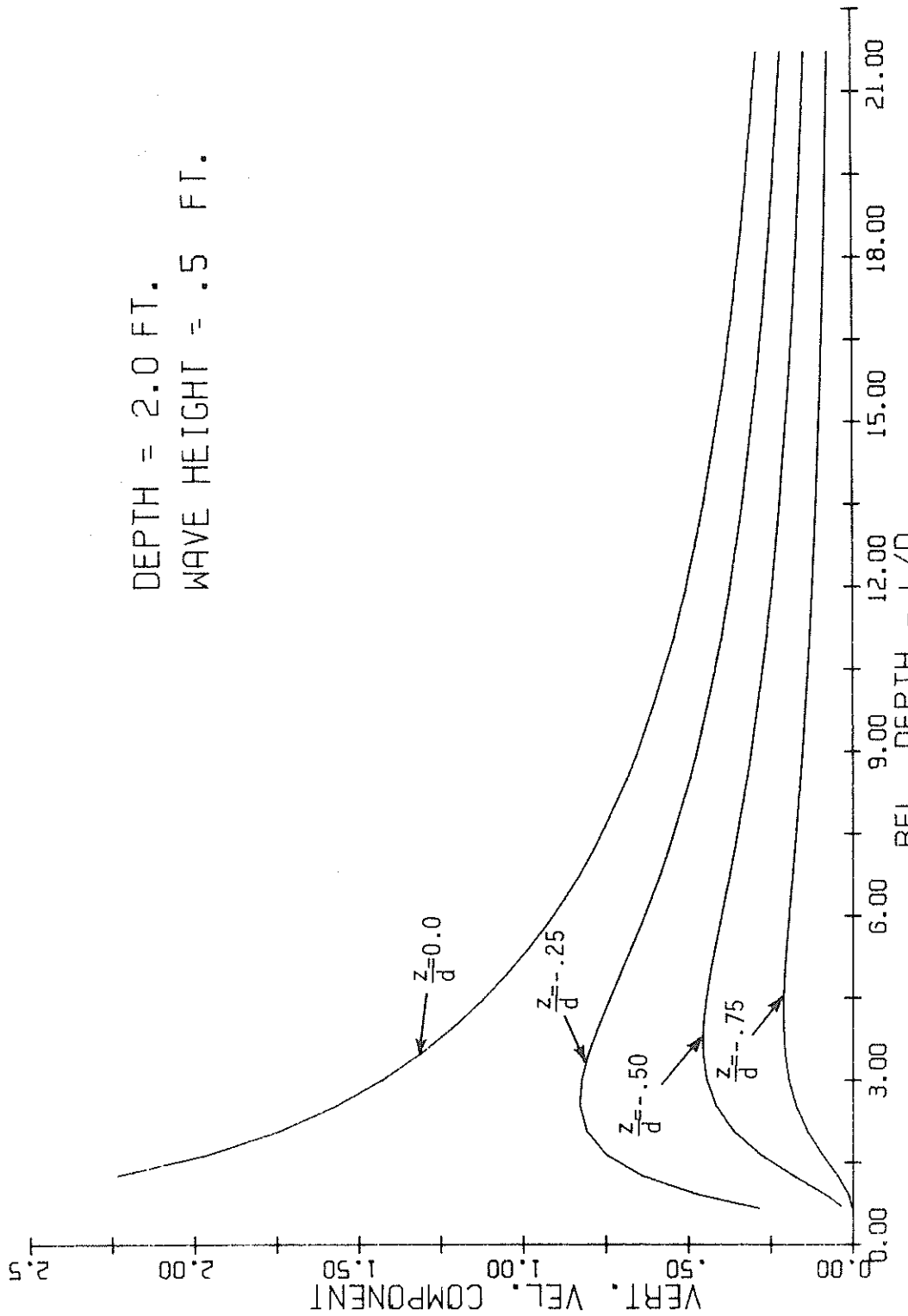

FIG. 25 VERTICAL PARTICLE VELOCITY VS. RELATIVE DEPTH

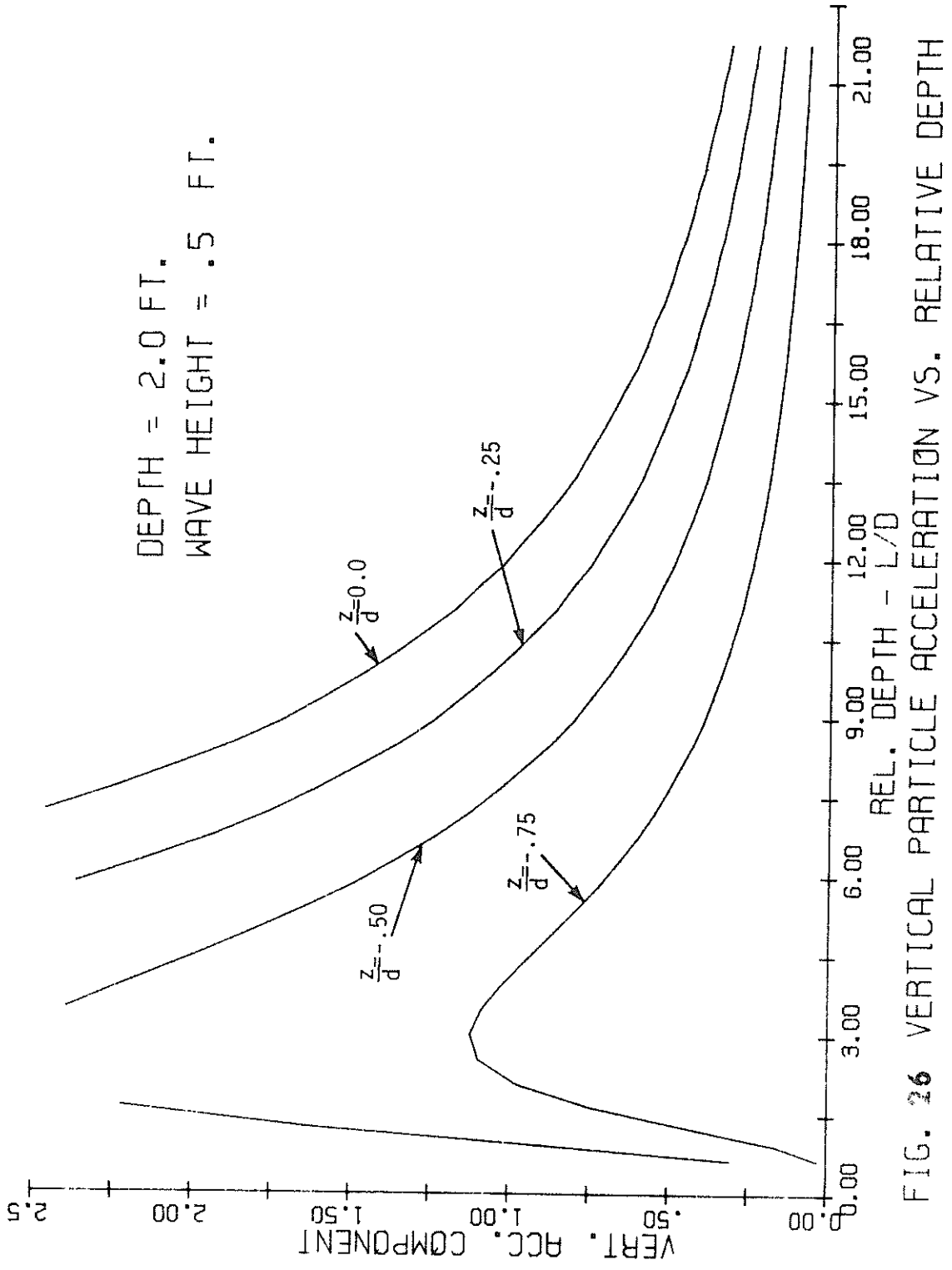

FIG. 26 VERTICAL PARTICLE ACCELERATION VS. RELATIVE DEPTH

measure both the force and phase angle. For large wave heights and for values of relative depth between 2.5 and 6.0, the contribution of the drag force to the total force should not be neglected. Theoretical force equations which are based on small wave height neglect the drag force.

Figs. 25 and 26 show the vertical particle velocity and acceleration (Eqs. 3.9 and 3.11) plotted versus relative depth (L/d). In the vertical direction, the particle velocity and displacement are small and viscous effects (drag forces) are negligible. The measured vertical dimensionless force should therefore agree closely with the theoretical vertical dimensionless force. The data for the vertical dimensionless force showed a slight tendency to increase with increasing wave steepness. The curves drawn in Fig. 19 and 21 are the upper bounds for the force measured on the model at the depth indicated. The variation due to the wave steepness was small enough that the single line drawn should accurately predict the wave force on the object for a wave steepness up to 0.09. Graphing the measured dimensionless force for a given model versus the relative displacement parameter shows that the vertical dimensionless force is nearly independent of wave height (Fig. 27).

In the vertical direction the dimensionless force depends on the water depth. For model 2, three distinct curves were drawn. For model 1 the curves for d = 1.5 ft. and 2.0 ft. coincide, and the curve for d = 1.1 ft. is distinct. The coefficient of mass for a given object submerged in a fluid has been shown to increase

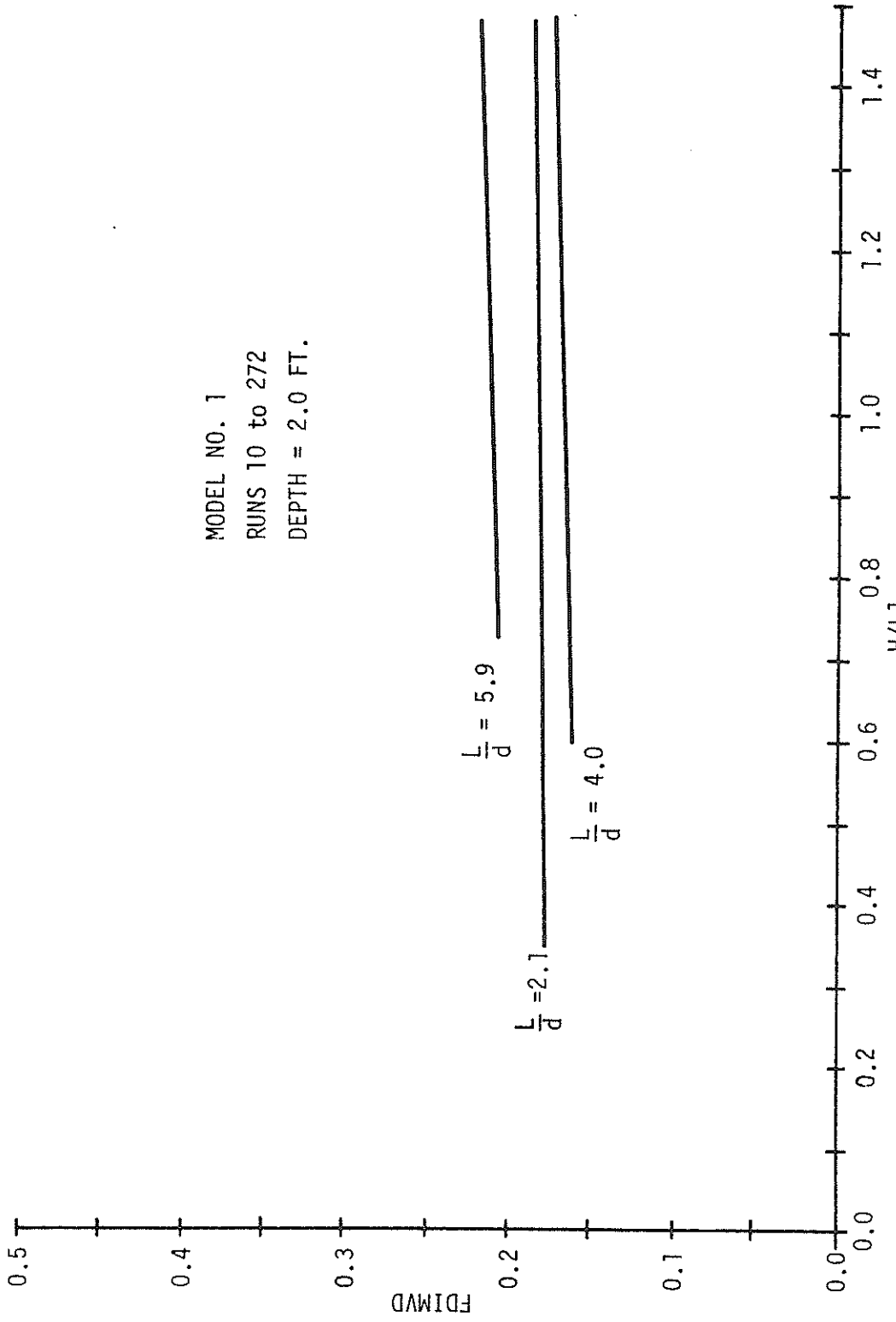

FIG. 27 - VERTICAL DIMENSIONLESS FORCE VS. RELATIVE DISPLACEMENT PARAMETER.

as the object approaches a boundary. This could be one explanation, as the water surface can be considered a boundary to the system. At the lower water depth, reflection from the model would result in larger forces on the model; however, no attempt was made to determine reflection at the model. The variation in force with water depth was not found for the horizontal direction.

The results of the model tests performed by the author are presented in Figs. 28 to 47. Figures 28 to 37 are the dimensionless plots for the maximum horizontal dimensionless force (FDIMHW) versus relative depth (L/d) and Figs. 38 to 47 are the dimensionless plots for the maximum vertical dimensionless force (FDIMVD) versus relative depth (L/d). Each plot is identified by model number, corresponding run numbers and water depth.

Although a theoretical analysis indicates that the horizontal dimensionless force is independent of wave height, examination of Figs. 28 to 37 shows the horizontal dimensionless force depends on the wave height (H). The value of the wave steepness (H/L) is indicated at each data point. It is noted that we may not actually say that the horizontal dimensionless force increases with increasing wave steepness from these graphs. The reason for this is the fact that in each graph the water depth (d) is constant and for each value of relative depth (L/d) points on a vertical line represent a constant wave length (L). Therefore, increasing values of wave steepness (H/L) only indicate the relative increase in wave height.

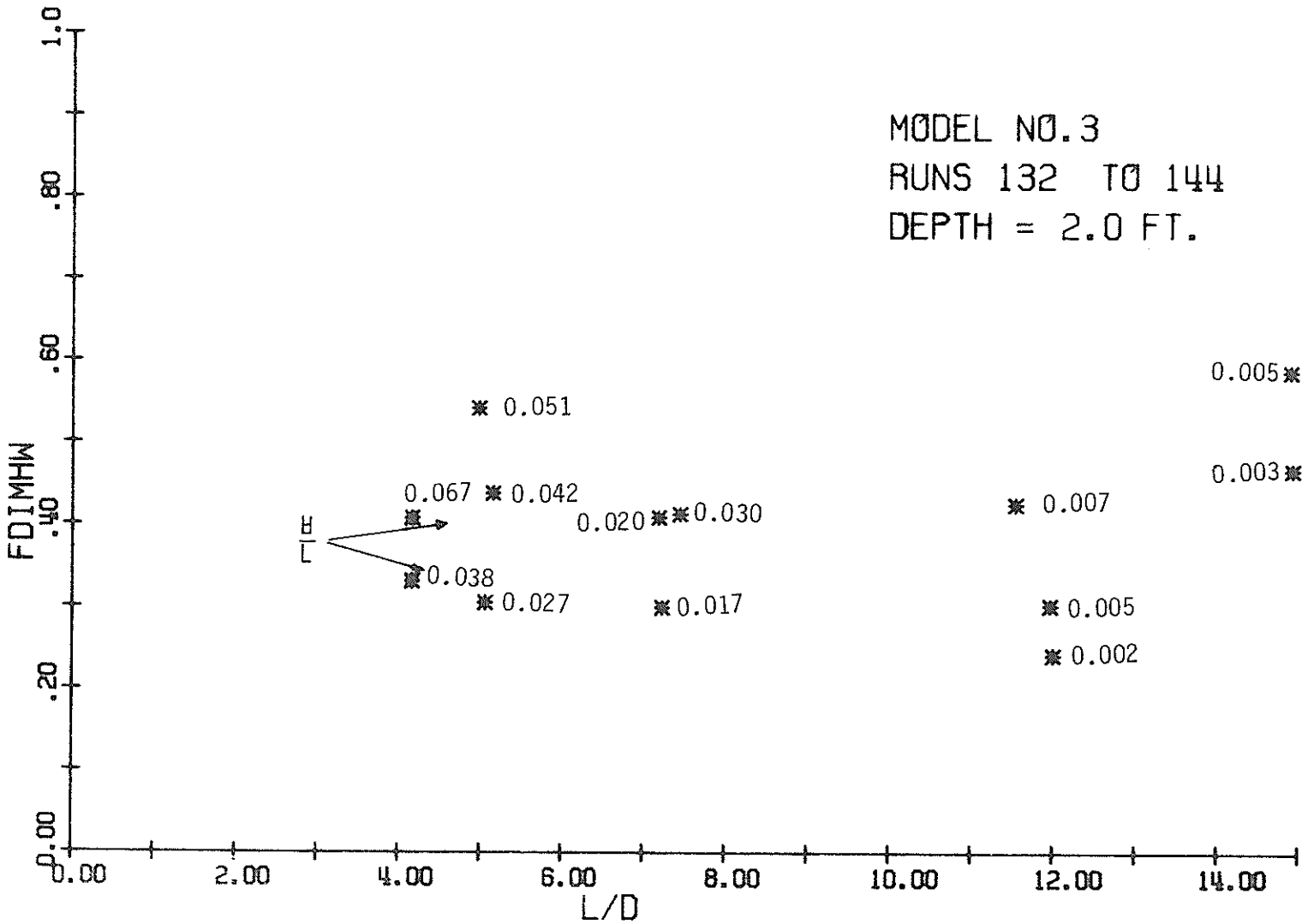

FIG. 28 HORIZONTAL DIMENSIONLESS FORCE VS. RELATIVE DEPTH

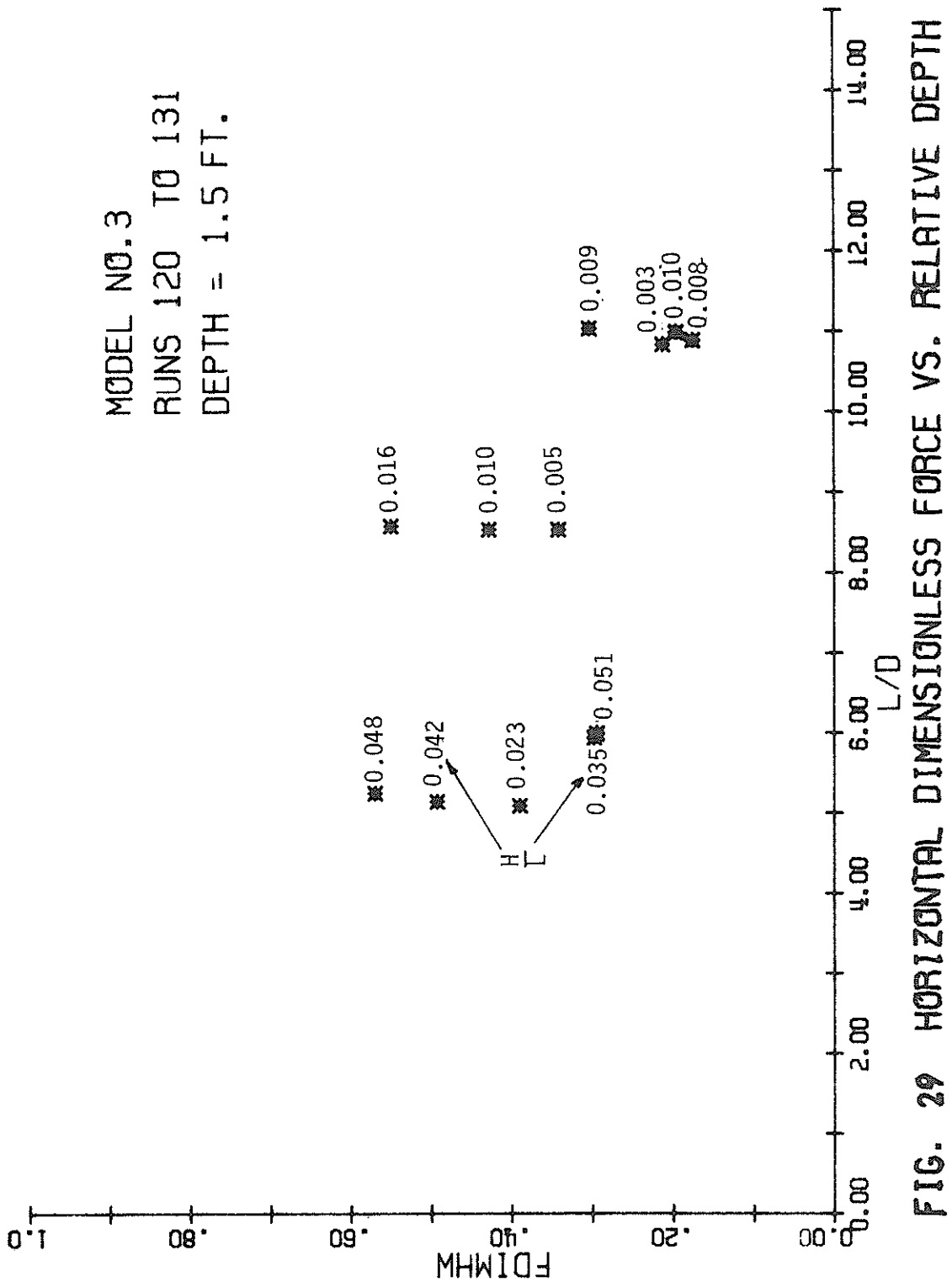

FIG. 29 HORIZONTAL DIMENSIONLESS FORCE VS. RELATIVE DEPTH

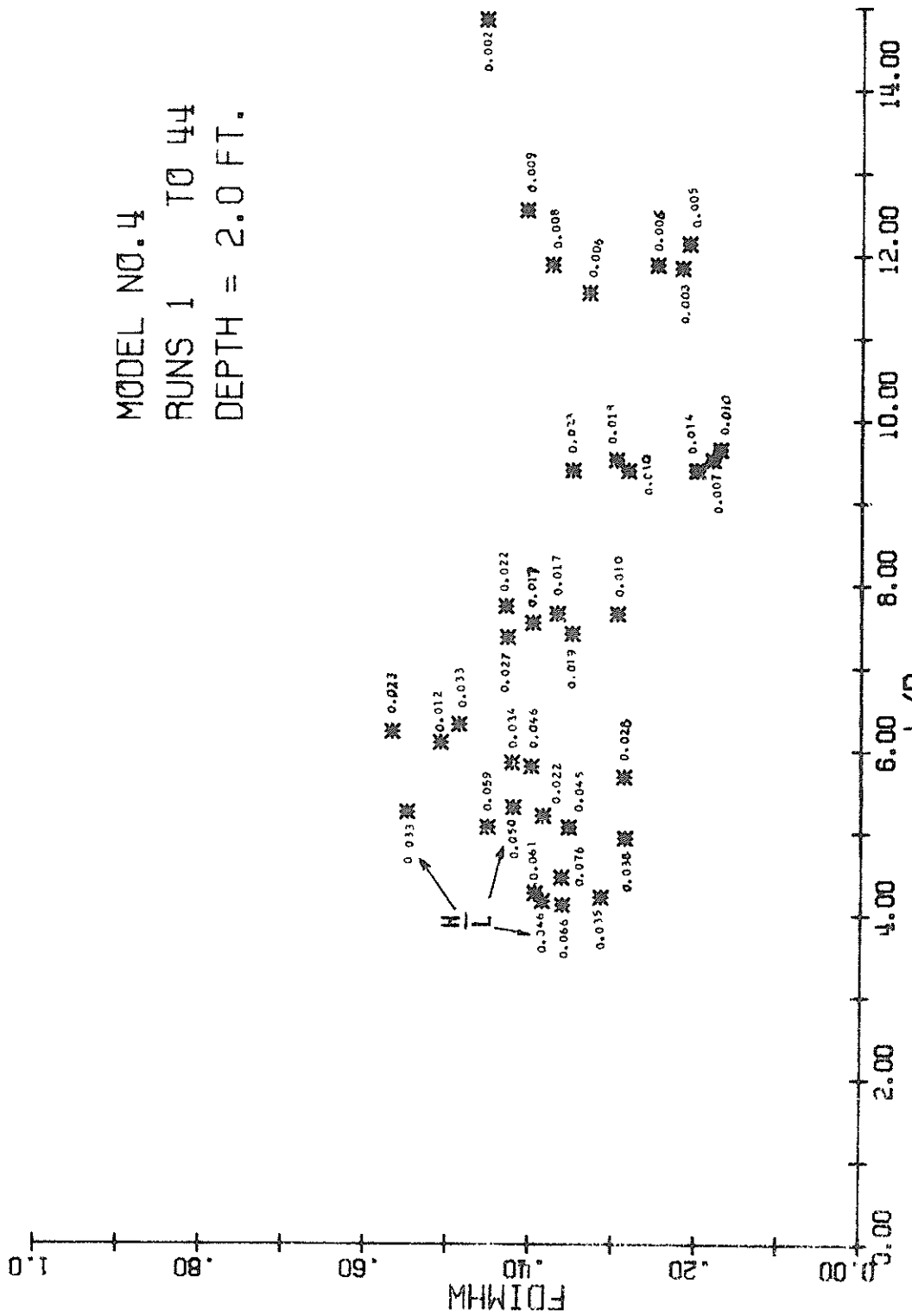

FIG. 30 HORIZONTAL DIMENSIONLESS FORCE VS. RELATIVE DEPTH

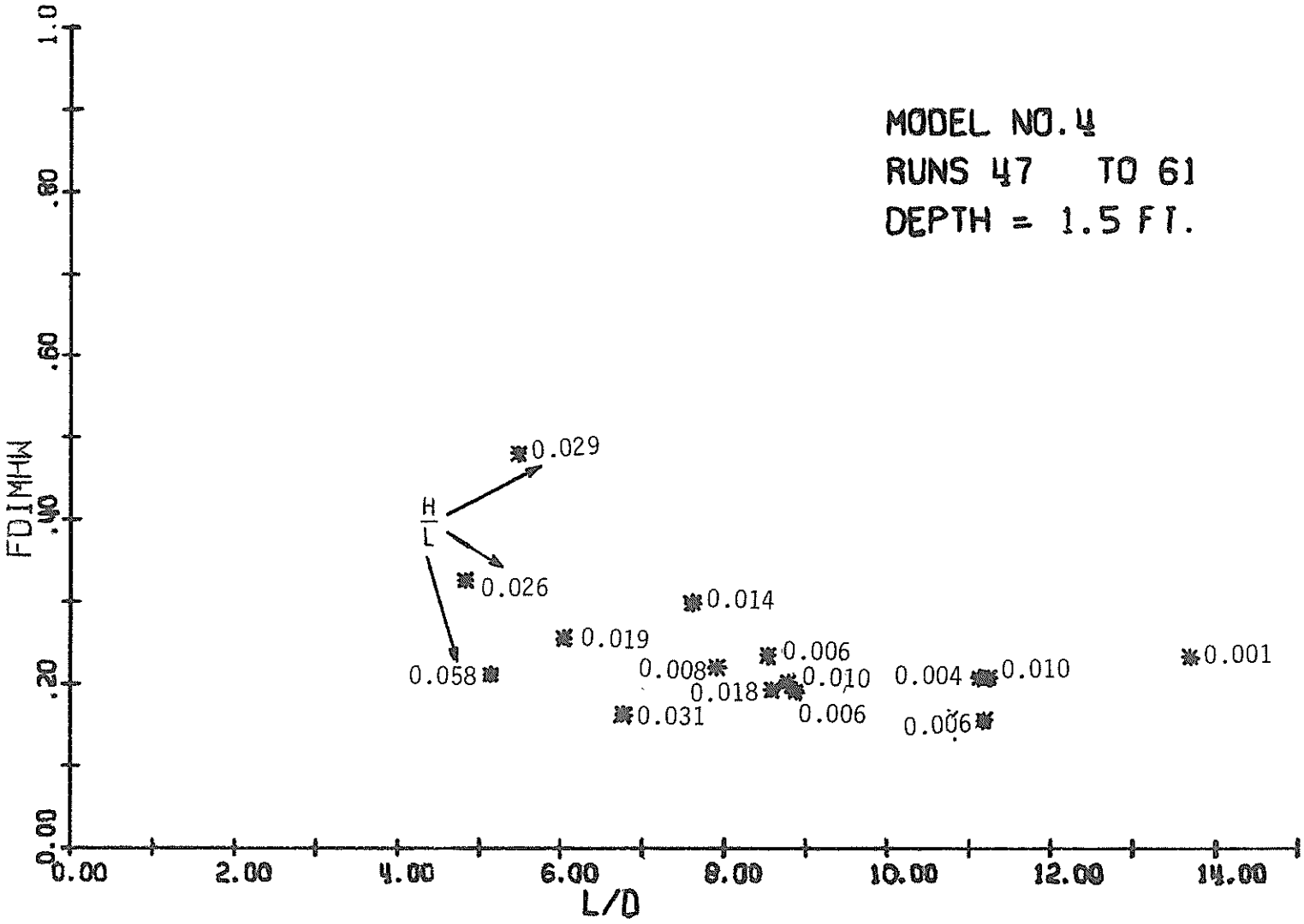

FIG. 31 HORIZONTAL DIMENSIONLESS FORCE VS. RELATIVE DEPTH

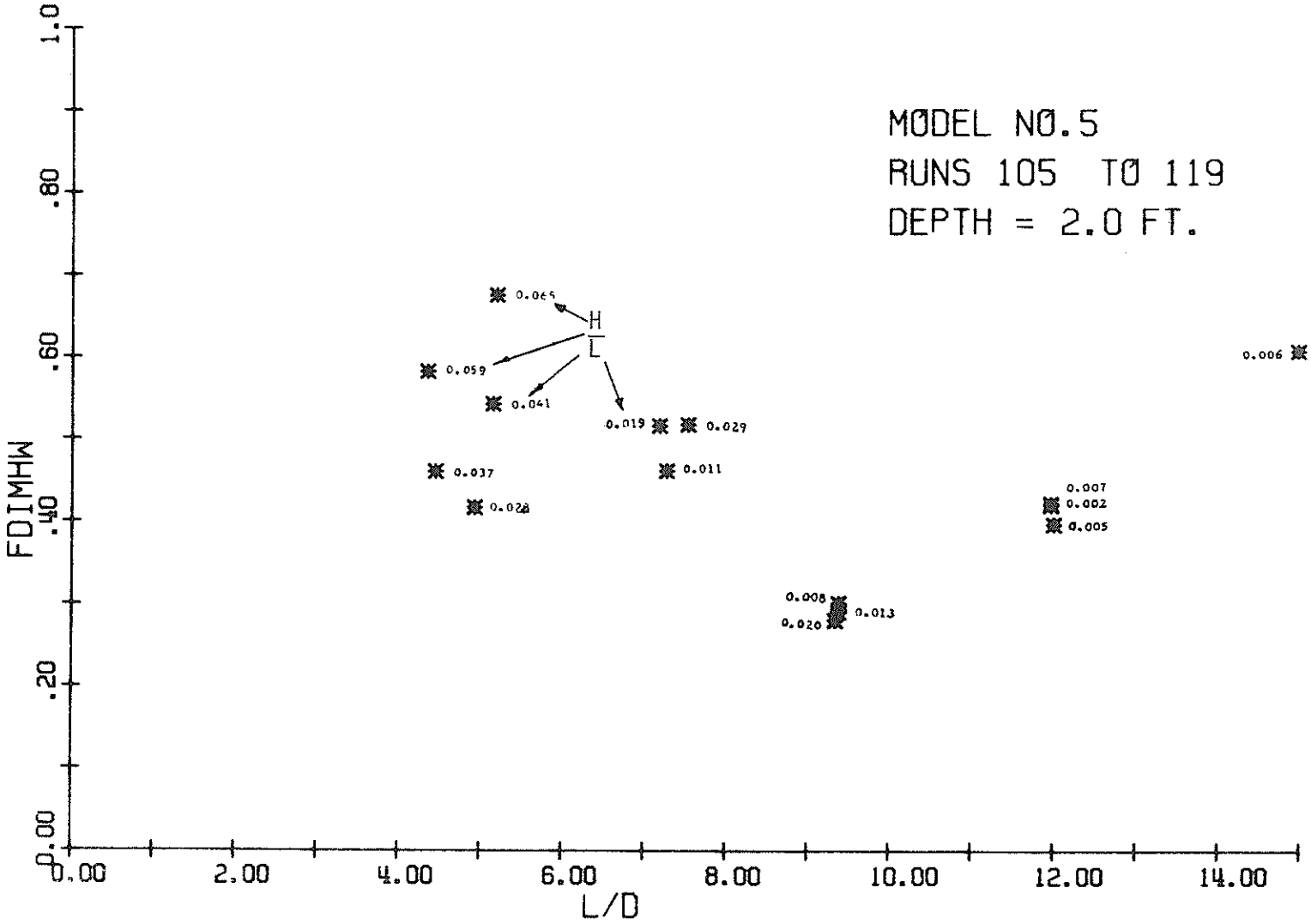

FIG. 32 HORIZONTAL DIMENSIONLESS FORCE VS. RELATIVE DEPTH

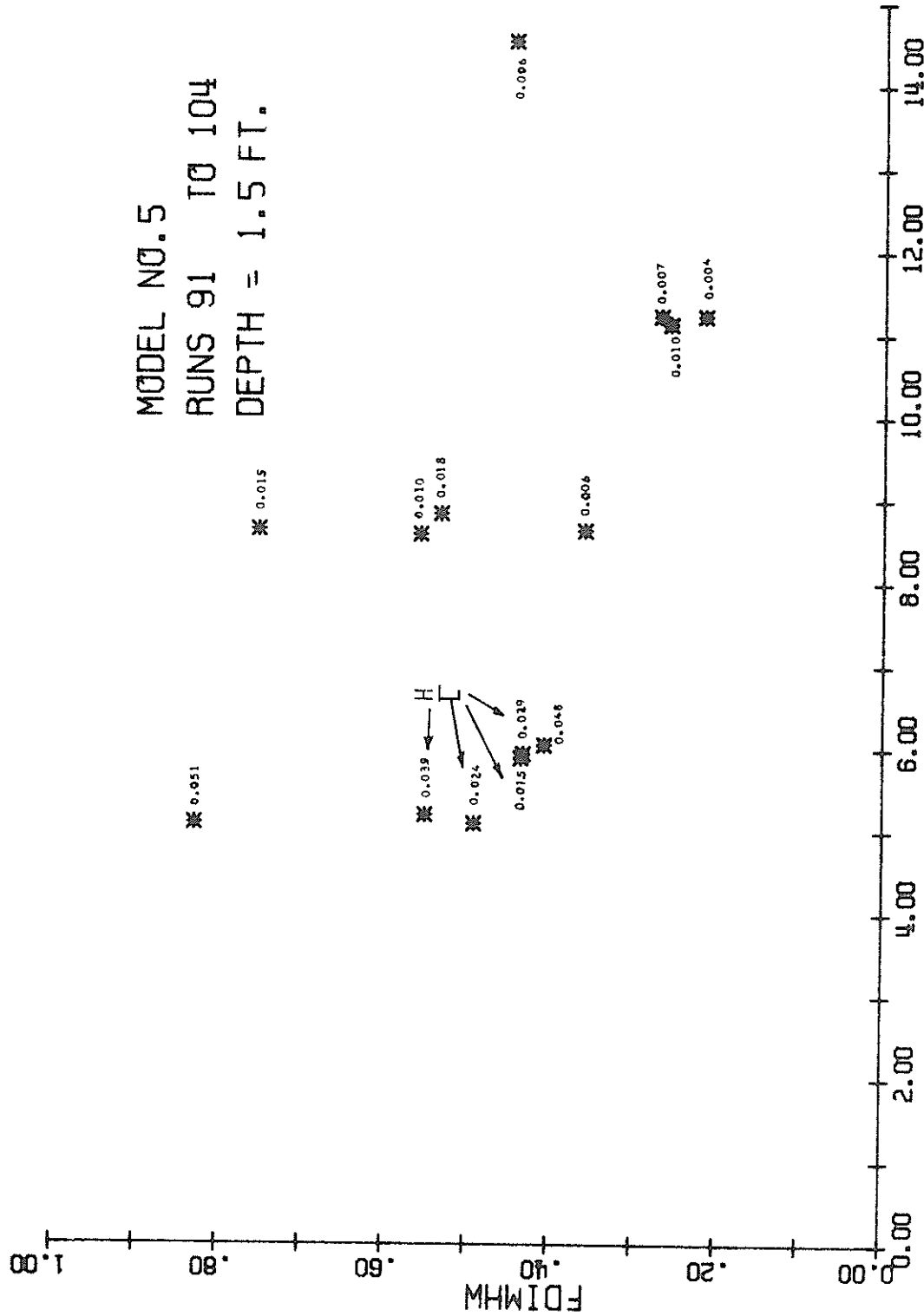

FIG. 33 HORIZONTAL DIMENSIONLESS FORCE VS. RELATIVE DEPTH

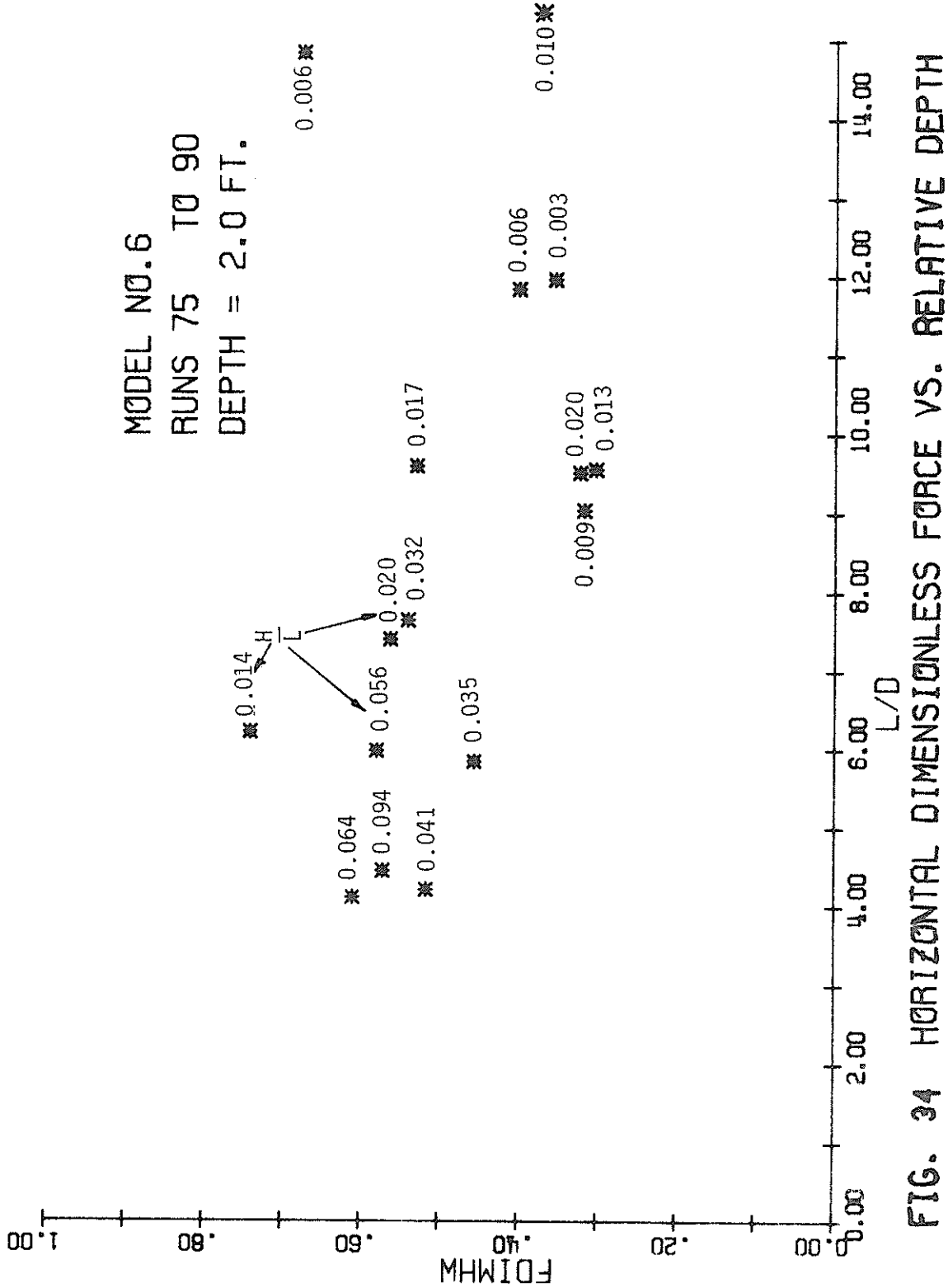

FIG. 34 HORIZONTAL DIMENSIONLESS FORCE VS. RELATIVE DEPTH

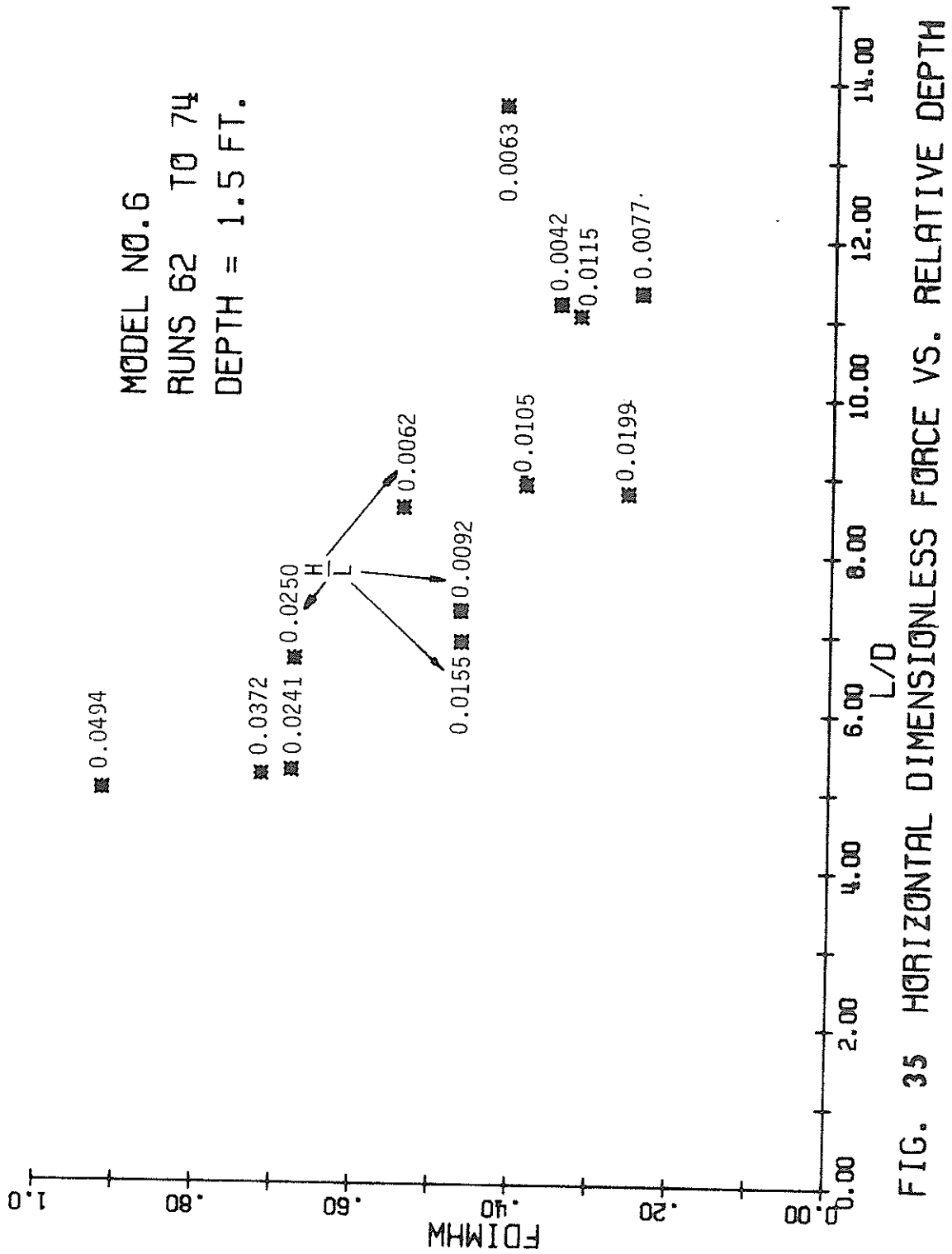

FIG. 35 HORIZONTAL DIMENSIONLESS FORCE VS. RELATIVE DEPTH

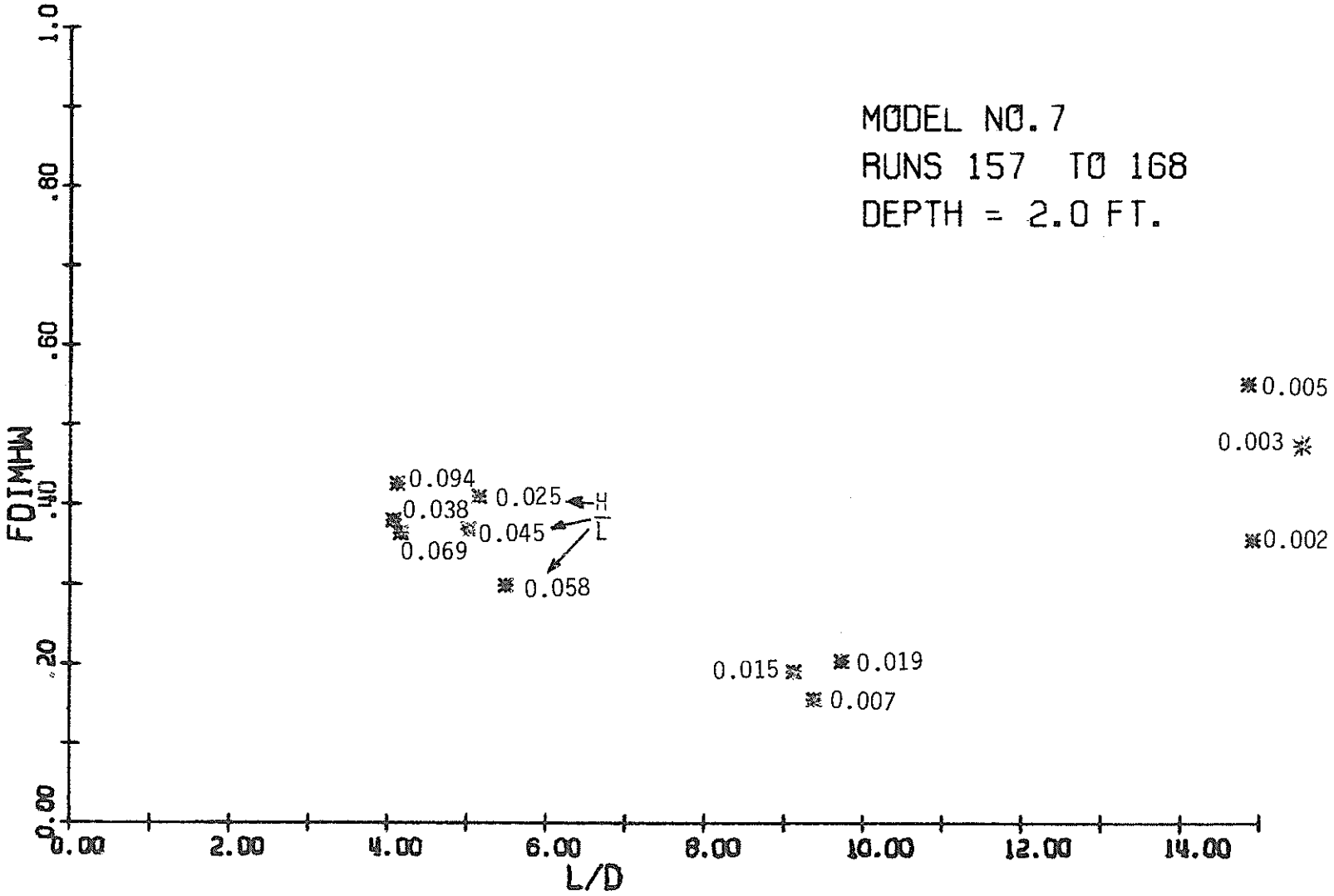

FIG. 36 HORIZONTAL DIMENSIONLESS FORCE VS. RELATIVE DEPTH

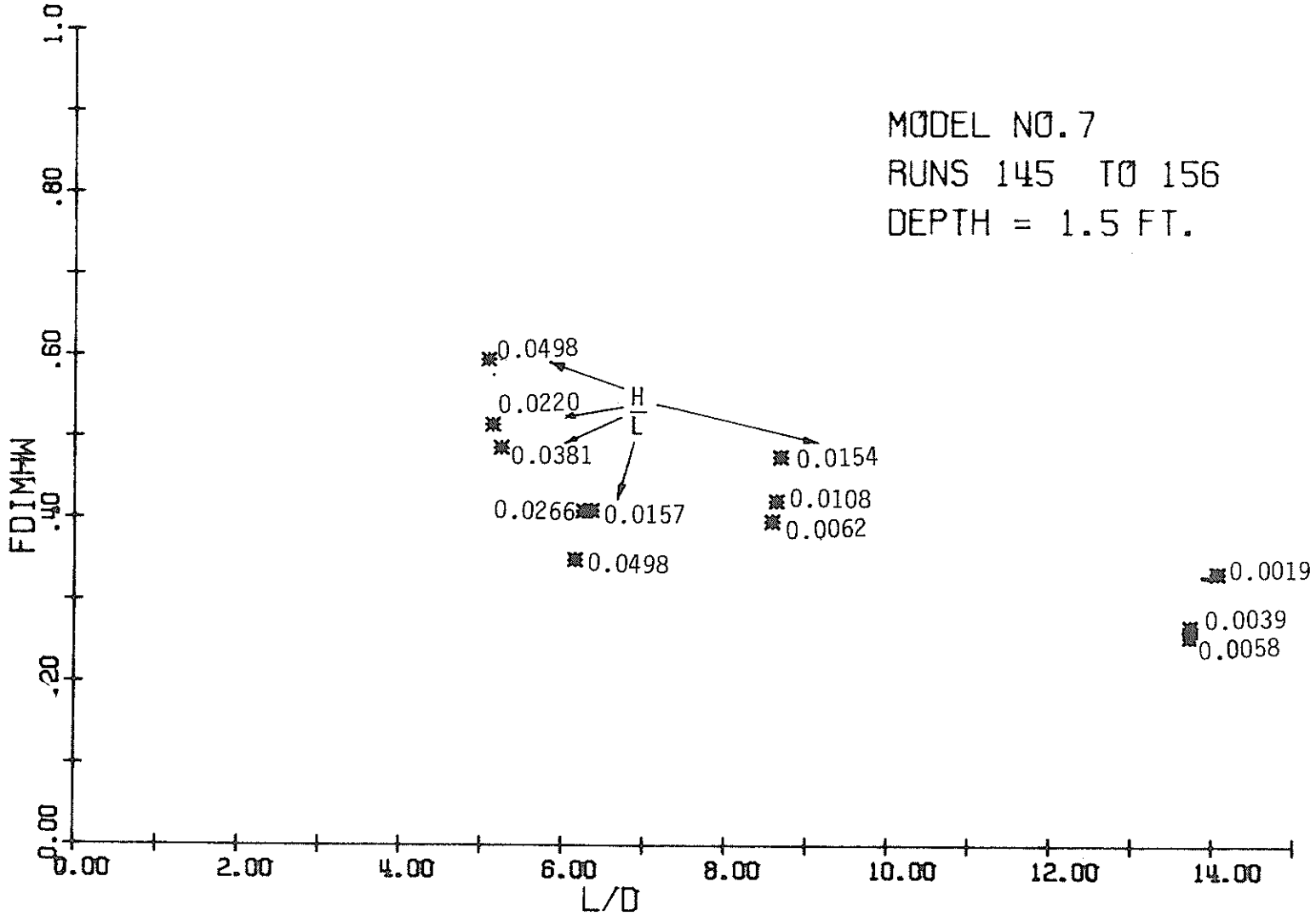

FIG. 37 HORIZONTAL DIMENSIONLESS FORCE VS. RELATIVE DEPTH

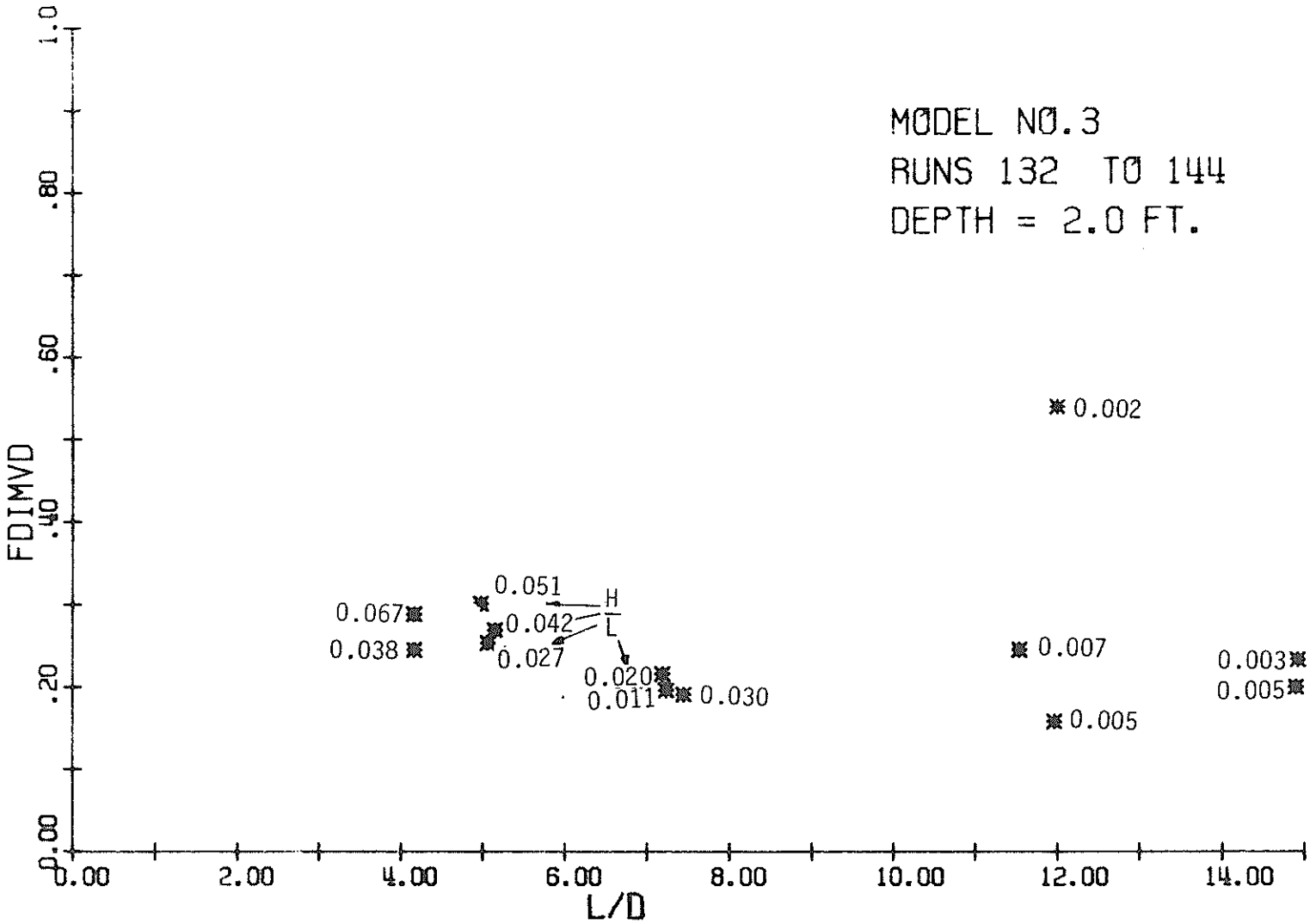

FIG. 38 VERTICAL DIMENSIONLESS FORCE VS. RELATIVE DEPTH

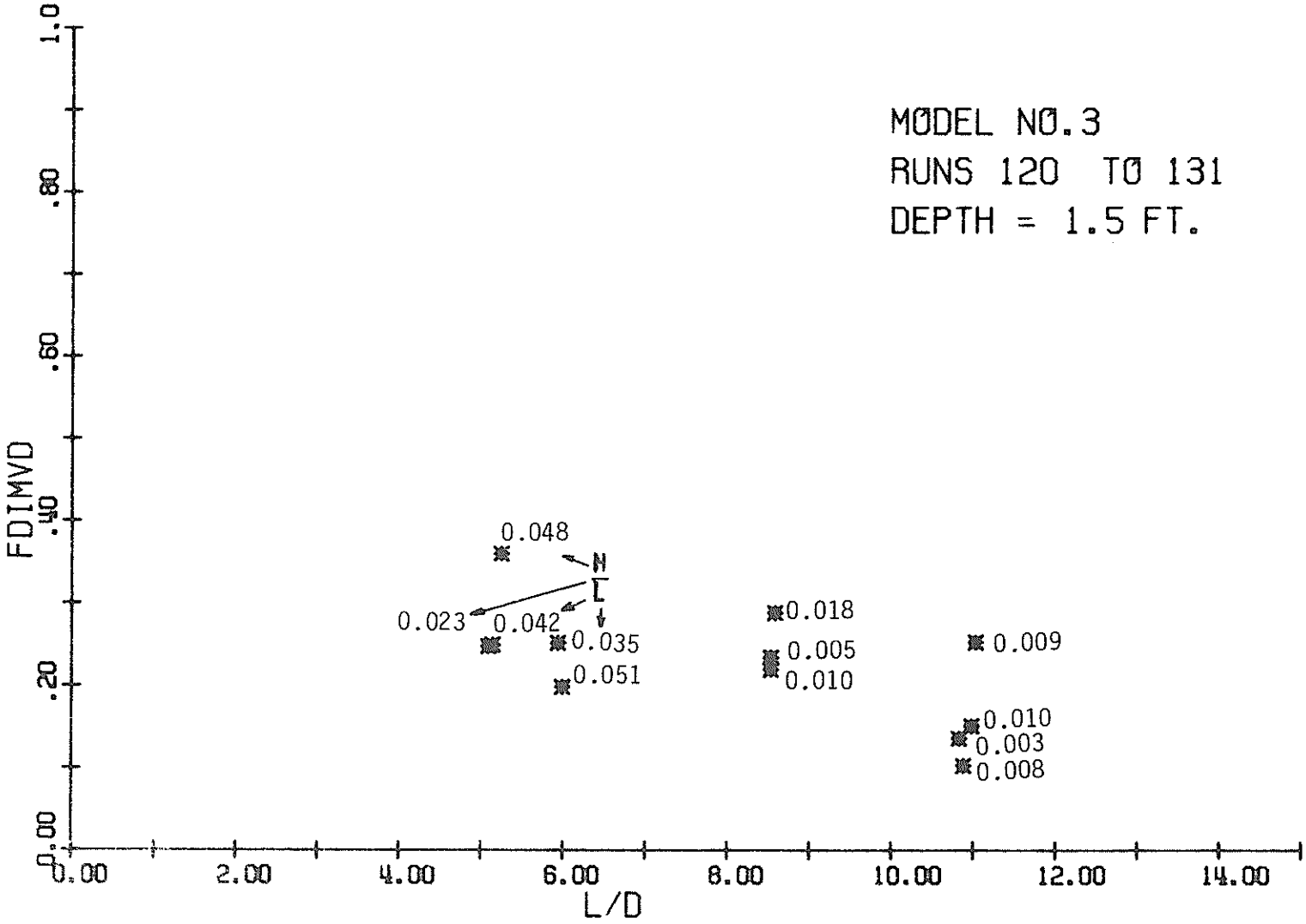

FIG. 39 VERTICAL DIMENSIONLESS FORCE VS. RELATIVE DEPTH

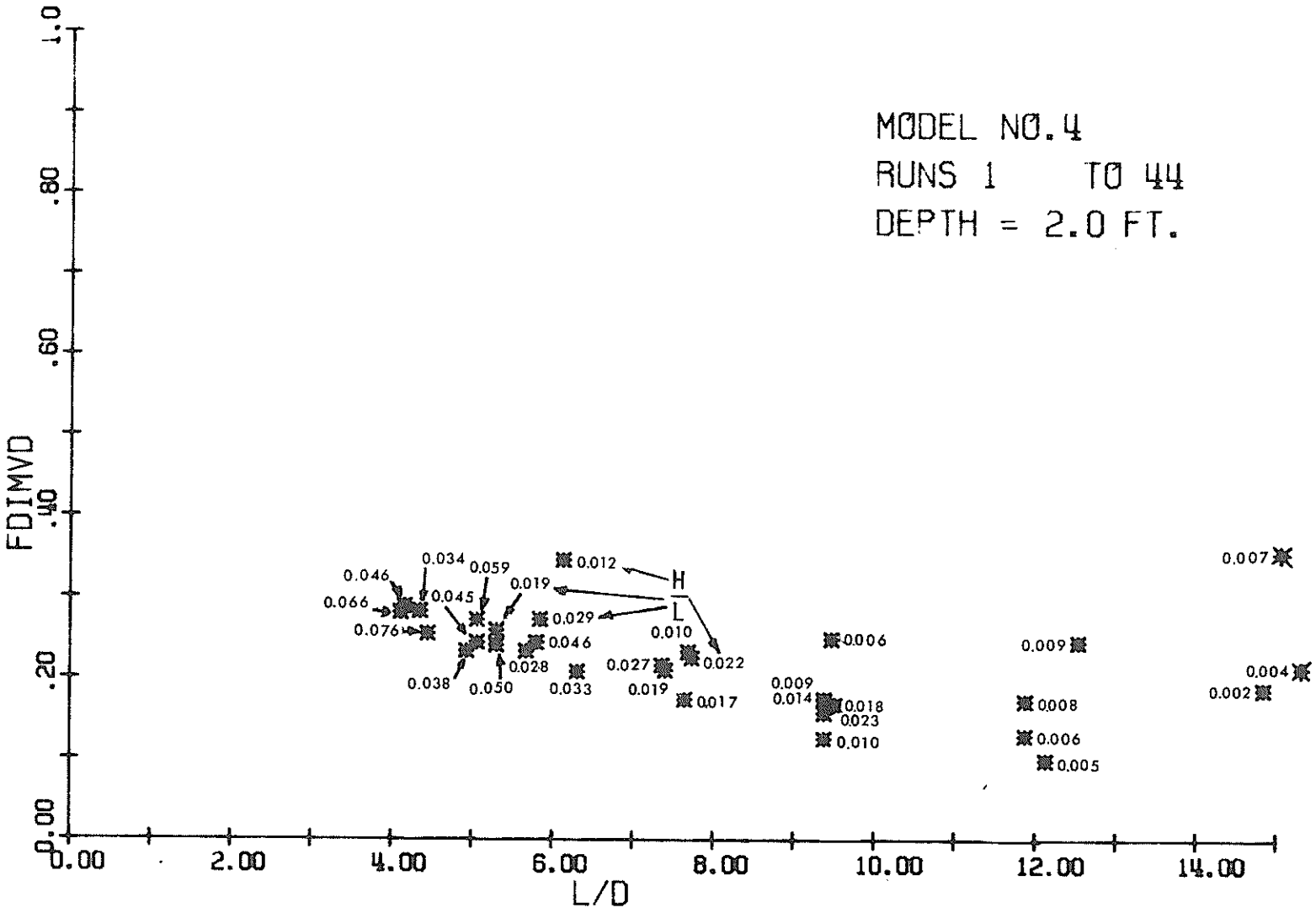

FIG. 40 VERTICAL DIMENSIONLESS FORCE VS. RELATIVE DEPTH

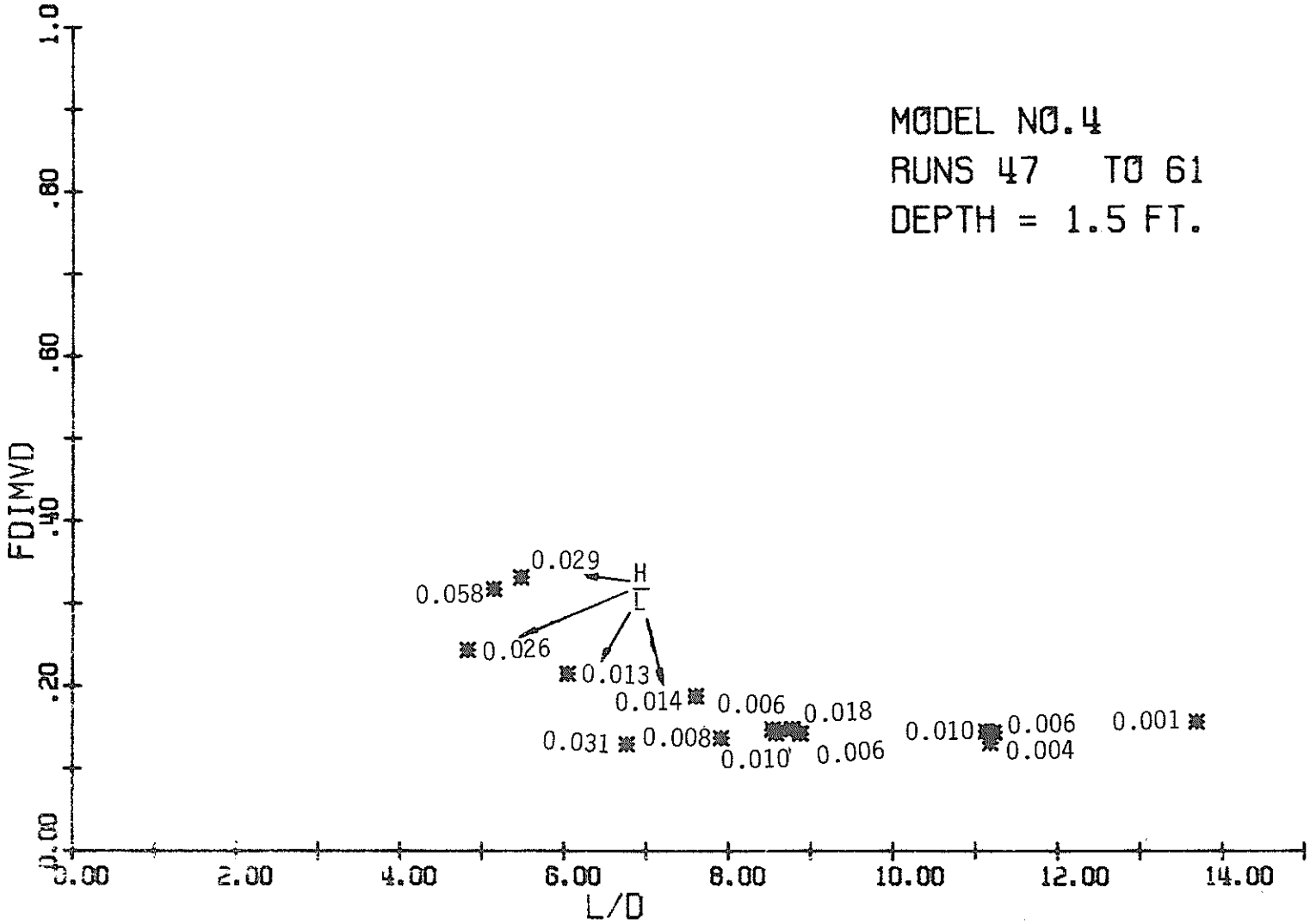

FIG. 41 VERTICAL DIMENSIONLESS FORCE VS. RELATIVE DEPTH

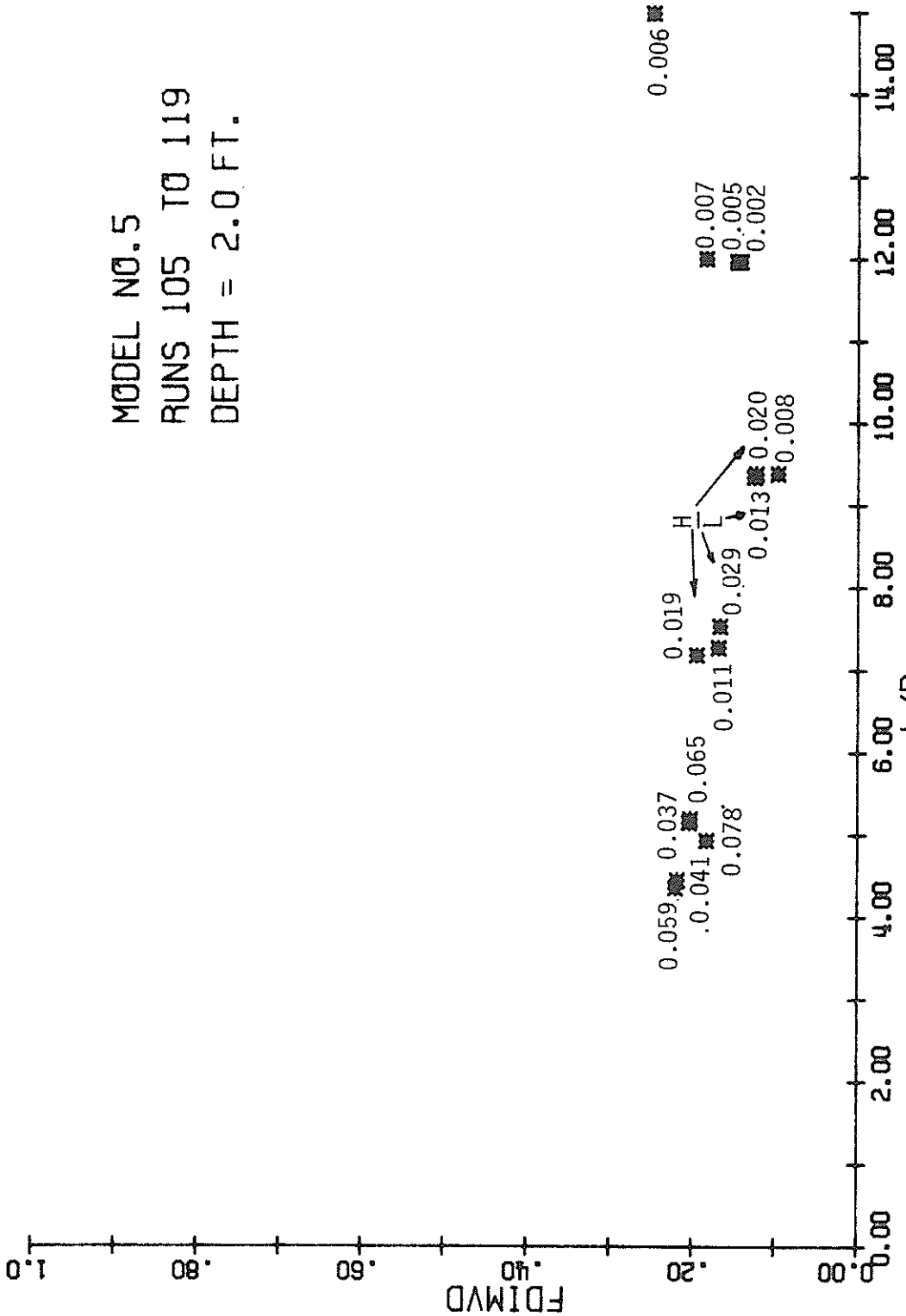

FIG. 42 VERTICAL DIMENSIONLESS FORCE VS. RELATIVE DEPTH

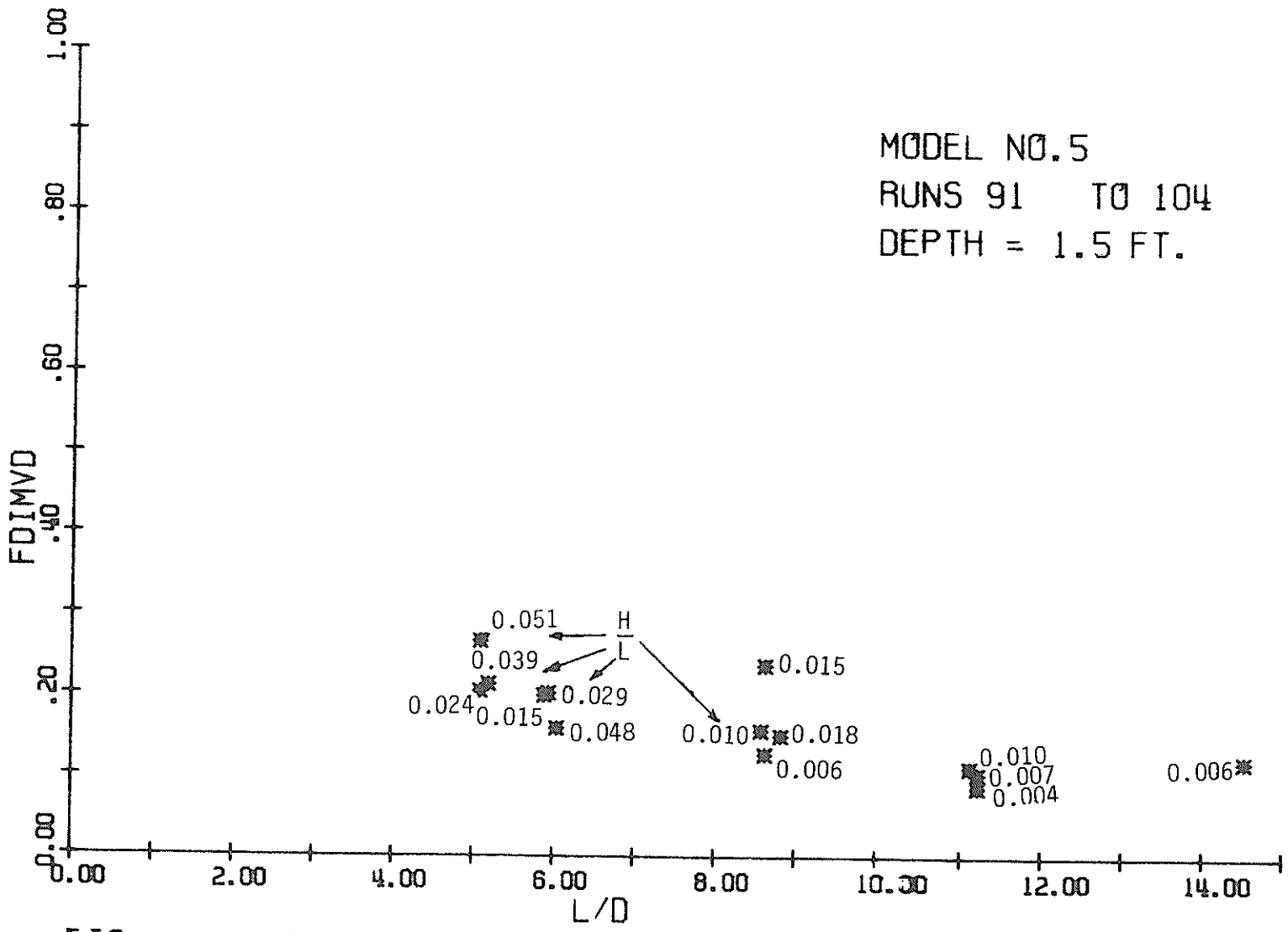

FIG. 43 VERTICAL DIMENSIONLESS FORCE VS. RELATIVE DEPTH

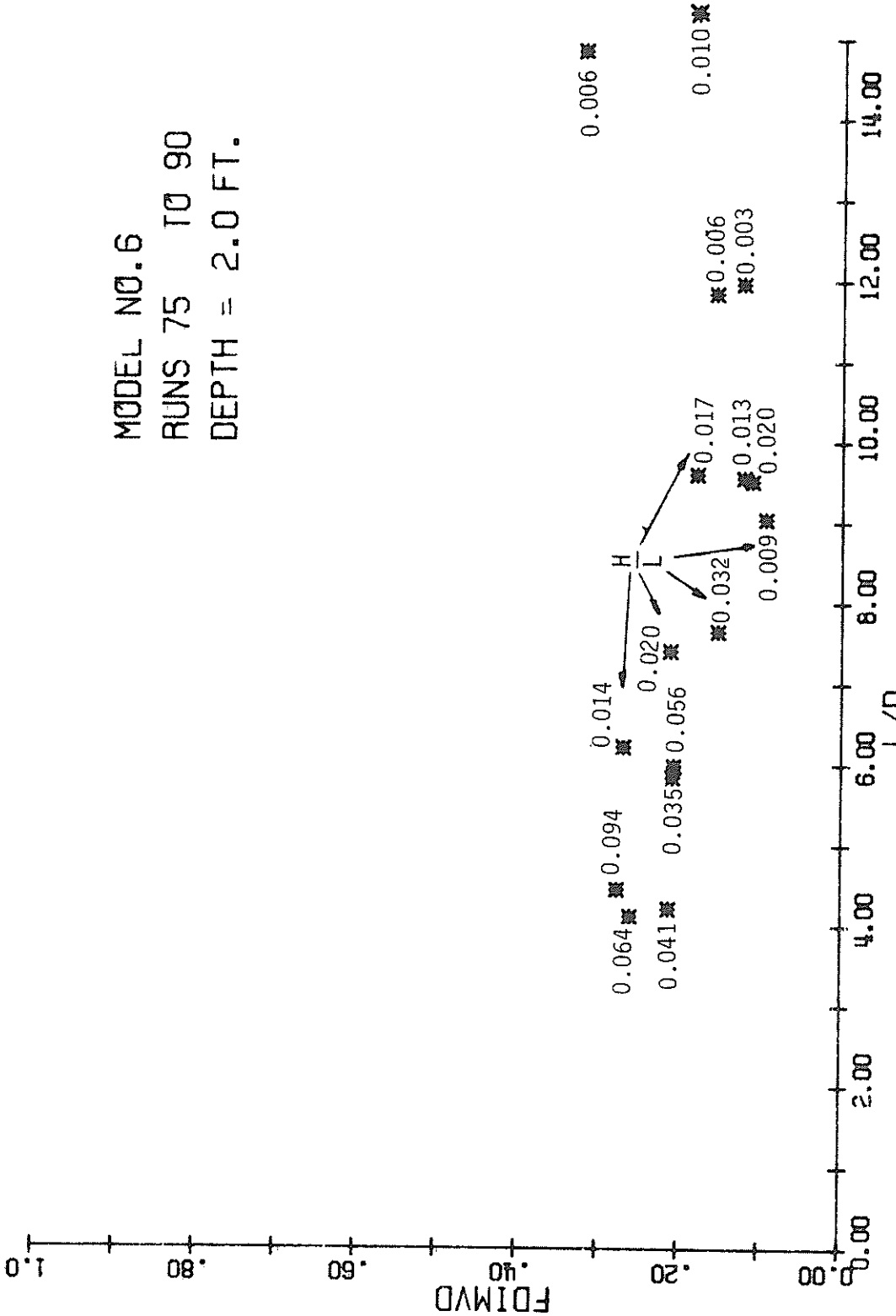

FIG. 44 VERTICAL DIMENSIONLESS FORCE VS. RELATIVE DEPTH

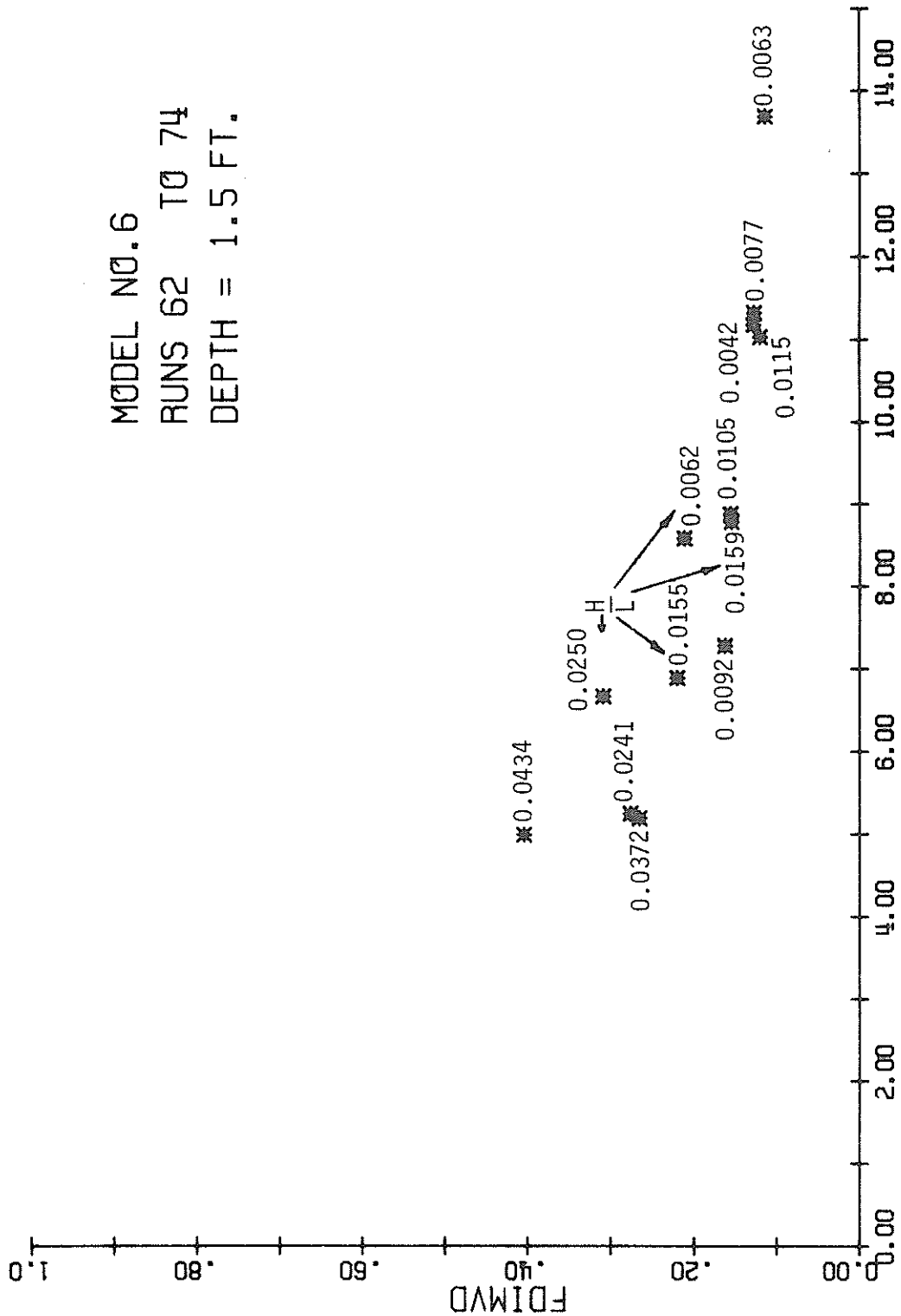

FIG. 45 VERTICAL DIMENSIONLESS FORCE VS. RELATIVE DEPTH

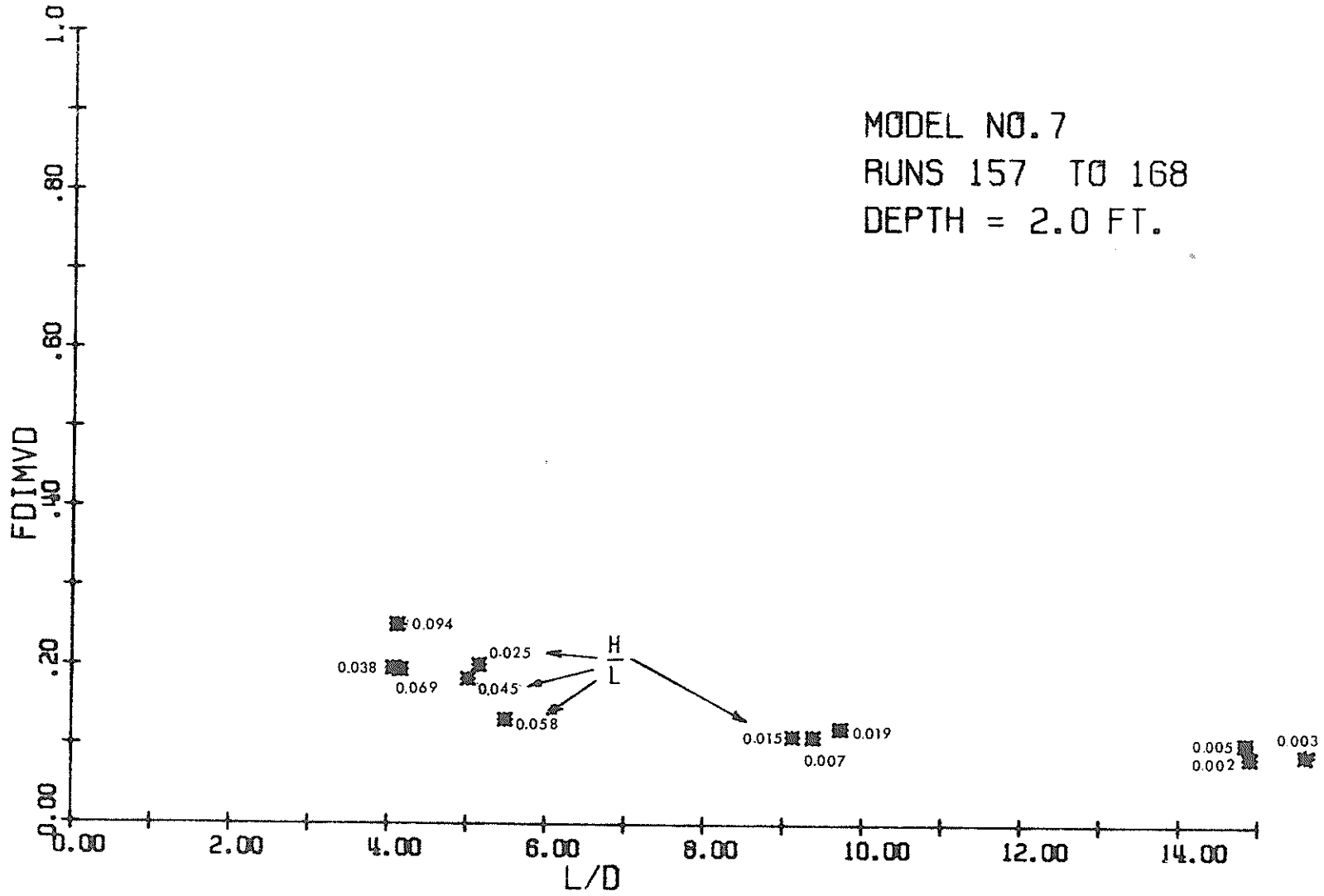

FIG. 46 VERTICAL DIMENSIONLESS FORCE VS. RELATIVE DEPTH

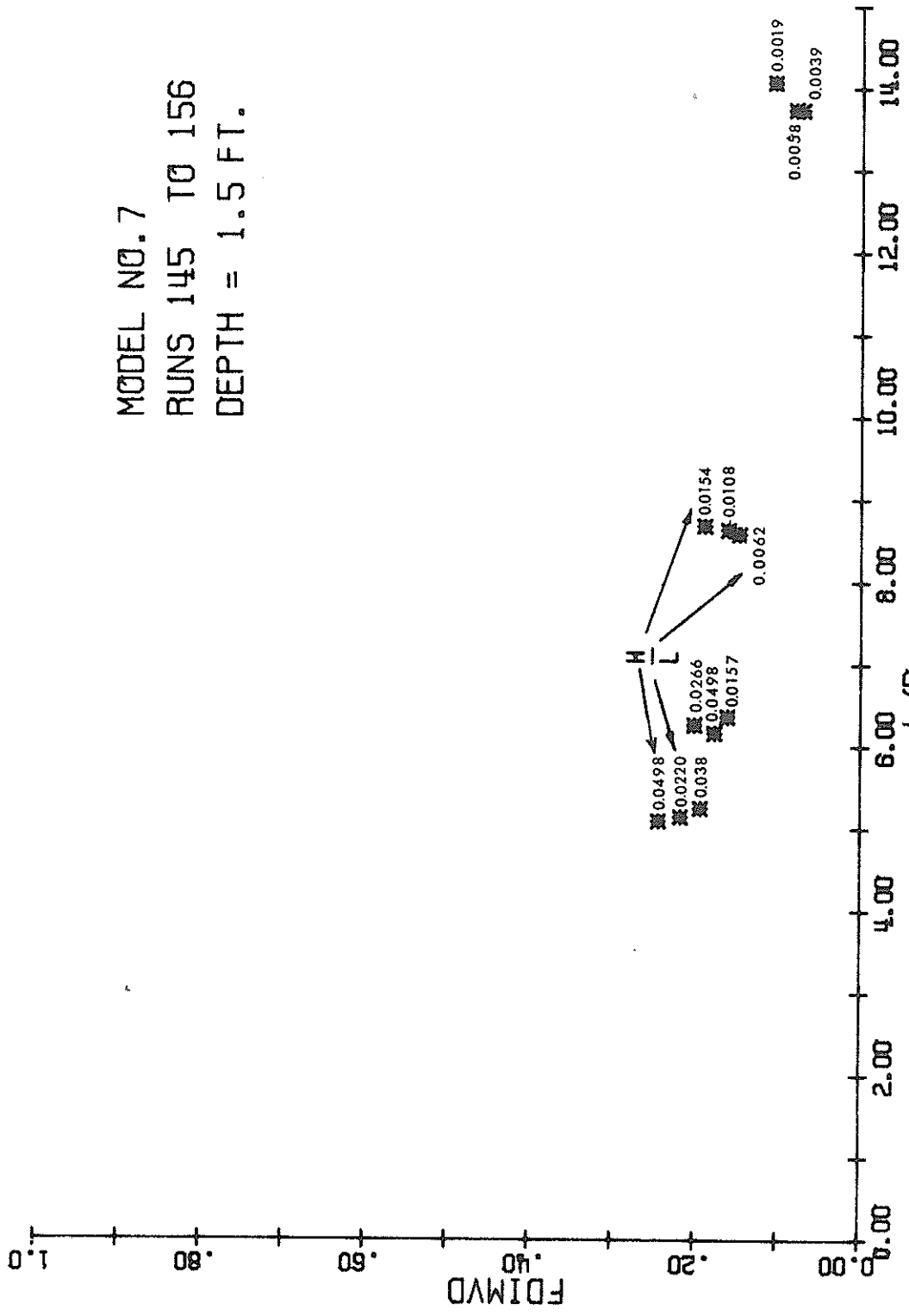

FIG. 47 VERTICAL DIMENSIONLESS FORCE VS. RELATIVE DEPTH

The data is plotted as discrete points to show the effect of wave height on the dimensionless force. The limitations of the wave generator prevented the determination of a constant wave steepness at all values of relative depth. The wave heights generated at large values of relative depth were smaller than those generated at low values of relative depth. Thus it was impossible to present a set of curves of horizontal dimensionless force versus relative depth for a constant wave steepness. In general, the horizontal dimensionless force increased with increasing wave height. Of notable exception are data points which fall in the relative depth region of maximum horizontal acceleration and have large values of wave height. For values of relative depth at the deep water end of the intermediate depth range the horizontal accelerations are a maximum and increase as the wave height increases. The high accelerations are the result of large pressure fields which are interrupted by the presence of the model and pressure differences at the edges of the model result in the spawning of vortices. Vortex formation results in a lowering of the coefficient of mass for the model and hence a decrease in dimensionless force. The increased pressure drag due to the formation of the vortices should show up a change in phase angle at which the maximum force occurs. To obtain a better understanding of this phenomenon phase angle measurements should be done. Equipment limitation made this difficult in these experiments.

The dimensionless vertical force data is plotted versus relative depth in Figs. 38 to 47. In the vertical direction both the particle

acceleration and velocity are small and the experimental results should agree more closely with the theoretical results. Although a slight increase in vertical dimensionless force with increasing wave height can be observed the experimental results do agree with the theoretical. This can be seen by comparing Fig. 6 with the vertical force results for each model provided a proper value of C_m is used. As with models 1 and 2 the results show a slightly higher dimensionless force at the lower water depth (d).

Both the horizontal and vertical dimensionless force plots show an increase in the dimensionless force at the larger values of relative depth (L/d). The theoretical dimensionless force, developed from Airy wave theory, indicates that the force should decrease. But Airy wave theory is developed for small amplitude waves in deep water, and another wave theory suitable for shallow water (e.g. Solitary Wave Theory) should be used in this region to describe the pressure, acceleration, and velocity fields.

The data for models 1 and 2 were obtained from experiments in a 2 ft. wide two-dimensional wave tank. The experiments on the remaining models were performed in a wide wave basin. The results, when compared, indicate that side wall effects in the two-dimensional wave flume were negligible. A dimensionless horizontal force of 0.42 was experimentally obtained for model #3 for L/d=5 and H/L=.042 (Fig. 28). Considering the coefficient of mass to be approximately equal for models 2 and 3, then we may predict a horizontal dimensionless force of 0.63 for model 2 (based on volume difference). Data for model 2

shows a value of .60 at H/L=.044 and L/d=5. It is to be recognized here that the coefficient of mass changes with both wave height and model dimensions.

The experimental data reported in this paper was obtained from models with open bottoms through which the wave pressure could enter the model. This type of model was used because of its apparent application as under water storage facilities for the oil industry. The theoretical dimensionless force equation were developed for a solid rectangular structure with the wave pressure acting at its boundaries. In order to compare the two cases a thin plate was attached to the bottom of model 4 (to be referred to as model 7). The model was positioned and filled with water and subjected to the series of waves. The results for model 7 are presented in Figs. 36, 37, 46, and 47. A comparison of these results with those for model 4 for the vertical forces (Figs. 40 and 41 with 46 and 47) indicates the vertical force on the open bottom model to be slightly higher than the vertical force on the closed bottom model. For the forces in the horizontal direction the data for the two models in two feet of water shows fair agreement (Figs. 30 and 36). At a water depth of 1.5 ft. (Figs. 31 and 37) the force on the closed bottom model is higher than the force on the model with the open bottom.

CHAPTER VII

CONCLUSIONS

The forces due to oscillatory waves on submerged objects have been studied both theoretically and experimentally. The theoretical approach is based on the assumption that the wave force is entirely inertial and can be obtained from the wave pressure distribution on the structure. The experimental results were obtained from model studies in a three-dimensional wave basin. Additional data from experiments in a two-dimensional wave flume on similar models was also used in this study. The conclusions are stated as follows:

1. —— The wave forces on the models tested were a function of the relative depth and wave steepness.

2. —— The dimensionless force term used in this research can be used as a model study parameter when plotted as a function of relative depth and wave steepness.

3. —— The experimentally determined vertical dimensionless force agreed closely with the theoretically determined dimensionless force. Wave steepness did not appreciably affect the vertical dimensionless force.

4. —— The effect of wave steepness was significant for the experimentally determined values of the horizontal dimensionless force. For large wave heights at the deep water end of

intermediate depth water, a complex flow situation was produced which resulted in greatly varying values of dimensionless horizontal force.

5. —— The research performed in this report could be greatly advanced by further experiments which determine the phase relationship between the maximum force and the crest of the wave. This would show the effect of the velocity-induced force (drag force) on the model which from these results may be appreciable.

6. —— The comparison of the data obtained by Herbich and Shank for the tests in the two-dimensional wave flume and the author's data from the three-dimensional wave basin are good, indicating that effects due to the proximity of the side walls in the smaller flume were negligible.

7. —— Until further model studies are performed in which phase angles can be measured and the drag force determined, the horizontal force on the submerged structure should be determined as the sum of the inertial and drag components of force.

APPENDIX I

REFERENCES

1. Bleakly, W.B., "Lockheed, Shell Flange Up Subsea Well", Oil and Gas Journal, Vol. 70, No. 43, Oct. 23, 1972, pp. 64-66.

2. Brater, E.F., McNown, J.S., and Stair, L.D., "Wave Forces on Submerged Structures", Journal of the Hydraulics Division, ASCE, Vol. 84, No. HY6, Proc. Paper 1833, Nov. 1958, pp. 1-26.

3. Brater, E.F., McNown, J.S., and Stair, L.D., "Wave Forces on Submerged Structures, with Discussions by Alterman, Hamlin, Sarphaya, and Herbich", Transactions, ASCE, Vol. 95, 1961.

4. Chakrabarti, S.K., "Discussion of 'Forces Due to Waves on Submerged Structures', by Herbich, J.B., and Shank, G.E.", Journal of the Water, Harbors and Coastal Engineering Division, ASCE, Vol. 97, No. WW3, Aug. 1971, pp. 92-94.

5. Chakrabarti, S.K., "Interaction of Waves with Submerged Objects", Journal of the Waterways, Harbors and Coastal Engineering Division, ASCE, Vol. 97, No. WW4, November 1971.

6. Clines, C.A., and Colonell, J.M., "Laboratory Modeling of Structural Response to Ocean Wave Excitation", University of Massachusetts, School of Engineering, Report No. UM-72-3, Amherst, April, 1972.

7. Cress, P., Dirksen, P., Graham, J.W., Fortran IV With Watfor and Watfiv, Prentice-Hall, Inc., New Jersey, 1970.

8. Daily, J.W., and Harleman, D.R.F., Fluid Dynamics, Addison-Wesley Publishing Company, Inc., Reading, Mass., 1966.

9. Dean, R.G. and Dalrymple, R.A., "Discussion of 'Forces Due to Waves on Submerged Structures' by Herbich, J.B. and Shank, G.E.", Journal of the Waterways, Harbors and Coastal Engineering Division, ASCE, Vol. 98, No. WW1, Feb., 1972.

10. Garrison, C.J., and Chow, P.Y., "Wave Forces on Submerged Bodies", Journal of the Waterways, Harbors and Coastal Engineering Division, ASCE, Vol. 98, No. WW3, Aug. 1972, pp. 375-392.

11. Garrison, C.J. and Snider, R.H., "Wave Forces on Large Submerged Tanks", Sea Grant Publication No. 210, Texas A&M University, January 1970.

12. Garrison, C.J., Rao, V.S., and Snider, R.H., "Wave Interaction with Large Submerged Objects", Proc. Second Offshore Technology Conference, Houston, OTC 1278, April 1970.

13. Grace, R.A., "The Effects of Clearance and Orientation on Wave Induced Forces on Pipelines: Results of Laboratory Experiments", University of Hawaii, Department of Ocean Engineering, James K.K. Look Laboratory, U Hawaii-Look Lab-71-15, April 1971.

14. Herbich, J.B. and Shank, G.E., "Forces Due to Waves on Submerged Structures", Journal of the Waterways, Harbors and Coastal Engineering Division, ASCE, Vol. 97, No. WW1, Proc. Paper 7870, Feb. 1971, pp. 57-71.

15. "Hewlett-Packard Manual-Model 321 Dual Channel Carrier Preamplifier Recorder" Hewlett-Packard Co., Houston, Texas.

16. Horning, J.I., and McCurry, G.L., "Dubai Expands Production System", Oil and Gas Journal, Vol. 70, No. 35, Aug. 28, 1972, pp. 53-57.

17. "Inland Ocean Ups Subsea Technology", Oil and Gas Journal, Vol. 69, No. 28, July 12, 1971, pp. 55-57.

18. Ippen, A.T., Editor, Estuary and Coastline Hydrodynamics, McGraw-Hill Co., New York, 1966.

19. Keulegan, G.H. and Carpenter, L.H., "Forces on Cylinders and Plates in an Oscillating Fluid", Journal of Research of the National Bureau of Standards, Vol. 60, No. 5, Paper No. 2857, May 1958.

20. Langhaar, H.L., Dimensional Analysis and Theory Models, John Wiley & Sons, Inc., New York, 1951.

21. Longuet-Higgins, M.S. and Stewart, R.W., "Radiation Stresses in Water Waves; A Physical Discussion, with Applications", Deep Sea Research, 1964, Vol. 11, pp. 529-562.

22. MacCamy, R.C. and Fuchs, R.A., "Wave Forces on Piles: A Diffraction Theory", Beach Erosion Board, Technical Memorandum No. 69, 1954.

23. Morison, J.R., "The Design of Pilings", Proc. First Conference on Coastal Engineering, pp. 254-258, 1951.

24. Morison, J.R., O'Brien, M.P., Johnson, J.W., and Schaaf, S.A., "The Force Exerted by Surface Waves on Piles", Petroleum Transactions, AIME, Vol. 189, 1950, pp. 149-154.

25. Morison, J.R. and Crooke, R.C., "The Mechanics of Deep Water, Shallow Water, and Breaking Waves", Technical Memorandum No. 40, Beach Erosion Board, Corps of Engineers, March 1953.

26. Morison, J.R., Johnson, J.W., and O'Brien, M.P., "Experimental Studies of Forces on Piles", Proceedings, Fourth Conference on Coastal Engineering, 1953, pp. 340-370.

27. O'Brien, M.P., and Morison, J.R., "The Forces Exerted by Waves on Objects", Trans, Amer. Geophys. Union, Vol. 33, No. 1, 1952.

28. Paape, A., and Breusers, H.N.C., "The Influence of Pipe Dimensions on Forces Exerted by Waves," Delft Hydraulics Lab., Publication No. 41, Oct. 1966, Delft, The Netherlands.

29. Rao, V.S., and Garrison, C.J., "Interaction of a Train of Regular Waves with a Rigid Submerged Ellipsoid", Sea Grant Publication No. TAMU-SG-71-209, Texas A&M University, College Station, Texas, May 1971.

30. Reid, R.O., "Horizontal and Vertical Forces on a Partially Submerged Platform for Maximum Wave Conditions in Lake Caddo, La.", Texas A&M University, Department of Oceanography, Project 45, Jan. 1954.

31. Reid, R.O., and Bretschneider, C.L., "Surface Waves and Offshore Structures: The Design Wave in Deep or Shallow Water, Storm Tide, and Forces on Vertical Piles and Large Submerged Objects", Texas A&M University, Oceanography Dept., Technical Report, Oct. 1953.

32. "Sanborn Manual-Model 150 Four Channel Carrier Preamplifier Recorder", Sanborn Co., Boston, Mass.

33. Sarpkaya, T., Garrison, C.J., "Vortex Formation and Resistance in Unsteady Flow", Transactions, ASME, March 1963.

34. Sarpkaya, T., "Lift, Drag, and Added-Mass Coefficients for a Circular Cylinder Immersed in a Time-Dependent Flow", Journal of Applied Mechanics, March 1963.

35. Shank, G.E., and Herbich, J.B., "Forces Due to Waves on Submerged Structures", Sea Grant Publication, No. TAMU-SG-70-212, Texas A&M University, College Station, Texas, May 1970.

36. Stokes, G.G., "On the Theory of Oscillatory Waves", Trans. Cambridge Philosophical Society, Vol. VIII, p. 441, 1847.

37. Streeter, V.L., Fluid Mechanics, McGraw-Hill, Inc., New York, 1966.

38. Wiegel, R.L., Oceanographical Engineering, Prentice-Hall, Inc., New Jersey, 1964.

APPENDIX II

NOTATION

The following symbols are used in this paper.[1]

Symbol	Description	Dimension
a	Wave amplitude	L
C	Celerity	L/T
C_M	Coefficient of mass	-
C_D	Coefficient of drag	-
C_{M_H}	C_M for horizontal direction	-
C_{M_V}	C_M for vertical direction	-
d	Water depth	L
D	Water depth on computer plots	L
F	Force	ML/T^2
F_H	Horizontal force	ML/T^2
F_V	Vertical force	ML/T^2
FHW	F_H in direction of wave advance	ML/T^2
FHO	F_H opposite to direction of wave advance	ML/T^2

[1] These symbols are consistent throughout the text with the exception of the literature survey. In the literature survey, the symbols are used as they appear in the cited literature, and are redefined for each author.

Symbol	Description	Dimension
FVD	Vertical force downward	ML/T^2
FVU	Vertical force upward	ML/T^2
FDIMHW	Dimensionless form of FHW	-
FDIMHO	Dimensionless form of FHO	-
FDIMVD	Dimensionless form of FVD	-
FDIMVU	Dimensionless form of FVU	-
g	Gravitational constant	L/T^2
H	Wave height	L
H/L	Wave steepness	-
k	Wave number	L^{-1}
L	Wave length	L
L/d	Relative depth	-
ℓ	Characteristic length	L
ℓ_1	Model length	L
ℓ_2	Model width	L
ℓ_3	Model height	L
MWL	Mean water level	L
P	Wave induced pressure	M/LT^2
S	Distance measured from bottom of tank upward	L
S'	Distance from bottom of tank to center of model	L
T	Wave period	T

Symbol	Description	Dimension
t	Time	T
u	Horizontal velocity component	L/T
$\frac{\partial u}{\partial t}$	Horizontal acceleration component	L/T^2
U	Velocity	L/T
$\forall$	Volume	L^3
w	Vertical velocity component	L/T
$\frac{\partial w}{\partial t}$	Vertical acceleration component	L/T^2
x	Horizontal coordinate	L
z	Vertical coordinate	L
γ	Specific weight of water	M/L^2T^2
ρ	Mass density of water	M/L^3
μ	Dynamic viscosity of water	$M/L\ T$
ϵ	Vertical water particle displacement	L
ξ	Horizontal water particle displacement	L
ω	Wave angular frequency	T^{-1}
π_n	n^{th} dimensionless term	-
η	Free surface elevation from MWL	L
Φ	Velocity potential	L^2/T

APPENDIX III

CALIBRATION

Force Transducers. - Since wave forces are oscillatory, the force transducers were required to measure the force in two directions. To accomplish this, each transducer was pretensioned, the vertical force transducers by the weight of the model, and the horizontal transducers by the spring in the horizontal constraint system. The wave induced forces oscillated about this static load. The procedure is as follows:

1. After positioning the model according to the procedure given in Appendix III, balance the half-bridge of the recording units[3] and set the pens to the center of recorder paper. The pen positions now represent zero wave loading of the model.

2. Calibrate the four vertical force transducers together. From each transducer hand a 50 gram load and adjust the recorder sensitivity to 10 millimeters of deflection. This gives a basic sensitivity of 5.0 grams per millimeter of pen deflection. Next, use the four calibration pulleys shown in Fig. 10 to put an upward load on the transducer. Note the distance each pen deflects.

3. Without changing recorder sensitivity, load the transducer first downward then upward with calibration loads of 100 and 200 grams. Note the amount of pen deflection for each loading. Plot the

[3]Balancing procedures can be found in references 15 and 32.

pen deflection as positive for an upward force and negative for a downward force for each transducer. The resulting curve is the calibration curve for each transducer.

4. Calibration of the horizontal transducer follows steps 2 and 3 except that the calibration loads are 100, 200, 400 and 800 grams. Plot a calibration curve for the horizontal force transducer.

5. Remove calibration pulleys and calibration weights from force transducers.

Wave Gauge. - A capacitance type wave gauge mounted on a vernier was used to measure the water surface elevation at the model. The procedure for calibration is as follows:

1. Lower the wave gauge into the water until 50% of the shank is submerged.

2. With the water surface quiescent and the gauge wire wetted, balance the full-bridge of the electronic recorder and set the recorder pen to the center of the recorder paper.

3. Using the vernier, lower the gauge 0.05 ft. and observe the pen deflection. Adjust the recorder sensitivity for a pen deflection of 5 mm.

4. Raise the gauge 0.05 ft. (back to gauge zero) and observe if the pen goes back to the center of the recorder paper. If not, rebalance and repeat step 3 until 0.05 ft. of gauge movement corresponds to 5 mm of pen deflection. This sets the basic sensitivity to 0.1 ft. per centimeter of pen deflection.

5. With the recorder paper feed running at 1.0 mm/sec and moving the vernier in jumps of 0.05 ft., raise the gauge to ±0.25 ft. then back through zero to -0.25 ft. then back to zero. The trace should be step-like and level off every 5 mm.

During calibration and testing, the sensing wire of the gauge should be kept wet. There are two reasons for this. The capacitance of the gauge differs depending on how much of the wire above the still water level is wet. During tests, the varying wave heights will wet different levels of the wire above the still water level assuming that drying occurs between tests. Thus, by wetting the gauge before each test, the capacitance of the wire should be more constant and the results truer. Secondly, due to water surface tension, a meniscus forms around the sensing wire of the wave gauge. As the water rises, the water surface at the wave gauge takes the form of profile X-X in Fig. 38. When the water level begins to drop, the meniscus remains attached at S until the water surface drops a distance Δt. This causes the wave records to be flat-topped at the crest. Wetting the sensing wire tends to pull the point of attachment of the meniscus up the wire and the wave records assume a truer shape.

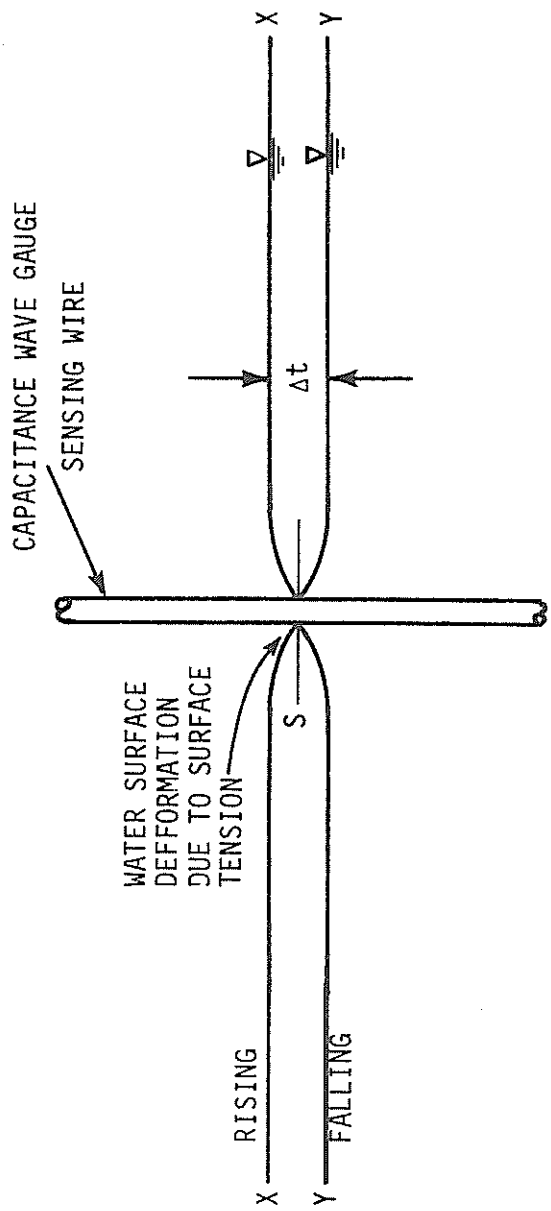

Fig. 48 SURFACE TENSION EFFECT ON CAPACITANCE WAVE GAUGE.

APPENDIX I V

PROCEDURE FOR ALIGNING MODEL IN TEST POSITION[1]

The procedure for positioning the model in the wave basin is as follows:

1. Place the vertical force transducer board in the cradle with the front edge parallel to the front edge of the cradle and 1.25 in. apart. This should align the four transducers over the corners of the model test position, the transducer board itself aligned with the wave generator.

2. Level the transducer board in the directions parallel and perpendicular to the wave crests, and secure the board to cradle using 2 in. C-clamps.

3. Suspend the model from the four force transducers using the four vertical support wires as shown in Fig. 17. When the model is at rest, the connecting points for the horizontal force leads located on the center of the front and rear model faces should be directly over the center line of the wave basin drawn on the floor. If the connecting points are not over the center line adjust the transducer board until they are. Adjust the threaded force transducer eye-bolts to level the model 0.25 in. above the basin floor. Mark the position of the model on the floor.[2]

---

[1]This procedure assumes that the cradle is properly aligned with the wave generator.

[2]This is the model test position. Steps 4 thru 7 constrain the model horizontally and adjust the model to the position as marked on the floor.

4. Adjust the height of the bottom of the pulley and the height of the studs to 2.4 in. above the floor to coincide with the level of the horizontal leader connecting points on the model (Fig. 17). Center the pulley and the forward support stud with the centerline of the model. Align the two lateral supports with the transverse centerline of the model.

5. Connect leader A as shown in Fig. 17. Adjust the position of the horizontal force transducer so that the extension of the tangent formed by the leader at the pully is perpendicular to the basin floor.

6. Connect the spring and leader B as shown in Fig. 17. By adjusting the threaded eye-bolts on the support stud and force transducer, bring the model to the test position drawn on the floor.

7. Connect lateral restraints as shown in Fig. 16. Adjust eye-bolts on studs to bring model to test position drawn on floor. This completes positioning of the model and the tank may be filled.

APPENDIX V

COMPUTER PROGRAM

The following pages include the computer program used in analyzing the model data. The program consists of four steps. Step 1 reads in the raw data from the model tests. Step two calculates the wave length (L) in the subroutine CALLEN. Step 3 calculates the dimensionless parameters used in the study. Step 4 outputs the data in the form of printed output and Calcomp or Gerber data plots.

```
C
C  ..................................................................
C
C           THIS COMPUTER PROGRAM PRODUCES THE DIMENSIONLESS QUANTITIES
C      USED IN THE WAVE FORCE ANALYSIS.  INPUT IS THE RAW DATA FROM THE
C      EXPERIMENTS.  OUTPUT IS THE DIMENSIONLESS TERMS USED IN PRESENTING
C      THE DATA.
C
C  ..................................................................
C
C                                INPUT
C
C      NN = TOTAL NUMBER OF INPUT CARDS
C      N = REFERS TO THE NEXT N CARDS OF DATA FOR A GIVEN MODEL AND DEPTH
C      DEPTH = WATER DEPTH
C      L1 = MODEL DIMENSION PARALLEL TO DIRECTION OF WAVE ADVANCE
C      L2 = MODEL DIMENSION PERPENDICULAR TO DIRECTION OF WAVE ADVANCE
C      L3 = MODEL HEIGHT
C      RUN = DATA RUN NUMBER
C      T = WAVE PERIOD
C      H = WAVE HEIGHT
C      FVD = MEASURED VERTICAL FORCE DOWNWARD
C      FVU = MEASURED VERTICAL FORCE UPWARD
C      FHW = MEASURED HORIZONTAL FORCE IN DIRECTION OF WAVE ADVANCE
C      FHW = MEASURED HORIZ. FORCE IN DIRECTION OPPOSITE TO WAVE ADVANCE
C
C  ..................................................................
C
      COMMON WAVLEN(500), T(500), DEPTH, FDIMHW(500), FDIMHO(500), FDIMVU(500
       1), FDIMVD(500),N,DDL(500), LDD(500), HDL(500), FHO(500), FHW(500),
     *FVU(500), FVD(500), DENOM(500), H(500), RUN(500), SUI(500), SHL3(500), J,
     *X(500),Y(500),Z(500),U(500),W(500),HDL'(500),L1DL(500),S(500),
     *R(500), FIN,ST,ZZ
      INTEGER RUN, ZZ1
```

```
      REAL L1, L2, L3, LDD,L1DL
C
C  ..........o.....................................................................
C
C            CONSTANTS AND OTHER QUANTITIES USED IN PROGRAM
C
C     A = CONVERSION FACTOR (GRAMS TO POUNDS)
C     V = MODEL VOLUME
C     GAMMA= UNIT WEIGHT OF WATER
C     CALLEN = SUBROUTINE FOR CALCULATING WAVE LENGTH
C     ZZ, ZZ1 = MODEL NUMBER
C
C  .....................................................................................
C
      PI = 3.14159265
      A = 0.00220462
      J = 0
      READ 19, NN
   19 FORMAT(I3)
   16 READ 205, N. DEPTH, L1, L2, L3
  205 FORMAT(I3,4F4,2)
      IF(J.GE.166) GO TO 88
      DO 101 I=1,N
      M = J+I
      READ 100, RUN(M), T(M), H(M), FHW(M), FHO(M), FVU(M), FVD(M)
  100 FORMAT(I3, 2F5.2, 4F5.0)
  101 CONTINUE
      GO TO 15
   88 DO 999 I=1,N
      M=J+I
      READ(5,777) RUN(M),T(M),H(M),FVD(M),FVU(M),FHW(M),FHO(M)
  777 FORMAT(I4,2X,F5,3,9X,F5,3,2X,F3,0,2X,F3,0,2X,F4.0)
   15 V=L1*L2*L3
```

```
      GAMMA = 62.4
      CALL CALLEN
      DO 50 I=1,N
      K=J+1
      SL1(K)=(SIN(PI*L1/WAVLEN(K)))/(PI*L1/WAVLEN(K))
      SHL3(K)=(SINH(PI*L3/WAVLEN(K)))/(PI*L3/WAVLEN(K))
      DENOM(K)=GAMMA*(H(K)/DEPTH)*V*SL1(K)*SHL3(K)
      FDIMHO(K)=FHO(K)/DENOM(K)*A
      FDIMHW(K)=FHW(K)/DENOM(K)*A
      FDIMVD(K)=FVD(K)/DENOM(K)*A
      FDIMVU(K)=FVU(K)/DENOM(K)*A
      LDD(K)=WAVLEN(K)/DEPTH
      DDL(K)=DEPTH/WAVLEN(K)
      HDL(K)=H(K)/WAVLEN(K)
      L1DL(K)=L1/WAVLEN(K)
      HDL1(K)=H(K)/L1
   50 CONTINUE
      ZZ = 4.0
      J=J+N
      IF (J.GE.60) ZZ=6.0
      IF(J.GF.89) ZZ=5.0
      IF(J.GE.118) ZZ=3.0
      IF(J.GE.143 ZZ=7.0
      IF (J.GE.167) ZZ=1.0
      IF(J.GE.272) ZZ=2.0
      ZZ1=ZZ
      J=J-N
C
C     ..........................................................................
C
C                                    OUTPUT
C
C     WAVLEN =WAVE LENGTH
C     LDD = L/D, WAVE LENGTH/DEPTH - RELATIVE DEPTH
C     DDL = INVERSE OF LDD
```

```
C       HDL = WAVE STEEPNESS
C       HDL1 = RELATIVE DISPLACEMENT PARAMETER
C       L1/L = RELATIVE SIZE PARAMETER
C       FDIMHW = THEORETICAL DIMENSIONLESS FORCE FOR FHW
C       FDIMHO = THEORETICAL DIMENSIONLESS FORCE FOR FHO
C       FDIMVD = THEORETICAL DIMENSIONLESS FORCE FOR FVD
C       FDIMVU = THEORETICAL DIMENSIONLESS FORCE FOR FVU
C       SL1 = CIRCULAR SINE PARAMETER
C       SHL3 = HYPERBOLIC SINE PARAMETER
C
C  ..............................................................................
C
        PRINT 99, ZZ1, L1,L2,L3,DEPTH
   99   FORMAT('1',28X,'MODEL NO.',I1,', DIMENSIONS* L1=',F5.2, ' FT., L2
       *=',F5.2,' FT., L3=',F5.2,'FT., DEPTH=', F3,1,' FT.')
        PRINT 212
  212   FORMAT('-',2X,'RUN',2X,'PEROID',6X,'H',6X,'L',6X,'L/D',5X,'D/L',5X
       *,'H/L',5X,'H/LI',5X,'L1/L',3X,'FDIMHW',3X,'FDIMHO',3X,FDIMVU',3X,
       *'FDIMVD',6X,'SL1',5X,'SHL3',2X,'DEPTH')
        DO 224 I=1,N
        M=J+I
        PRINT 35,RUN(M),T(M),H(M),WAVLEN(M),LDD(M),HDL(M),HDL1(M),
       *L1DL(M),FDIMHW(M),FDIMHO(M),FDIMVU(M),FDIMVD(M),SL1(M),SHL3(M),
       *DEPTH
    35 FORMAT (16,F8.2,2F7.2,F9.4,2F8.4,2F9.4,4F9.4,2F9.5,F7.2)
   224 CONTINUE
       DO 33 I=1,N
       M=J+1
       X(I)-LDD(M)
       Y(I)-FIDMHW(M)
       Z(I)=FDIMHO(M)
       U(I)=FDIMVU(M)
       W(I)-FDIMVD(M)
       R(I)=HDL1(M)
```

```
      S(I) = L1DL(M)
   33 CONTINUE
      ST=RUN(J+1)
      FIN=RUN(J+N)
      JP=0
   45 JP=JP+1
      CALL LINE1(15.0,0.,1.,0.,2.,.2)
      CALL AXIS1(0.,0.,'L/D',-3,7.5,0.,0.,2.0,20.0)
      CALL SYMBOL(5.0,4.35,.15,'MODEL NO.',0.,9)
      CALL NUMBER(6.16,4.35,.15,ZZ,0.,-1)
      CALL SYMBOL(5.0,4.05,.15,'RUNS
      CALL NUMBER(565,4.05,.15,ST,0,-1)
      CALL NUMBER(6.67,4.05,.15,FIN,0.,-1)
      CALL SYMBOL(5.0,3.75,.15,'DEPTH =    FT.',0.,15)
      CALL NUMBER(6.05,3.75,.15,DEPTH,0.,1)
      IF (JP.EQ.1)GO TO 10
      IF (JP.EQ.2)GO TO 20
      IF (JP.EQ.3)GO TO 30
      IF (JP.EQ.4)GO TO 40
   10 CALL AXIS1(0.,0.,'FDIMHW',6,5.,90.,0.,.20,20.)
      CALL SYMBOL(0.,-0.65,.15,'FIG.     HORIZONTAL DIMENSIONLESS FORCE
     *VS. RELATIVE DEPTH',0.,58)
      CALL LINE2(X,Y,N,11,1,1)
      CALL LINE3(10.0)
      CAOO OPSTOP
      GO TO 45
   20 CALL AXIS1(0.0,0.0,'FDIMHO',6,5.0,90.0,0.0,0.20,20.0)
      CALL SYMBOL(0.,-0.65,.15,'FIG.     HORIZONTAL DIMENSIONLESS FORCE
     *VS. RELATIVE DEPTH',0.,58)
      CALL LINE 2(X,Z,N,11,1,1)
      CALL LINE 3(10.0)
      CALL OPSTOP
      GO TO 45
```

```
30  CALL AXIS1(0.0,0.0,'FDIMVU',6,5.0,90,0,0.0,0.20,20.0)
    CALL SYMBOL(0.,-.65,.15,'FIG.     VERTICAL DIMENSIONLES FORCES VS.
   * RELATIVE DEPTH',0.,56)
    CALL LINE2(X,U,N,11,1,1)
    CALL LINE3(10.0)
    CALL OPSTOP
    GO TO 45
40  CALL AXIS1(0.0,0.0,'FDIMVD',6,5.0,90.0.0,0.0,0.20,20.0)
    CALL SYMBOL(0.0-.65,.15,'GIH.     VERTICAL DIMENSIONLESS FORCE VS.
   * RELATIVE DEPTH',0.,56)
    CALL LINE 2(X,W,N,11,1,1)
    CALL LINE 3(10.0)
    CALL OPSTOP
    J=J+N
    IF(J.EQ.NN) GO TO 41
    GO TO 16
41  CALL LINE4
    STOP
    END
```

CALLEN

```
      SUBROUTINE CALLEN
      COMMON WAVLEN(500),T(500),DEPTH,FDIMHW(500),FDIMHD(500),FDIMVU(500
     1),FDIMVD(500),N,DDL(500),LDD(500),HDL(500),FHO(500),FHW(500),
     *FVU(500),FVD(500),DENOM(500),H(500),RUN(500),SL1(500),SHL3(500),J,
     *X(500),Y(500),Z(500),U(500),W(500),HDL1(500,L1DL(500),S(500),
     *R(500),FIN,ST,ZZ
      REAL LO,LNOW, LENG,LENGO
      DO 400 I-1,N
      M-J+I
      LO=5.12*T(M)**2.0
      DLO=DEPTH/LO
      IF(DLO-.04)10,1,1
    1 IF(DLO-.15) 20,2,2
    2 IF(DLO-0.39) 30,40,40
   10 DL=0.43*DLO**0.511
      GO TO 100
   20 DL=0.54*DLO**0.58
      GO TO 100
   40 DL=DLO
  100 LNOW=DEPTH/DL
      PID=6.2832*DEPTH
      LENG=LO*TANH(PID/LNOW)
      DO 300 K=1,500
      LENGO=LENG
      LENG=LO*TANH(PID/LENGO)
      IF(0.005*LENGO,GE.ABS(LENGO-LENG)) GO TO 200
  300 CONTINUE
  200 WAVLEN(M)=LENG
  400 CONTINUE
      RETURN
      END
```

MODEL NO. 4, DIMENSIONS= L1= 1.29 FT., L2= 0.66 FT., L3= 0.37 FT., DEPTH=1.5 FT.

RUN	PERIOD	H	L	L/D	D/L	H/L	H/L1	L1/L	FDIMHW	FDIMHD	FDIMVU	FDIMVD	SLI	SHLI
47	3.05	0.04	20.93	13.6875	0.0731	0.0019	0.0310	0.0628	0.7327	0.2981	0.0977	0.1565	0.99387	1.00083
48	2.34	0.07	16.77	11.1798	0.0894	0.0042	0.0543	0.0769	0.1552	0.1485	0.1067	0.1309	0.99029	1.00080
49	2.00	0.08	12.90	8.5334	0.1172	0.0062	0.0620	0.1008	0.2349	0.1751	0.1495	0.1671	0.98338	1.00137
50	2.07	0.09	11.32	8.8786	0.1126	0.0068	0.0694	0.0969	0.1919	0.1417	0.1499	0.1427	0.98444	1.00127
51	1.87	0.10	11.87	7.9104	0.1264	0.0084	0.0775	0.1087	0.2100	0.1740	0.1124	0.1370	0.99047	1.00160
52	1.51	0.13	9.07	6.0441	0.1654	0.0199	0.1395	0.1423	0.2564	0.2265	0.2199	0.2140	0.96701	1.00274
53	1.29	0.19	7.24	4.8258	0.2072	0.0262	0.1473	0.1782	0.3253	0.3392	0.2677	0.2494	0.96857	1.00430
54	2.53	0.11	16.70	11.1308	0.0898	0.0066	0.0853	0.0773	0.2068	0.1543	0.1157	0.1451	0.99021	1.00081
55	2.01	0.14	12.87	8.5828	0.1165	0.0109	0.1095	0.1002	0.1925	0.1464	0.1867	0.1427	0.98357	1.00134
56	1.81	0.17	11.41	7.6038	0.1315	0.0149	0.1319	0.1131	0.2987	0.3188	0.2361	0.1977	0.97008	1.00173
57	1.40	0.26	8.21	5.4737	0.1827	0.0317	0.2016	0.1571	0.4804	0.5106	0.2560	0.3312	0.95089	1.00334
58	2.35	0.15	16.84	11.2288	0.0891	0.0107	0.1395	0.0766	0.2074	0.1509	0.1094	0.1443	0.99038	1.00079
59	2.04	0.24	13.17	8.7801	0.1139	0.0192	0.1860	0.0979	0.2020	0.1565	0.1664	0.1478	0.98429	1.00130
60	1.65	0.30	10.15	6.7664	0.1478	0.0296	0.2326	0.1271	0.1632	0.1724	0.2195	0.1293	0.97364	1.00219
61	1.34	0.43	7.71	5.1422	0.1945	0.0583	0.3488	0.1672	0.2107	0.2536	0.3282	0.3172	0.95462	1.00379

MODEL NO. 5, DIMENSIONS= L1= 0.66 FT., L2= 0.96 FT., L3= 0.37 FT., DEPTH=1.5 FT.

RUN	PERIOD	H	L	L/D	D/L	H/L	H/L1	L1/L	FDIMHW	FDIMHD	FDIMVU	FDIMVD	SLI	SHLI
91	3.24	0.13	21.30	14.9326	0.0698	0.0060	0.1970	0.0303	0.4444	0.3196	0.1233	0.1198	0.99842	1.00068
92	2.06	0.25	13.24	8.5293	0.1135	0.0180	0.3788	0.0498	0.5317	0.3436	0.1655	0.1501	0.99509	1.00129
93	2.53	0.17	16.70	11.1308	0.0898	0.0102	0.2576	0.0395	0.2577	0.2019	0.0901	0.1116	0.99749	1.00081
94	2.07	0.20	12.95	8.6322	0.1158	0.0156	0.3030	0.0510	0.7518	0.5878	0.1764	0.2374	0.99877	1.00134
95	1.51	0.44	9.07	6.0441	0.1654	0.0485	0.6667	0.0728	0.4062	0.4897	0.2082	0.1588	0.99131	1.00774
96	1.33	0.39	7.63	5.0893	0.1965	0.0511	0.5909	0.0865	0.8278	0.7578	0.3125	0.2664	0.98776	1.00380
97	2.35	0.12	16.84	11.2288	0.0891	0.0071	0.1818	0.0392	0.2691	0.2447	0.0772	0.1038	0.99748	1.00080
98	2.01	0.13	12.87	8.5828	0.1165	0.0101	0.1970	0.0513	0.5566	0.4557	0.1692	0.1565	0.99568	1.00137
99	1.49	0.26	8.91	5.9379	0.1684	0.0292	0.3939	0.0741	0.4319	0.4886	0.2242	0.2024	0.99090	1.00286
100	1.35	0.31	7.79	5.1949	0.1925	0.0398	0.4697	0.0947	0.5499	0.5719	0.2110	0.2134	0.98824	1.00373
101	2.35	0.07	16.84	11.2288	0.0891	0.0042	0.1061	0.0392	0.2162	0.2129	0.0742	0.0871	0.99748	1.00080
102	2.02	0.08	12.95	8.6322	0.1158	0.0062	0.1212	0.0510	0.3590	0.2911	0.1187	0.1272	0.99577	1.00135
103	1.48	0.14	8.83	5.8847	0.1699	0.0459	0.2121	0.0748	0.4343	0.4376	0.2220	0.1993	0.99083	1.00291
104	1.33	0.19	7.63	5.0893	0.1965	0.0249	0.2879	0.0865	0.4906	0.5864	0.2310	0.2046	0.98775	1.00380

MODEL NO. 6, DIMENSIONS= L1= 0.66 FT., L2= 1.29 FT., L3= 0.37 FT., DEPTH=1.5 FT.

RUN	PERIOD	H	L	L/D	D/L	H/L	H/L1	L1/L	FDIMHW	FDIMHD	FDIMVU	FDIMVD	SLI	SHLI
62	2.51	0.19	16.55	11.0329	0.0906	0.0115	0.2879	0.0399	0.3193	0.2235	0.0905	0.1197	0.99739	1.00097
63	2.05	0.21	13.17	8.7801	0.1139	0.0159	0.3182	0.0501	0.3471	0.2330	0.1758	0.1442	0.99587	1.00139
64	1.63	0.25	10.00	6.6665	0.1500	0.0250	0.3788	0.0660	0.6762	0.7439	0.2739	0.3084	0.99245	1.00225
65	1.31	0.37	7.49	4.9926	0.2003	0.0494	0.5606	0.0891	0.9176	0.8715	0.4642	0.4017	0.98737	1.00429
66	3.05	0.13	23.53	15.6875	0.0731	0.0063	0.1970	0.0321	0.4146	0.3109	0.1259	0.1140	0.99339	1.00083
67	2.56	0.13	16.93	11.2938	0.0891	0.0077	0.1970	0.0496	0.2424	0.2933	0.0995	0.1370	0.99753	1.00094
68	2.07	0.14	13.32	8.9786	0.1126	0.0105	0.2121	0.0496	0.3956	0.3276	0.1773	0.1564	0.99594	1.00127
69	1.67	0.16	10.33	6.8880	0.1452	0.0155	0.2424	0.0639	0.4648	0.5493	0.2240	0.2107	0.99330	1.00211
70	1.35	0.29	7.79	5.1949	0.1925	0.0373	0.4394	0.0947	0.7164	0.6872	0.2901	0.3443	0.99026	1.00371
71	2.54	0.07	16.77	11.1798	0.0894	0.0062	0.1061	0.0394	0.3443	0.2613	0.1197	0.1274	0.99745	1.00080
72	2.01	0.08	12.87	8.5828	0.1165	0.0062	0.1212	0.0511	0.4300	0.5263	0.1781	0.2139	0.99569	1.00134
73	1.49	0.13	10.32	7.2794	0.1376	0.0092	0.1515	0.0605	0.4667	0.4730	0.2112	0.1853	0.99400	1.00189
74	1.34	0.19	7.67	5.2478	0.1906	0.0251	0.2879	0.1339	0.6783	0.6962	0.3124	0.2756	0.98847	1.00364

Fig. 49 Sample Computer Output

MODEL NO. 2, DIMENSIONS= L1= 0.66 FT., L2= 0.64 FT., L3= 0.37 FT., DEPTH=1.1 FT.

RUN	PERIOD	H	L	L/D	D/L	H/L	H/L1	L1/L	FDIMW	FDIMHO	FDIMVU	FDIMVD	SL1	SHL3
1700	1.30	0.08	6.67	6.1728	0.1620	0.0114	0.1152	0.0990	0.5101	0.5101	0.2296	0.2327	0.98396	1.00518
1701	1.30	0.08	6.67	6.1728	0.1620	0.0114	0.1152	0.0990	0.5423	0.5867	0.2519	0.2465	0.98396	1.00518
1702	1.29	0.08	6.63	6.1428	0.1628	0.0116	0.1167	0.0995	0.6043	0.5476	0.2581	0.2473	0.98380	1.00524
1711	1.30	0.14	6.67	6.1728	0.1620	0.0240	0.2424	0.0990	0.6179	0.6361	0.2499	0.2635	0.98396	1.00518
1720	1.27	0.25	6.45	5.9735	0.1674	0.0384	0.3758	0.1023	0.6297	0.6258	0.2621	0.2669	0.98287	1.00554
1730	1.26	0.33	6.42	5.9422	0.1683	0.0517	0.5030	0.1028	0.6954	0.6721	0.2798	0.2466	0.98269	1.00560
1740	1.24	0.37	6.25	5.7854	0.1728	0.0592	0.5606	0.1056	0.8238	0.8186	0.2401	0.2243	0.98175	1.00590
1750	1.24	0.41	6.25	5.7854	0.1728	0.0656	0.6219	0.1056	0.6819	0.6677	0.2587	0.2368	0.98175	1.00590
1760	1.05	0.11	4.96	4.5901	0.2179	0.0219	0.1636	0.1331	0.5297	0.5207	0.3240	0.3260	0.97110	1.00939
1770	1.04	0.22	4.92	4.5575	0.2194	0.0439	0.3273	0.1341	0.6431	0.6295	0.3182	0.3261	0.97069	1.00952
1780	1.04	0.32	4.99	4.5249	0.2211	0.0653	0.4833	0.1351	0.7056	0.6503	0.4042	0.3673	0.97027	1.00966
1790	1.03	0.44	4.82	4.4567	0.2243	0.0922	0.6727	0.1370	0.6616	0.6043	0.3639	0.3799	0.96940	1.00995
1800	1.01	0.33	4.68	4.3292	0.2310	0.0710	0.5030	0.1412	0.6645	0.6497	0.4334	0.4098	0.96754	1.01056
1810	0.89	0.10	3.83	3.5430	0.2822	0.0272	0.1576	0.1725	0.5721	0.5721	0.3985	0.3504	0.95178	1.01579
1820	0.89	0.21	3.83	3.5430	0.2822	0.0554	0.3212	0.1725	0.5285	0.5145	0.3835	0.3403	0.95178	1.01579
1821	0.89	0.20	3.83	3.5430	0.2822	0.0523	0.3030	0.1725	0.5553	0.5478	0.4028	0.3458	0.95178	1.01579
1830	0.89	0.30	3.83	3.5430	0.2822	0.0784	0.4545	0.1725	0.5288	0.5255	0.3727	0.3611	0.95178	1.01579
1840	0.88	0.34	3.79	3.5101	0.2849	0.0892	0.5121	0.1741	0.5577	0.5284	0.3662	0.3567	0.95088	1.01609
1850	0.89	0.29	3.83	3.5430	0.2822	0.0758	0.4394	0.1725	0.5095	0.5129	0.3787	0.3488	0.95178	1.01579
1860	0.75	0.10	2.87	2.6554	0.3766	0.0335	0.1455	0.2301	0.3714	0.3449	0.3980	0.4086	0.91513	1.02821
1870	0.75	0.19	2.87	2.6554	0.3766	0.0659	0.2864	0.2301	0.4151	0.4124	0.3652	0.3760	0.91513	1.02821
1880	0.75	0.24	2.83	2.6230	0.3812	0.0914	0.4182	0.2330	0.4344	0.4021	0.3512	0.3318	0.91307	1.02892
1890	0.75	0.27	2.87	2.6554	0.3766	0.0955	0.4152	0.2301	0.4648	0.4090	0.3514	0.3597	0.91513	1.02821
1900	0.75	0.23	2.87	2.6554	0.3766	0.0795	0.3455	0.2301	0.4580	0.4022	0.3977	0.3888	0.91513	1.02821
1910	0.71	0.10	2.59	2.3981	0.4170	0.0371	0.1455	0.2548	0.3768	0.3230	0.4198	0.4037	0.89655	1.03465
1920	0.71	0.19	2.56	2.3664	0.4226	0.0751	0.2909	0.2582	0.3984	0.3371	0.3816	0.3870	0.89385	1.03560
1930	0.71	0.25	2.56	2.3664	0.4226	0.0990	0.3833	0.2582	0.3930	0.3428	0.3704	0.3909	0.89385	1.03560
1931	0.71	0.25	2.56	2.3664	0.4226	0.0986	0.3819	0.2582	0.4356	0.3658	0.3873	0.4027	0.89385	1.03560
1940	0.71	0.23	2.56	2.3664	0.4226	0.0908	0.3515	0.2582	0.4062	0.3348	0.3638	0.3872	0.89385	1.03560
1950	0.70	0.22	2.52	2.3348	0.4283	0.0888	0.3394	0.2617	0.7830	0.6950	0.3753	0.3753	0.89105	1.03658

MODEL NO. 3, DIMENSIONS= L1= 0.96 FT., L2= 0.66 FT., L3= 0.37 FT., DEPTH=2.0 FT.

RUN	PERIOD	H	L	L/D	D/L	H/L	H/L1	L1/L	FDIMW	FDIMHO	FDIMVU	FDIMVD	SL1	SHL3
132	3.13	0.07	24.01	12.0042	0.0833	0.0029	0.0729	0.0400	0.2410	0.2582	0.5423	0.5380	0.99737	1.00039
133	2.01	0.17	14.46	7.2318	0.1383	0.0119	0.1771	0.0664	0.2989	0.2989	0.1850	0.1957	0.99277	1.00108
134	1.53	0.28	10.13	5.0628	0.1975	0.0277	0.2917	0.0948	0.3044	0.3370	0.2381	0.2533	0.98528	1.00221
135	1.34	0.32	8.33	4.1641	0.2401	0.0384	0.3333	0.1153	0.3302	0.3733	0.2316	0.2450	0.97829	1.00327
136	3.92	0.11	29.85	14.9249	0.0670	0.0037	0.1146	0.0322	0.4652	0.3695	0.1533	0.2226	0.99830	1.00025
137	3.12	0.13	23.93	11.9651	0.0836	0.0054	0.1354	0.0401	0.3013	0.3245	0.1344	0.1576	0.99735	1.00030
138	2.00	0.29	14.38	7.1882	0.1391	0.0202	0.3021	0.0668	0.4078	0.4055	0.1836	0.2159	0.99268	1.00109
139	1.56	0.44	10.31	5.1546	0.1940	0.0427	0.4583	0.0931	0.4371	0.4218	0.2324	0.2690	0.98580	1.00213
140	1.34	0.56	8.33	4.1641	0.2401	0.0672	0.5833	0.1153	0.4069	0.4375	0.2395	0.2882	0.97829	1.00327
141	3.93	0.16	29.80	14.9096	0.0671	0.0054	0.1667	0.0322	0.5651	0.4440	0.1580	0.1994	0.99829	1.00025
142	3.02	0.17	23.09	11.5417	0.0866	0.0074	0.1771	0.0416	0.4236	0.4431	0.1347	0.2446	0.99716	1.00042
143	2.06	0.46	14.90	7.4496	0.1342	0.0308	0.4697	0.0644	0.4119	0.5106	0.1651	0.1908	0.99318	1.00102
144	1.51	0.51	9.96	4.9796	0.2008	0.0512	0.5313	0.0964	0.5434	0.5374	0.2697	0.3210	0.98479	1.00228

Fig. 50 Sample Computer Output